SPECTROSCOPIC AND THERMODYNAMIC STUDIES OF THE ADSORPTION OF

ATMOSPHERICALLY RELEVANT DICARBOXYLIC ACIDS AT THE

VAPOR/WATER INTERFACE

by

PATRICK GEORGES BLOWER

A DISSERTATION

Presented to the Department of Chemistry
and the Graduate School of the University of Oregon
in partial fulfillment of the requirements
for the degree of
Doctor of Philosophy

June 2013

DISSERTATION APPROVAL PAGE

Student: Patrick Georges Blower

Title: Spectroscopic and Thermodynamic Studies of the Adsorption of Atmospherically Relevant Dicarboxylic Acids at the Vapor/Water Interface

This dissertation has been accepted and approved in partial fulfillment of the requirements for the Doctor of Philosophy degree in the Department of Chemistry by:

Dr. Paul C. Engelking   Chair
Dr. Geraldine L. Richmond   Advisor
Dr. Michael E. Kellman   Member
Dr. Thomas R. Dyke   Member
Dr. Katharine V. Cashman   Outside Member

and

Kimberly Andrews Espy   Vice President for Research and Innovation
                             Dean of the Graduate School

Original approval signatures are on file with the University of Oregon Graduate School.

Degree awarded June 2013

DISSERTATION ABSTRACT

Patrick Georges Blower

Doctor of Philosophy

Department of Chemistry

June 2013

Title: Spectroscopic and Thermodynamic Studies of the Adsorption of Atmospherically Relevant Dicarboxylic Acids at the Vapor/Water Interface

Many important atmospheric processes are determined by the chemical composition of aerosols, including organic material. Dicarboxylic acids are a commonly detected class of organic material in urban, rural, and remote sites across the globe. Understanding the surface behavior of these molecules is imperative in characterizing the atmospheric fate of these molecules in aerosols, especially at an aerosol surface. In fact, little is known about their orientation, solvation, or pH dependence.

This dissertation explores in molecular level detail the concentration and pH behavior of low molecular weight dicarboxylic acids at the air/water interface, which is used as a model for an aerosol surface. The solvation of the carboxylic head groups is shown to be dependent upon the length of the alkyl backbone. Indeed, the solvation of the head groups changes dramatically from very weakly solvated to typical surface solvation to near bulk solvation as the backbone increases. The orientation and conformation at the surface is fully explored to explain these differences in solvation. The pH dependence of surface adsorption is characterized, and it is shown that some acids are only surface active if they are fully protonated while others may still be surface active in singly or fully deprotonated forms.

Using a combination of vibrational sum frequency spectroscopy (VSFS), surface tension, and computational modeling, the behavior at the air/water interface of four of the most relevant surface-active dicarboxylic acids (malonic, succinic, glutaric, and adipic acid) is completely described. VSFS, a surface specific optical technique, provides details about the solvation, orientation, and number density at the surface while surface tension measurements provide corollary information about the surface density. The use of computational modeling aids and confirms the spectral analysis while also providing molecular level details about the surface adsorption of the acids studied. By investigating the concentration and pH dependence of these molecules, molecular level detail is obtained which enables a complete description of these acids at an air/water interface and provides pertinent surface information on these atmospherically important organic molecules.

This dissertation includes both previously published and unpublished co-authored material.

CURRICULUM VITAE

NAME OF AUTHOR: Patrick Georges Blower

GRADUATE AND UNDERGRADUATE SCHOOLS ATTENDED:

     University of Oregon, Eugene, Oregon
     New College of Florida, Sarasota, Florida

DEGREES AWARDED:

     Doctor of Philosophy, Chemistry, 2013, University of Oregon
     Bachelor of Arts in Chemistry, 2004, New College of Florida

AREAS OF SPECIAL INTEREST:

     Laser Spectroscopy, Surface Science, Atmospheric Chemistry, Physical
          Chemistry

PROFESSIONAL EXPERIENCE:

     Research Assistant in the Richmond Laboratory, University of Oregon, Eugene,
          OR (2005-present)

     Graduate Teaching Assistant, Instrumental Analysis, University of Oregon,
          Eugene, OR (2006)

     Graduate Teaching Assistant, General Chemistry Laboratory, University of
          Oregon, Eugene, OR (2004-2005)

PUBLICATIONS:

P. Blower, E. Shamay, L. Kringle, S. Ota, and G.L. Richmond. Surface Behavior of Malonic Acid Adsorption at the Air/Water Interface. *J. Phys. Chem. A*, **2013**, 117 (12), pp 2529-2542.

M. Kido-Soule, P. Blower, and G.L. Richmond. Nonlinear Vibrational Spectroscopic Studies of the Adsorption and Speciation of Nitric Acid at the Vapor/Acid Solution Interface. *J. Phys. Chem. A*, **2007**, *111* (17), pp 3349–3357

M. Kido-Soule, P. Blower, and G.L. Richmond. Effects of Atmospherically Important Solvated Ions on Organic Acid Adsorption at the Surface of Aqueous Solutions. *J. Phys. Chem. B*, **2007**, *111* (49), pp 13703–13713

ACKNOWLEDGMENTS

Some journeys are longer than others but the destination is never the goal.

While this dissertation represents the work that I have done here as a graduate student, it does not necessarily reflect the people who have supported me. To that end, I would like to thank first the Richmond group members, both past and present. To Stephanie, I thank you for being a friend in our first year as well as an excellent source of support throughout our time in the lab. Without your help, I would probably still be fitting spectra today. To Nick and Eric, my computational saviors, thanks for all the great discussions and incredible work. Ellen, you were my first REU student and I am proud to have seen you turn into an accomplished researcher. Laura, Jet, and Brandon, my advice is simple: don't get discouraged (even when the laser breaks). To the members who have graduated in my time, including Melissa, Teresa, Dave, Cathryn, Dan, and Adam, I thank each of you for helping me along to become a better scientist. To the post-docs who have come through our lab including Dennis, Davida, Simon, Hristina, Katy, and Jenny, thank you for your help and support as well. And of course, none of this would have been possible without Geri, who has been an amazing advisor. When things were down, you helped me see the big picture. When things went well, you challenged me to do more. Thank you for your patience and support over the years.

I would also like to thank my committee members, Profs. Paul Engelking, Tom Dyke, Michael Kellman, and Kathy Cashman. Your valuable insight has helped me develop as a scientist. A big thanks goes out to Priscilla Lewis, who single-handedly keeps everything running smoothly and is always there with a piece of candy and a good conversation. To Fred, you continue to be the oracle for our group and I know your

contributions to the lab are invaluable. To Larry, you are an incredible source of knowledge and I can honestly say that your support will never be underestimated. The time you spent with me will always be some of the most enlightening, as well as enjoyable times, during graduate school.

In addition, I would be remiss in not recognizing friends who have made a huge difference in my well being during the rigors of grad school. To Calden and Pat, thanks for the lunches and beers. Our conversations often made a tough day better. To Byron and Caitlin, who have kept me in shape both mentally and physically, thank you for pushing me to my limits in more ways than one. To others, including but not limited to Matt, Brian and Kaila, Andy and Leni, Jay, Rick, Roger, Eric, Carey, Danielle W, Danielle H, and Mary, thanks for being great friends and great people.

I would also like to thank my parents, David and Elizabeth. While I know it was hard on you to have your only son move over 3000 miles away, you supported my decision and provided me with help and care along the way. I wish there was a better to way to communicate how deeply I appreciate your love and respect. Finally, to my best friend and furry dog, your wagging tail has gotten me through many bad days. You're my girl, Blue.

Dedicated to my parents, David and Elizabeth

TABLE OF CONTENTS

LIST OF FIGURES

Figure   Page

LIST OF TABLES

CHAPTER I

INTRODUCTION

Aerosols are defined as suspensions of fine solid or liquid particles dispersed in a gas,[1] but in its more common use the term aerosol describes particulate matter in the atmosphere. As such, aerosols incorporate many different types of particulate matter such as dusts, fogs, fumes, hazes, mists, smog, smoke, and soot. Aerosols can range in size from a few nanometers to tens of microns. Most importantly, without aerosols in our atmosphere, clouds could not form. As one of the most significant elements of the atmosphere, clouds are a major factor in the Earth's radiation budget, the hydrologic cycle, as well as a medium for aqueous-phase chemical reactions and secondary species.

Organic materials are ubiquitous in the atmosphere of the earth and their presence in aerosols play an important role in climate conditions.[1,2] Aerosols affect climate forcing directly through scatter and absorption of radiation or indirectly through cloud formation. Aerosols often contain a large quantity of organic matter, up to 90% of the total mass of some tropospheric aerosols depending upon their location.[3] Consequently, there is increasing interest in the study of how organic matter affects aerosol surface and bulk properties.

Organic acids are a particularly important class of organic material found in aerosols, varying in size and complexity from low molecular weight formic acid to large humic-like substances (HULIS). Dicarboxylic acids represent a sizeable fraction of organic matter in aerosols and are of low molecular weight, are soluble in water, and have low vapor pressures; thus, these acids partition preferentially to aerosols over the

1

gas phase. These dicarboxylic acids, with their hygroscopic and doubly ionizable acid groups, are prevalent in the atmosphere occurring in urban, rural, remote, and marine environments.[4-13]

Sources for dicarboxylic acids have been shown to be from biogenic and anthropogenic sources. However, their biogenic sources are thought to be small and thus anthropogenic sources are the primary emission source.[14,15] In addition, the persistence of these molecules, as evidenced by their global detection, is further indication that dicarboxylic acid molecules are mainly produced through oxidation of precursors, commonly referred to as secondary organic aerosol (SOA) formation.[16] A current model of an aerosol is that of an inverted micelle, with an aqueous core and an organic coating. The surface composition of organic material at an aerosol surface are expected to change as atmospheric processing oxidizes organic material to higher oxygen:carbon ratios.[17,18] The properties of aerosols, and specifically surface properties, are then expected to change as the organic material undergoes chemical changes.

Dicarboxylic acids are often the dominant class of water-soluble organics in the environment. Deliquescence,[3] phase transitions,[19] water activities,[20] and surface tension[21-24] have been investigated for binary systems containing dicarboxylic acids in order to aid in the predictability and modeling of these binary systems as cloud condensation nuclei (CCN).[25] While these studies have provided a better understanding of the bulk thermodynamic properties of dicarboxylic containing aerosols vis à vis their stability for CCN, they do not address the heterogeneous reactions[26] that can take place at the surfaces of these aerosols. Furthermore, the surface to volume ratio of aerosols can be large; indicating that aerosol surfaces may play a more important role than is currently

understood. For example, a recent study on halogen activation on water surfaces (i.e. a heterogeneous reaction) shows how weak acids, such as malonic acid, at a water surface can actually enhance $I_2(g)$ production in the marine boundary layer when compared to a neat water surface.[27] Another study has shown that glutaric acid coated particles increase the CCN activation for a $(NH_4)_2SO_4$ particle.[28]

It is known from surface tension measurements[21-23] that short-chain dicarboxylic acids are surface active. However, unlike traditional ionic alkyl surfactant molecules that have well defined hydrophobic and hydrophilic parts, low molecular weight dicarboxylic acids have two hydrophilic ends (carboxylic acid moieties) connected by a hydrophobic spacer $(CH_2)_n$. With a traditional surfactant, the orientation (and subsequent behavior) can be assumed, but the structure of dicarboxylic acids makes any assumptions made completely speculative. Given the prevalence of dicarboxylic acids in aerosols, surprisingly few molecular-level investigations of the behavior of dicarboxylic acids at aqueous surfaces have been conducted.

Therefore, it is the aim of this dissertation to investigate and fully characterize the orientation and solvation environment of low molecular weight dicarboxylic acids at the air/water interface. This will be completed through examining both the concentration and pH dependence of four dicarboxylic acids: malonic, succinic, glutaric, and adipic acid. These dicarboxylic acids differ only by the number of methylene units along the alkyl backbone. At first look, these diacids appear to be very similar and would thus behave in a comparable manner. However, these acids are known to have alternating odd/even effects for properties such as vapor pressure, melting point, and solubility.[29-32] In addition, the surface behavior of dicarboxylic acids will be dependent upon the

delicate balance between the hydrophobic carbon backbone and the hydrophilic carboxylic end groups. These acids are also diprotic and have different pK_a values. The surface behavior as a function of pH has not been studied before and may be an important factor in surface adsorption. Thus, the behavior of these acids must be examined carefully.

Through the use of Vibrational Sum Frequency Spectroscopy (VSFS), surface tension measurements, and computational modeling, a complete picture can be formed for the adsorption conditions of these atmospherically relevant acids. VSFS is a surface specific spectroscopy that is excellently suited for exploring the surface properties of these aqueous organic systems. As a second order non-linear vibrational spectroscopic method, VSFS is surface specific and can impart valuable information about the structure and orientation of an adsorbate as well as the alteration of surface water molecules due to the presence of the adsorbate. Surface tension measurements provide data about the number density of adsorbates at the interface, which can be used to corroborate the spectral results from VSFS as well as provide surface adsorption information. To complete the picture, molecular dynamics (MD) simulations are reported that validate the experimentally derived conclusions and assist in spectroscopic interpretations by directly assessing the specific orientations and geometries of dicarboxylic acids on a water surface. These studies provide not only crucial information relevant to the adsorption of these molecules but also develop a platform for understanding the interactions of ternary aqueous organic/inorganic systems, which closely resemble those of atmospheric systems.

The organization of this dissertation begins with a brief overview of the necessary background for VSFS and surface tension measurements. The following chapter details the experimental methods used throughout the remainder of the dissertation. Each subsequent chapter will use VSFS, surface tension, and computational modeling to characterize the four different dicarboxylic acids properties at the air/water interface. Chapter IV examines malonic acid, the smallest dicarboxylic acid studied here. Chapter V investigates succinic acid. Chapter VI explores glutaric acid and Chapter VII documents adipic acid, the largest dicarboxylic acid studied here. Finally, Chapter VII summarizes the main conclusions as well as some preliminary results from further studies performed with the addition of atmospherically relevant ions. The material in Chapter IV has been published in the Journal of Physical Chemistry A with co-authors Eric Shamay, Stephanie Ota, and Loni Kringle. The material in Chapter V will be published with co-authors Stephanie Ota, Nicholas Valley, and Suzzanah Wood. The material in Chapters VI and VII will be published with co-authors Nicholas Valley, Katy Plath, and Suzzanah Wood.

CHAPTER II

THEORY AND BACKGROUND OF VIBRATIONAL SUM FREQUENCY

SPECTROSCOPY AND SURFACE TENSION

<u>Introduction</u>

This chapter provides a brief, review of the necessary background theory for understanding non-linear optical effects as required for VSFS. Beginning with the interaction of light with matter, the non-linear optical effects which give rise to sum frequency generation are developed. The non-linear susceptibility is described and developed for a symmetry appropriate interface. A description of the relevant properties for the susceptibility is presented; the relation to molecular properties is also discussed in detail. Finally, the role of individual molecular vibrations are presented to elucidate the effect of bond strength, orientation, and number density at an interface. In addition, a brief overview of surface tension measurement and theory are reviewed.

<u>The Interaction of Light with Matter: Nonlinear Effects</u>

The optical effects that we see around us on a daily basis, such as reflection, transmission, and refraction, are dominated by linear optics. In these scenarios, there is an induced dipole that results from the incident electric field in the medium (molecules or atoms). This can be written as

$$\boldsymbol{\mu} = \boldsymbol{\mu}_0 + \alpha \boldsymbol{E} \tag{2.1}$$

Where $\boldsymbol{\mu}_0$ is the static (or permananet) dipole, α is the polarizability of the medium, and $\boldsymbol{E}$ is the incident electric field. The electron distribution in the molecule responds

harmonically to the incident electric field and thus, the induced dipole is proportional to the strength of the electric field. In a condensed phase, the individual molecular electric dipoles are summed together to give a dipole moment per unit volume, the bulk polarization $\boldsymbol{P}$. Equation 2.1 is rewritten as

$$\boldsymbol{P} = \boldsymbol{P_0} + \varepsilon_o \chi^{(1)} \boldsymbol{E} \tag{2.2}$$

Where $\boldsymbol{P_0}$ is the static polarization, $\chi^{(1)}$ is the macroscopic average of α (and is referred to as the linear susceptibility) and ε_o is the vacuum permittivity. Since most materials do not possess a static polarization, $\boldsymbol{P_0}$ can be dropped from the equation and only the oscillation from the incident electric field is considered.

When the strength of the electric field is increased (such as that from a laser source), these stronger fields can be comparable to those experienced by the electrons in a molecule. Therefore, electrons no longer respond harmonically and higher order terms are necessary to describe the molecular response.

$$\boldsymbol{P} = \boldsymbol{P_1} + \boldsymbol{P_2} + \boldsymbol{P_3} + \cdots$$

$$= \varepsilon_0(\chi^{(1)} \boldsymbol{E} + \chi^{(2)} : \boldsymbol{EE} + \chi^{(3)} \vdots \boldsymbol{EEE} + \cdots) \tag{2.3}$$

This equation describes the higher order, nonlinear terms where $\chi^{(2)}$ and $\chi^{(3)}$ are referred to as the second- and third-order nonlinear susceptibilities, respectively. $\chi^{(2)}$ is a third rank tensor and optical processes that result from it are referred to as second-order non-linear effects.

Up to this point, the electric field has been only described by its strength. The electric field as a frequency dependent entity can be written as

$$\boldsymbol{E} = E_1 \cos \omega t \tag{2.4}$$

Where ω is the frequency of the incident light and E_1 is the amplitude. The induced polarization from 2.3 can thus be expressed as

$$P = \varepsilon_0\left(\chi^{(1)}(E_1\cos\omega t) + \chi^{(2)}(E_1\cos\omega t)^2 + \chi^{(3)}(E_1\cos\omega t)^3 + \cdots\right) \quad (2.5)$$

Which can also be written as

$$P = \varepsilon_0(\chi^{(1)}E_1\cos\omega t + \frac{\chi^{(2)}}{2}E_1^2(1 + \cos 2\omega t) + \frac{\chi^{(3)}}{4}E_1^3(3\cos\omega t + \cos 3\omega t) +$$

$$+ \cdots) \quad\quad\quad (2.6)$$

So a direct consequence of the inclusion of higher order terms from the intense electric field is that the induced polarization (and hence the emitted light) can oscillate at frequencies different than the incident frequency. In this case, the frequencies emitted are the doubled and tripled frequency of the original incident frequency.

A description of the signal from a sum frequency experiment can be shown through a similar treatment. In this case, the surface electric field is expressed as the sum of two different oscillating fields incident upon the material. The electric field of two laser beams with frequencies ω_1 and ω_2 are thus expressed as

$$E = E_1\cos\omega_1 t + E_2\cos\omega_2 t \quad\quad\quad (2.7)$$

By considering only the second order term of the polarization and using the above definition for the electric fields, the nonlinear polarization is written as

$$P^{(2)} = \varepsilon_0\chi^{(2)}(E_1\cos\omega_1 t + E_2\cos\omega_2 t)^2 \quad\quad\quad (2.8)$$

After performing trigonometric substitution the equation results in terms that include a frequency independent term ($E_1^2 + E_2^2$), second harmonic at each incident frequency ($E_1^2\cos 2\omega_1 t + E_2^2\cos 2\omega_2 t$), a difference frequency term ($E_1 E_2\cos(\omega_1 - \omega_2)t$) as well as a sum frequency term ($E_1 E_2\cos(\omega_1 + \omega_2)t$). The difference frequency conversion is an important aspect of the creation of femtosecond infrared pulses used in the VSFS

studies conducted in this work and will be discussed in the following chapter. Without including the time dependence of the electric field, the most basic description of sum frequency generation is now written as

$$P^{(2)} = \varepsilon_0 \chi^{(2)} E_1 E_2 \qquad (2.9)$$

Where $\chi^{(2)}$ is the second-order nonlinear susceptibility and is a third rank tensor that describes the interaction of the two incident electric fields E_1 and E_2 with a resulting vector $P^{(2)}$. This simple approach is not meant to be exhaustive and further, rigorous derivation is available.[1,2]

Second-order Susceptibility and Sum Frequency Generation

The properties of the second-order susceptibility give rise to the unique surface sensitivity of VSFS. As mentioned previously, $\chi^{(2)}$ is a third rank tensor, which is comprised of 27 elements, $\chi^{(2)}_{ijk}$. In centrosymmetric media (media possessing inversion symmetry), all directions are equivalent. Inversion symmetry requires that any and all elements must be equal to its inversion,

$$\chi^{(2)}_{ijk} = \chi^{(2)}_{-i-j-k} = -\chi^{(2)}_{ijk} \qquad (2.10)$$
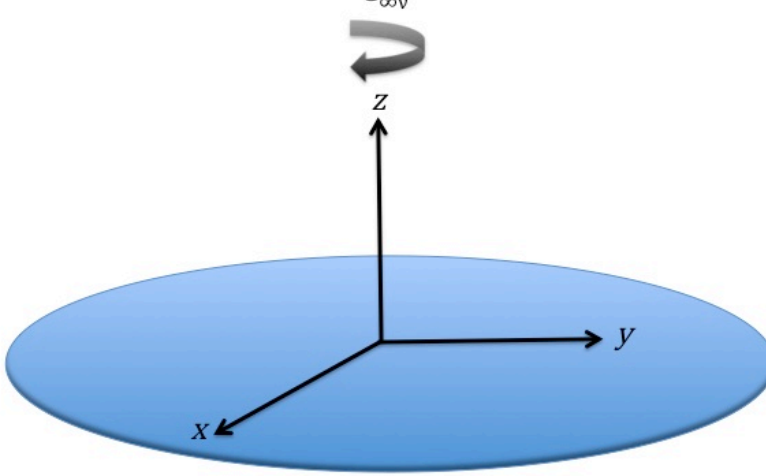
The only way to satisfy these requirements is $\chi^{(2)}_{ijk} = 0$. Most bulk media phases are centrosymmetric, (aqueous solutions being a pertinent example). However, at the boundaries of two materials, this centrosymmetry is broken. This property is what gives VSFS its exceptional surface sensitivity. The "interfacial region" that is probed through a VSFS experiment is the very thin region where the anisotropy between two bulk phases exists.

The 27 elements contained in $\chi_{ijk}^{(2)}$ can be simplified by applying symmetry constraints to the surface of investigation. Most surfaces can be described by $C_{\infty v}$ symmetry (x and y directions are indistinguishable); this is illustrated in Figure 2.1. The surface plane is designated as the xy plane with z normal to the surface. This symmetry constraint reduces the 27 tensor elements to seven elements, of which four are unique (see Figure 2.1). These elements can be selectively probed via careful control of the incident and resultant beams in a VSFS experiment.

$$\begin{bmatrix} \chi_{xxx} & \chi_{xxy} & \chi_{xxz} & \chi_{xyx} & \chi_{xyy} & \chi_{xyz} & \chi_{xzx} & \chi_{xzy} & \chi_{xzz} \\ \chi_{yxx} & \chi_{yxy} & \chi_{yxz} & \chi_{yyx} & \chi_{yyy} & \chi_{yyz} & \chi_{yzx} & \chi_{yzy} & \chi_{yzz} \\ \chi_{zxx} & \chi_{zxy} & \chi_{zxz} & \chi_{zyx} & \chi_{zyy} & \chi_{zyz} & \chi_{zzx} & \chi_{zzy} & \chi_{zzz} \end{bmatrix}$$

$$\chi_{zzz}^{(2)} ; \chi_{zxx}^{(2)} = \chi_{zyy}^{(2)} ; \chi_{xzx}^{(2)} = \chi_{yzy}^{(2)} ; \chi_{xxz}^{(2)} = \chi_{yyz}^{(2)}$$

Figure 2.1. Full $\chi^{(2)}$ tensor, schematic of $C_{\infty v}$ surface, and unique $\chi^{(2)}$ elements from assuming a $C_{\infty v}$ surface.

All incoming and outgoing beams are described in reference to the plane of incidence (Figure 2.2). By selectively resolving the polarization of these beams as either S (perpendicular to the plane of incidence) or P (parallel to plane of incidence), the

unique elements of $\chi^{(2)}$ can be measured. The convention used to describe the polarizations goes in order from highest energy to lowest energy (Sum frequency, visible, infrared). Therefore, a VSFS experiment performed in SSP has the sum frequency beam polarized perpendicular to the plane, the visible beam polarized perpendicular to the plane, and the infrared beam polarized parallel to the plane. This SSP combination will selectively probe the $\chi^{(2)}_{xxz}$ component as demonstrated in Figure 2.2. When there is an IR transition dipole with a component in the plane of the surface, it is interrogated via S polarization in the infrared, or SPS, whereas transition dipoles with a component normal to the surface are interrogated via P polarization in the infrared, or SSP.

$$I_{SSP} \propto \left| \chi^{(2)}_{NR,xxz} + \sum_\nu \chi^{(2)}_{R_\nu,xxz} \right|^2$$
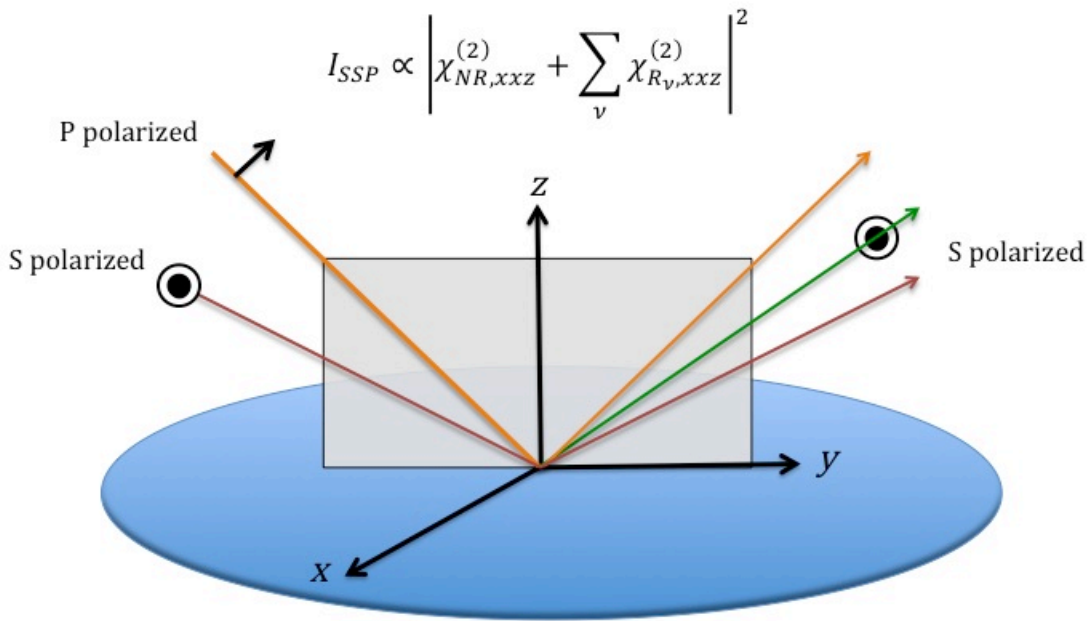
Figure 2.2. Polarization of incident beams used in polarized VSFS studies. The gray rectangle represents the plane of incidence.

11

Now that the second order susceptibility has been described, the VSFS process can be described further. In a typical VSFS experiment, two pulsed laser beams are overlapped in space and time upon the surface or interface of interest. One of these beams is fixed in frequency, off resonance, and is located in the visible region. The other beam is tunable in frequency and is located in the infrared region and resonant with vibrational modes of molecules of interest. When these two beams are overlapped, the induced polarization radiates at the sum of the two frequencies, $\omega_{SF} = \omega_{Vis} + \omega_{IR}$. All experiments performed in this work are done in the co-propagating reflecting geometry (Figure 2.3). The intensity of the generated sum frequency signal (I_{SFG}) is proportional to the square of the induced polarization,

$$I_{SFG} \propto \left| \vec{P}^{(2)} \right|^2 \propto \left| \chi_{eff}^{(2)} \right|^2 I_{vis} I_{IR} \tag{2.11}$$

which is itself proportional to the square of $\chi_{eff}^{(2)}$ times the intensities of the visible and infrared pulses. $\chi_{eff}^{(2)}$ is related to $\chi^{(2)}$ via Fresnel coefficients and unit polarization vectors for each beam,

$$\chi_{eff}^{(2)} = [\hat{e}(\omega) L(\omega)] \cdot \chi^{(2)} : [L(\omega_{Vis}) \cdot \hat{e}(\omega_{Vis})][L(\omega_{IR}) \cdot \hat{e}(\omega_{IR})] \tag{2.12}$$

Where $\hat{e}(\omega)$ are the unit polarization vectors which reflect (no pun intended) how the geometry of the experimental set up impacts the projection of the electric fields in the lab coordinates and $L(\omega)$ are the Fresnel coefficients which account for the amount of the electric field that is reflected or transmitted. The Fresnel coefficients depend upon the incident angle as well as the index of refraction.[3] By knowing the index of refraction and the incident angles, the Fresnels can be removed from $\chi_{eff}^{(2)}$ to yield $\chi^{(2)}$. It has been

shown that for the region[4] between 1600-1900 cm^{-1} as well as the region[5] between 2700-4000 cm^{-1}, the Fresnel corrections do not affect the frequency or linewidths of vibrational modes but only the relative intensity. Therefore, $\chi_{eff}^{(2)}$ is used throughout this work with no loss of information.

$$I_{SFG} \propto \left|\vec{P}^{(2)}\right|^2 \propto \left|\chi_{eff}^{(2)}\right|^2 I_{vis}I_{IR}$$
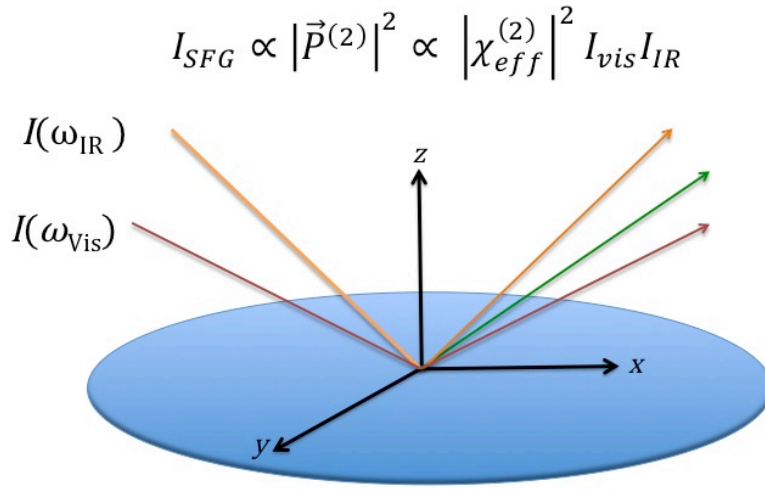
Figure 2.3. Example of beam geometry in co-propagating reflection geometry.

$\chi^{(2)}$ can be written out as the sum of all resonant terms summed with a nonresonant term,

$$I_{sfg} \propto \left|\chi_{NR}^{(2)} + \Sigma_v \chi_{R,v}^{(2)}\right|^2 I_{Vis}I_{IR} \tag{2.13}$$

$$I_{sfg} \propto \left|A_{NR}e^{i\varphi_{NR}} + \Sigma_v A_{R,v}e^{i\phi_v}\right|^2 I_{Vis}I_{IR} \tag{2.14}$$

13

Each $\chi^{(2)}$ term has an amplitude and phase associated with it. When both ω_{Vis} and ω_{sfg} are off resonance (far away from any electronic absorptions), the non-resonant component can be modeled as real and constant. The resonant components describe when the incoming IR photons are in resonance with a vibrational mode of the medium. The IR beam is tuned to various frequency ranges (e.g. 1600-1900 cm^{-1} for the C=O mode) to probe the vibrational modes of interest in the medium. In this manner, a surface vibrational spectrum of oriented, surface molecules can be generated. Due to the coherent nature of this technique and the phase relationships for each component, there can be interferences that requires the deconvolution of the spectrum. This is achieved through spectral fitting and will be addressed in the next chapter.

Connecting Macroscopic Susceptibility to Molecular Hyperpolarizability

Up to this point, the susceptibility has been defined macroscopically and it is necessary to connect this macroscopic susceptibility to the molecular frame. The macroscopic susceptibility, $\chi_R^{(2)}$, can be written as the orientational average of the individual molecular hyperpolarizabilities , β_ν,

$$\chi_R^{(2)} = \frac{N}{\varepsilon_0}\langle\beta_\nu\rangle \tag{2.15}$$

Where N is the number of molecules, or modes, contributing to the sum frequency response and β_ν is a third rank tensor (analogous to $\chi^{(2)}$) that is based in the molecular axis frame.

While perturbation theory[1] has been used to formulate a general expression for β_ν, it can be reduced greatly by assuming that only the infrared pulses are resonant (i.e.

14

ω_{sfg} and ω_{Vis} are from resonance) and only the electric dipoles are considered (neglect of quadrupoles and other higher order effects). The simplified form of β_ν is thus written as

$$\beta_{lmn,\nu} = \frac{\langle g|\alpha_{lm}|\nu\rangle\langle\nu|\mu_n|g\rangle}{2\hbar(\omega_\nu-\omega_{IR}-i\Gamma_\nu)}$$ (2.16)

Where the subscripts l, m, and n are in reference to the molecular frame (not the laboratory frame). $|g\rangle$ and $|\nu\rangle$ represent ground and excited vibrational states, respectively, while α_{lm} is the Raman transition probabitily and μ_n is the IR transition dipole. Thus, the numerator represents the strength (or amplitude) of the transition and the absolute square of the numerator can be thought of as an effective transition probability. This leads to a specific condition for which a local mode is sum frequency active; the mode must have nonzero Raman and IR transition probability. The denominator shows that as the IR frequency is tuned through a vibrational transition, there will be a resonant enhancement. The Γ_ν term represents the damping constant for the transition.

Now that the molecular picture has been established, the final piece is to connect the molecular frame back to the lab frame. This is achieved by performing an Euler transformation from β_ν to $\chi^{(2)}$. By using a rotation matrix ($\boldsymbol{\mu}_{IJK:lmn}$), each element of β_ν will be transformed to the lab frame,

$$\chi_{IJK,\nu} = \sum_{lmn} \boldsymbol{\mu}_{IJK:lmn} \cdot \beta_{lmn,\nu}$$ (2.17)

Where the lab frame coordinates xyz are represented by the indices IJK and the molecular coordinates abc by the indices lmn. With the transformation complete, an expression for the resonant macroscopic susceptibility based on the individual molecular responses is achieved,

$$\chi_{R,\nu}^{(2)} = \frac{N}{\varepsilon_0} \frac{M_{IJ}A_K}{(\hbar\omega_\nu-\hbar\omega_{IR}-i\Gamma_\nu)}$$ (2.18)

15

Where M_{IJ} is the Raman transition probability and A_K is the IR transition dipole moment. It is now evident that since the intensity of the sum frequency signal is proportional to the square of the second order susceptibility, the signal intensity will be a function of transition strength, number density, and orientation. These aspects of the sum frequency signal will be used throughout this work to explore and elucidate the air/water interface described herein.

Surface Tension

It is many times necessary to differentiate between the effects of number density and molecular orientation in VSFS experiments. The preceding section developed the microscopic response for VSFS ending with an expression relating the intensity of the VSFS signal as a function of the number density and orientation. Surface tension measurements provide a macroscopic measurement of an interface and relate the concentration differences that may exist between an interface and the bulk. By performing surface tension measurements, the number density value can be obtained and compared against VSFS results. This involves relating the square root of the VSFS signal (the concentration dependence of the sum frequency field is the square root of the intensity)[6] versus the excess surface concentration (number density) for bulk concentration changes. If field intensity changes are varies linearly with the number density obtained from surface tension measurements, this would indicate that the adsorption does not change orientation as a function of concentration. A non-linear plot would indicate that there are concentration dependent changes to the surface orientation.

16

Measuring the surface tension of aqueous solutions was done using the Wilhelmy plate method,[7] which involves a thin platinum (Pt) plate attached to a sensitive force balance (Figure 2.4). In essence, the plate (assuming completer wettability or zero contact angle) will support a meniscus whose weight can be accurately described by an "ideal" equation,

$$W_{tot} = W_{plate} + \gamma p \qquad (2.19)$$

where W_{tot} is the total weight measured of the plate just immersed in the solution of interest, W_{plate} is the weight of the plate, γ is the surface tension, and p is the perimeter

$$\gamma = \frac{F}{p \cdot \cos \theta}$$
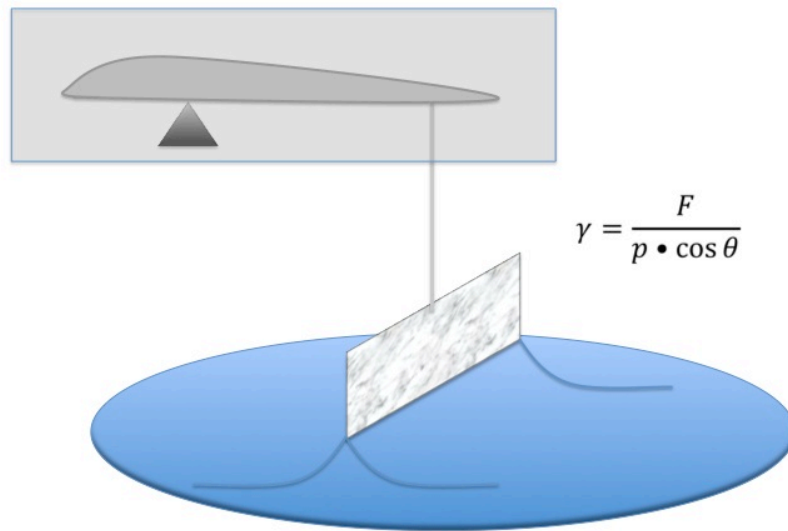
Figure 2.4. Wilhelmy plate submerged in aqueous solution and the force measured by a force balance.

of the bottom of the plate (2l+2w). This can be recast as

$$\gamma \cos \theta = \frac{F}{p} \qquad (2.20)$$

where the explicit contact angle is included ($\cos\theta$), and F is the force measured on the plate (achieved through taring of the weight of the balance before the plate is in contact with the solution). Once the surface tension value is measured, it can be converted to surface pressure via

$$\gamma_0 - \gamma = \pi \tag{2.21}$$

where γ_0 is the surface tension of pure water and π is surface pressure.

Surface pressure isotherms are recorded for various solutions. The maximum surface excess is obtained through a fit to the Gibbs adsorption equation,

$$\Gamma_i = \frac{1}{nRT}\left(\frac{\partial\pi}{\partial\ln(a_i)}\right)_T \tag{2.22}$$

where Γ_i is the surface excess concentration at maximum surface coverage, π is the surface pressure, and a_i is the activity of the solution. It should be noted that the surface excess concentration can be positive or negative and at low concentrations, the activity can be replaced with the bulk concentration. The surface area per molecule can be calculated via

$$a_1^s = {10^{23}}/{N\Gamma_i} \tag{2.23}$$

where a_1^s is the area per molecule (Å^2/molecule) and N is Avogadro's number.[8]

Once the maximum surface excess, Γ_i, is obtained the surface excess for a given bulk concentration can be calculated via the Frumkin isotherm,

$$\pi_2 = -RT\Gamma_i\ln\left[1 - \frac{\Gamma_2}{\Gamma_i}\right] \tag{2.24}$$

where π_2 is the surface pressure at a given bulk concentration and Γ_2 is the surface excess for that bulk concentration. The values for the surface excess can then be plotted against the VSFS intensities as described above. For a thorough thermodynamic treatment on the

Gibbs equation, the Frumkin equation, and other aspects on the theory of surface tension, an interested reader is recommended to peruse the literature.[9,10]

CHAPTER III

EXPERIMENTAL CONSIDERATIONS

This chapter provides a detailed examination of the broadband sum frequency spectrometer used for probing the C=O infrared region. This includes a brief description of the equipment used to create the initial femtosecond pulses and their amplification. The aspects of the creation of picosecond visible pulses and femtosecond infrared pulses are described. The detection set up as well as general and specific sum frequency considerations are also briefly discussed. Spectral analysis and fitting schemes are introduced and explained in detail. Finally, the surface tension apparatus and sample preparation aspects are detailed.

Previous Laser System

The laser system used for these experiments is based on a previous design[1] that was itself an alternative design to that first developed by Richter et al.[2] The previous system consisted of a home-built Ti:Sapphire oscillator pumped by 4W of 532 nm light from a diode-pumped cw Nd:YVO4 laser (Millenia V, Spectra Physics). The seed pulses from the oscillator were then amplified by a regenerative amplifier (Spitfire, Spectra Physics). The seed pulse was stretched, amplified by ~8.5W of 527nm light from a Nd:YLF laser (Evolution, Spectra Physics), and then compressed to produce ~1 W (at 1 kHz repetition rate) of light at 800nm with <130 fs pulse duration. The amplified pulse was then split with 85% going to the OPA for mid-infrared photon generation and the

remaining 15% was used for the production of picosecond pulses. These components were all upgraded in 2008.

Current Laser System

A general schematic of the laser is outlined in Figure 3.1. The laser system used for these experiments consists of a Ti:Sapphire oscillator (Tsunami, Spectra Physics) pumped by ~4.7 W of 532 nm light from a diode-pumped cw Nd:YVO4 laser. The mode-locked oscillator produces light pulses with a duration of ~100 fs centered at 800 nm with power between 750-800 mW with a repetition rate of nominally 80 MHz. These pulses are then amplified in a regenerative amplifier (Spitfire Pro XP, Spectra Physics). Although a Ti:Sapphire crystal is very robust, especially when compared to other optics-based crystals, it cannot handle the intense peak powers from direct amplification. Therefore, the technique of chirped pulse amplification is used to safely, and stably, amplify the pulses. Chirped pulse amplification, or CPA, stretches the pulse out temporally before amplification and then compresses the pulse nearly back to its original duration after amplification. The stretching of the pulse is achieved through the use of dispersive optics; in this case a diffraction grating is employed. The seed pulse is dispersed off of a grating, which results in the higher frequency, or bluer, components of the pulse traveling further than the lower, or redder, frequencies. This is referred to as positive group velocity dispersion (GVD). The seed pulse is thus "stretched" through the stretcher allowing safe amplification in the amplification stage.
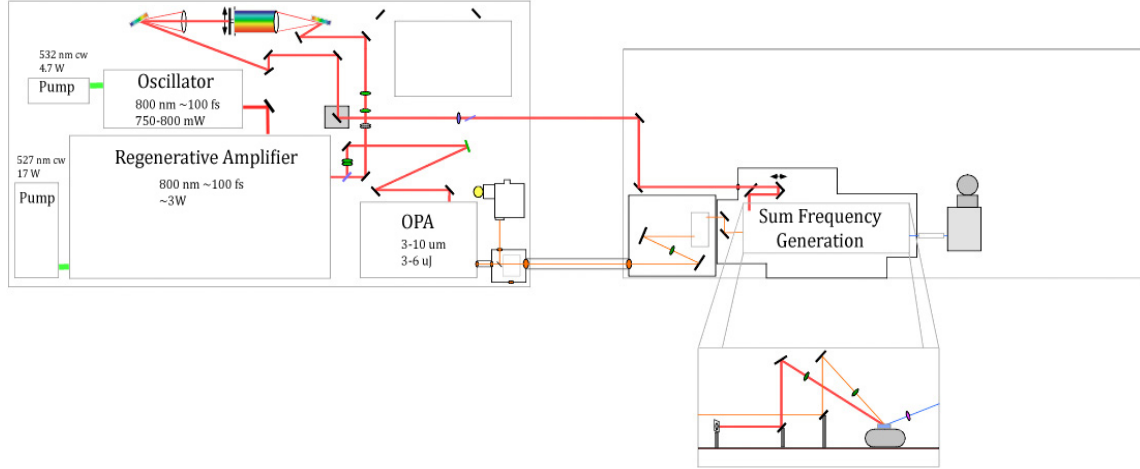
Figure 3.1. Schematic of BBSFG experimental design and layout.

The amplification of the stretched seed pulse is achieved by injecting the pulse into a multi-pass amplifier cavity. This cavity is pumped by >17W from a diode-pumped cw Nd:YLF (Empower, Spectra Physics). The cavity is designed to select, and then optically confine, an individual pulse from the train of mode-locked pulses (i.e. seed pulses) that have passed through the stretcher. This confinement is controlled by the use of polarization selective optics and two Pockels cells. The Pockels cells are birefringent crystals, which can be electrically excited. These electro-optics are passive (allowing unaltered transmission) when there is no applied voltage but act as a 1/4 waveplate (which rotates the polarization 45° upon each pass through) when a properly applied voltage is used. By using the appropriately polarized pulses, pulses can be selected for injection, retention, and ejection. Once the seed pulse is injected through an active Pockels cell, it remains in the cavity until it is ejected through the same mechanism as injection (i.e. polarization change). The timing of these events is controlled through the Timing and Delay Generator (TDG). After the pulse has passed through the gain media (in this case a Ti:Sapphire cavity) enough times to amplify the pulse but before the gain is

22

saturated, the pulse is ejected out of the cavity and then sent to the compressor.

The compressor is essentially the reverse of the stretching process process where the redder pulse components travel further than the bluer pulse components when dispersed (negative GVD). The amplified pulses are "compressed" via a four-stage pass process off of a diffraction grating. This results in amplified pulses of ~100 fs centered at 800 nm with an average power of ~3 W and a 1kHz repetition rate. This output is then used for both the generation of mid-infrared femtosecond pulses as well as picosecond visible pulses.

Mid-infrared Generation

Mid-infrared generation is possible through the use of an optical parametric amplifier (OPA) and is shown schematically in Figure 3.2. An OPA derives gain from a non-linear frequency conversion process (as described in the Chapter II). The parametric processes that occur in an OPA are achieved between the interaction of the oscillating electromagnetic field of the laser pulses and the bonded electrons in the non-linear gain media. For optical parametric amplification, a high intensity pump pulse is used to amplify a seed pulse (usually low intensity). Every pump photon is separated into two lower energy photons and is, by convention, referred to as signal for the higher energy pulse and idler for lower intensity pulse. Due to energy conservation, the sum of the frequencies of the signal (ω_s) and idler (ω_i) are equal to the pump frequency (ω_p). Tuning the angle of the non-linear gain medium with respect to the incident beams results in changes of the refractive indices and subsequently the frequencies of the signal and idler.

Figure 3.2. OPA Schematic. Red indicates 800 nm pulses, dark blue indicates white light continuum pulses, green and light blue are signal and idler (respectively) from first BBO pass, yellow is amplified idler and signal (from second pass).

The generation of femtosecond mid-infrared pulses requires a four-stage process in the OPA (OPA-800C, Spectra Physics). About 1W of the 3W is split from the output of the amplifier. These pulses (800 nm) are down collimated slightly and steered into the OPA (see Figure 3.1) where it is split into a white light generation (seed) stage and an amplification stage (pump). In the first stage (white light generation), roughly 5% of the beam is split and focused into a sapphire plate to produce a white light continuum. The remaining 95% are used for the two optical parametric amplification stages: "pre-amplification" and "power amplification".

In the pre-amplification stage, the white light seed is overlapped with ~15% of the pump, both temporally and spatially, in a type II BBO (Beta-Barium Borate) crystal.

This produces ~5-20 µJ of signal and idler photons. The pre-amplified signal and idler pulses are passed through a dichroic mirror, which allows only the amplified idler pulses retro reflected to the BBO. This amplified idler pulse is now the seed that will be used for the power amplification stage. In this stage, the amplified idler and remaining pump (~85%) are once again overlapped in space and time in the BBO to produce ~200-240 µJ of signal and idler. The signal is tunable between 1.1 to 1.6 µm and the idler between 1.6 to 3 µm through angle tuning of the BBO crystal.

In the final stage of mid-infrared generation, the signal and idler produced from the power amplification stage are overlapped, spatially and temporally, in a silver gallium sulfide ($AgGaS_2$) crystal; this is referred to as the DFG crystal since the optimized optical process is difference frequency generation. The signal and idler pulses are difference frequency mixed to produce the mid-infrared pulses used in the sum-frequency experiments. The DFG crystal is also angle-tuned to produce the best possible spatial, spectral, and energy output of the mixed signal. The mid-infrared pulses that are generated propagate along with other frequencies of light from residual signal and idler, residual pump, and other non-linear processes. To separate the mid-infrared pulses a Germanium filter is used. The pulses are then sent to a 150 mm focal length monochrometer (Acton SP-150) where the pulse is dispersed (150grooves/mm, 4 µm blaze) and detected with a liquid nitrogen cooled MCT detector. The signal from the detector is sent to a boxcar integrator (Stanford Research Systems) where it is gated and collected by a National Instruments DAQ board and transformed into a spectrum with the use of a home-built LabVIEW graphing program.

In the experiments presented in this work, most of the mid-infrared generation is

between 5.4 and 6 μm. Unfortunately, there are numerous absorptions for water vapor in this region. These absorptions serve to both reduce the overall intensity of the pulses as well as distort them. It is therefore necessary to purge the water from the beam path of the mid-infrared pulse. This is achieved through a system of boxes (home-built polyacrylic boxes) and lens tubes (Thor Labs) which are purged with a dry-air generator (PneuDri MIDAS, Parker). The dry-air generator takes in house dry air (~85 psi) and further dries to 0% RH. The pressure from the generator is set at 25 psi. If the boxes/tubes were airtight, this amount of pressure would cause the polyacrylic to crack so the boxes are designed to be "leaky". This allows water vapor in the boxes/tubes to be replaced by dry air as the generator is used. In the experiments conducted in this work in the C=O region, the relative humidity was measured at different places in the purge system and around 0% RH. The use of this purge system results in greatly suppressed absorption from water in the mid-infrared region.

<div align="center">Picosecond Visible Generation</div>

While it is possible to use the output pulses from the amplifier for the sum-frequency experiments, they are very broad in frequency since they are very short pulses. To improve the resolution of the experiment, the femtosecond pulses are sent through a beam shaper, referred to as a slicer. The pulses from the amplifier are first steered into a 3:1 telescope to reduce the beam size. The slicer consists of a grating-lens-slit-lens-grating combination; all of these optical elements are set one focal length from each other and is shown schematically in Figure 3.3. The beam is steered onto a grating (1800 grooves/mm, 500 nm blaze). Once dispersed off of the grating, the stripe passes through

a 200 mm focal length lens placed as close to one focal length from the grating as possible so that stripe is now collimated. The lenses are placed on a single axis translation stage while the mechanical slit is placed on a double axis translation stage. These translation stages allow for the focal lengths to be adjusted. The collimated stripe is then sent through a mechanical adjustable slit that passes a small portion of the stripe. The extra axis on the mechanical slit stage allows for centering the slit such that the sliced beam is centered at 800 nm. Once the stripe has passed through the slit, it is
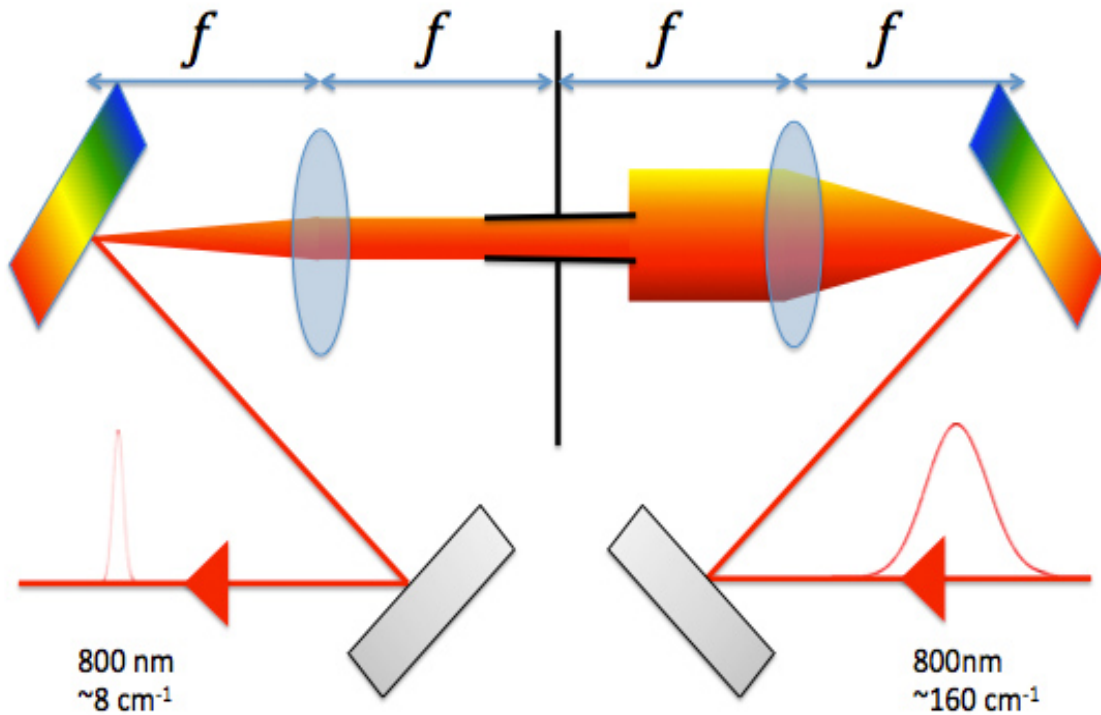
Figure 3.3. Slicer schematic. Incoming pulses are dispersed, collimated, sliced, focused, and recombined to provide shorter temporal profile resulting in better spectral resolution.

focused by another 200 mm focal length lens onto the final grating. When the focused output from the slit is dispersed off of the grating, the individual frequencies are combined into a roughly Gaussian beam. Great care is taken to make sure that the beam

is well aligned through the entire slicer apparatus. The bandwidth and energy of the resulting pulse is dependent upon the mechanical slit. By opening the slit up, more energy but larger bandwidths are available whereas closing the slit results in lower energy but smaller bandwidth. For these experiments, the slit was opened such that the resulting energy was ~40 μJ with a bandwidth ~8 cm^{-1}.

Sum Frequency Generation

Once the beam has been sliced, the picosecond pulse is steered through a half wave plate to allow for the selection of s or p polarizations for the sum frequency experiments. Since it is necessary to achieve temporal as well as spatial overlap for experiments, a retro-reflector is employed along the visible beam path. By translating the retro-reflector stage, the visible pulse train can be temporally overlapped with the femtosecond mid-infrared pulses since the path lengths of the beams are equal. The visible pulse is steered to the interface and is focused by a 250 mm focal length BK7 lens to the interface. Since the energy from these visible pulses is high enough, the focus of the beam is actually slightly beyond the interface; this prevents local heating/damage at the interface. The angle of the visible beam is 60° from normal to the interface.

The mid-infrared pulse is steered through a lens (500mm f) to slowly focus the beam as it approaches the interface. The alignment of the mid-infrared pulses is not trivial since the pulses cannot be seen by conventional methods. Therefore, heat paper attached to a lens mount with left/right and up/down axes marked by fishing line is used as an iris for alignment. After passing through the lens, the mid-infrared pulse is steered through a periscope design that can either retain the polarization (normal periscope) or

flip the polarization (90° offset periscope). The different periscopes are built on different kinematic bases, which are magnetically attached to a base; switching polarizations simply requires switching bases for the appropriate periscope. Once through the polarization periscope, the beam is steered to the interface and focused directly onto the interface with a BaF$_2$ 150 mm focal length lens. The angle of the mid-infrared beam is 45° from normal to the interface.

The choice of incoming angles is not trivial for sum frequency generation. The beam angles for both mid-infrared and visible are chosen such that they maximize the intensity for the resulting SF pulse; this is based on the Fresnel coefficients for the SF, visible, and mid-infrared pulses. For the experiments presented here, the angles of the mid-infrared and visible are chosen to maximize the response in the SPS polarization scheme. Due to fewer orienting forces at an air/water interface, the response from the SPS polarization is generally less than the SSP polarization scheme. Therefore, this set-up allows for maximal SPS response while still retaining good response (nearly maximal) in SSP. In addition to maximizing the polarization response, another important consideration is the spatial separation of the SF pulse and reflected visible pulse. The produced SF pulses must obey phase-matching conditions, $\mathbf{k}_{sfg} = \mathbf{k}_{vis} + \mathbf{k}_{IR}$. Since the wave vector $\mathbf{k}$ is $\mathbf{k}_i=(n_i[\omega_i])\omega_i/c$ (where n is the frequency dependent index of refraction, ω is the frequency, and c is the speed of light), by including the angles of the visible and mid-infrared, the angle of the sum frequency pulse can be calculated,

$$\sin\theta_{sfg} = \frac{\omega_{IR}n_{IR}}{\omega_{sfg}n_{sfg}}\sin\theta_{IR} + \frac{\omega_{vis}n_{vis}}{\omega_{sfg}n_{sfg}}\sin\theta_{vis} \tag{3.1}$$

With the angles chosen (θ_{IR}=45° and θ_{vis}=60°), the SF pulse is separated from the visible pulse by a few degrees and can be seen in Figure 3.4. This ensures that any residual

29

visible pulses are separated from the sum frequency pulses for subsequent collection.
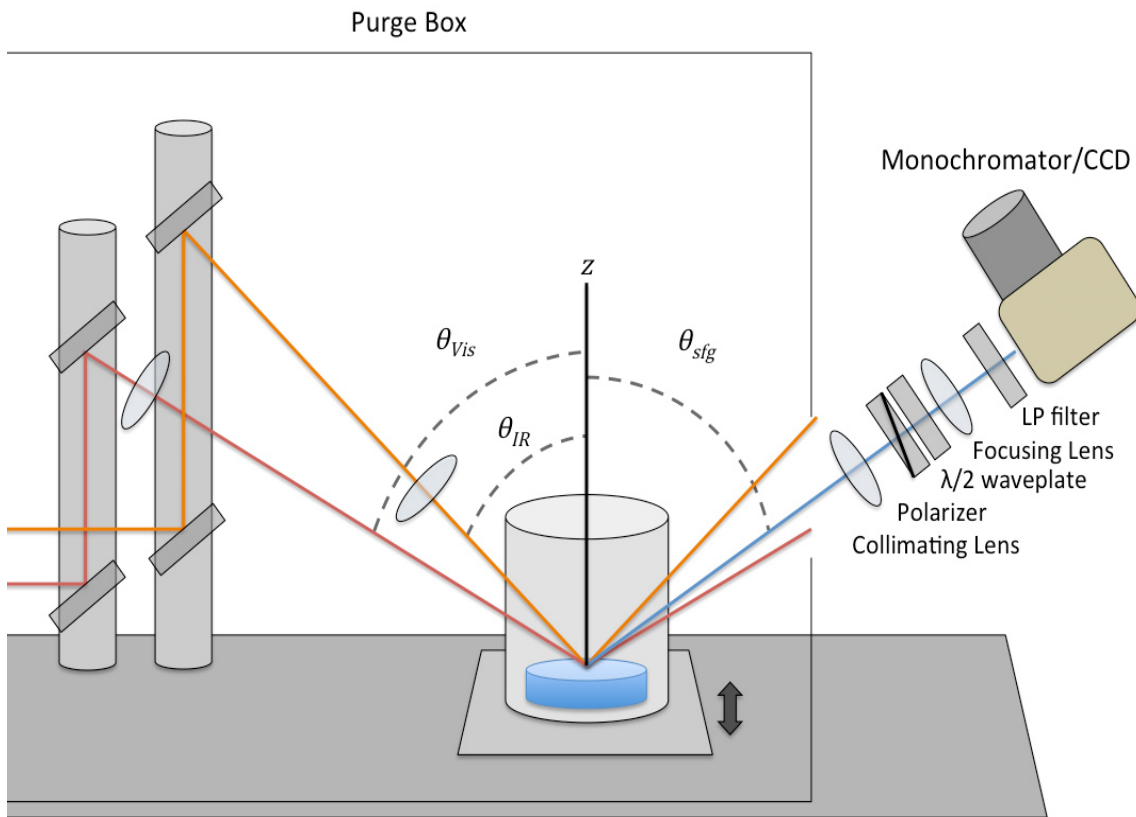
Figure 3.4. Schematic of sample cell and detection optics for BBSFG experiment.

Once the beams are overlapped at the interface, the resulting sum frequency pulse is sent through a collimating lens, a Glan-Thompson polarizer, an achromatic half waveplate, and a Raman edge filter (SEMROCK, RazorEdge). The sum frequency pulse passes through a focusing lens, which places the focus at the slit of the spectrometer (SpectraPro 150, Acton Research). The spectrometer collects the pulse and disperses it onto a liquid nitrogen cooled CCD camera (VersArray512B, Princeton Instruments). This set-up is shown in Figure 3.4. The collimating lens is set about a focal length away

from the interface. The GT polarizer and half waveplate combination are used to pick the polarization of the SF pulse as well as to rotate the pulse so that the optimum transmission through the spectrometer can be achieved (the spectrometer has a ~90% efficiency for p-polarized light vs ~40% for s-polarized light). The edge filter cuts off >99% of light at 800nm and is used to cut down on the scattered visible light from the interface. The final lens is set so the focus is at the slit entrance to the spectrometer so that instead of using the slit for the diffraction required for the spectrometer, the beam diverges at the slit interface to provide the spectral dispersion required. This has the added benefits of being able to close down the slits around the focus spot so that stray light entering the spectrometer can be minimized while also maximizing spectral resolution and creating a small spot size on the CCD. For any spectral acquisition, the spectrometer grating is dispersed at the sum-frequency wavelengths (~700nm). Since any visible light that gets through is near ~800 nm, the dispersion also biases the spectral acquisition for SF pulses over visible pulses/scatter. The liquid nitrogen cooled CCD, in addition to the dispersion grating, contribute to the ability of the system to measure weak SF pulses on a high background. During spectral acquisition, all lights are turned off and the sample area is blocked from stray light as much as possible.

Data Transformation

Once the data acquisition is complete, the raw spectra require extensive manipulations to obtain the finalized spectra. During a typical day of experiments, eight spectra from an uncoated amorphous gold surface (three normal spectra, three with a polystyrene standard placed in the IR beam path, and two with the IR blocked from

reaching the interface) are acquired. These spectra are used to both assess the viability of using the instrument on that day as well as for normalization. Sample spectra are usually acquired in 20-minute intervals. Three sample spectra are typically acquired along with one background spectrum (IR blocked from reaching the interface). These three spectra are then averaged together to improve the signal-to-noise ratio. Spectra are then averaged with sample spectra taken from other days to further improve the overall spectral quality.

For the experiments, the shutter on the CCD stays open during the spectral acquisition. This allows cosmic rays to hit the CCD array and be collected along with the SF spectra. These cosmic rays show up as sharply peaked (usually only a pixel or two) and are usually of much greater intensity. The raw spectra are therefore inspected for any cosmic rays before any averaging or normalization. The rays are carefully removed from the spectra by inspecting the intensity of data points on either side of the cosmic ray and averaging those points to replace the cosmic rays. This removal, as well as any other data manipulations, is done in the software program IGOR (Wavemetrics, Inc).

Once all cosmic rays are removed from the spectra, the data for a given sample set are averaged together. Background spectra are taken on samples over the same time period as a data scan. Background spectra consist of the same experimental setup used for a VSFS spectrum except the IR beam is blocked. This prevents any sum frequency generation and provides a background spectrum resulting from constant stray light sources as well as any scattering from the visible that may have not been fully extinguished through the filters. Background spectra are also averaged and subtracted from the averaged sample set. After background subtraction and data averaging, the averaged data set is then divided by the non-resonant response from the uncoated gold

surface. This normalization ensures that data from day to day can be meaningfully compared by eliminating the dependence upon incoming beam angles, degree of overlap, and intensity differences arising from pulse energies for both visible and IR.

The final step for converting raw spectra into VSFS data is the calibration of the frequencies. This is necessary since the sum frequency signal is in the visible spectrum. To calibrate the data, a thin film polystyrene sample is placed in the IR beam path and the non-resonant gold sum frequency signal is recorded, analogous to the gold spectra used for normalization. In addition, the IR beam is sent to a separate monochromator and MCT detector. The spectra are measured with no polystyrene as well as with polystyrene in the beam path. The absorptions from the polystyrene film appear as dips in the spectra for both the IR spectra as well as the non-resonant gold sum frequency spectra. By comparing these polystyrene spectra to the unaltered spectra, the known absorption in the IR (1602 cm^{-1})[3] can be pinned to the sum frequency spectra. Due to water vapor in the IR beam path, there are also adsorptions occurring in both the IR spectra and the non-resonant gold spectra. These dips are then correlated between the IR and non-resonant gold sum frequency (Figure 3.5). A linear regression is used to fit the points from the IR and gold spectra. The raw sum frequency wavelengths are converted from nm to cm^{-1}, multiplied by the slope of the regression, and the y-intercept value is subtracted. This yields calibrated frequencies in the appropriate IR region for the VSFS data for a given day. This procedure is performed daily to ensure accurate calibration of the frequencies.
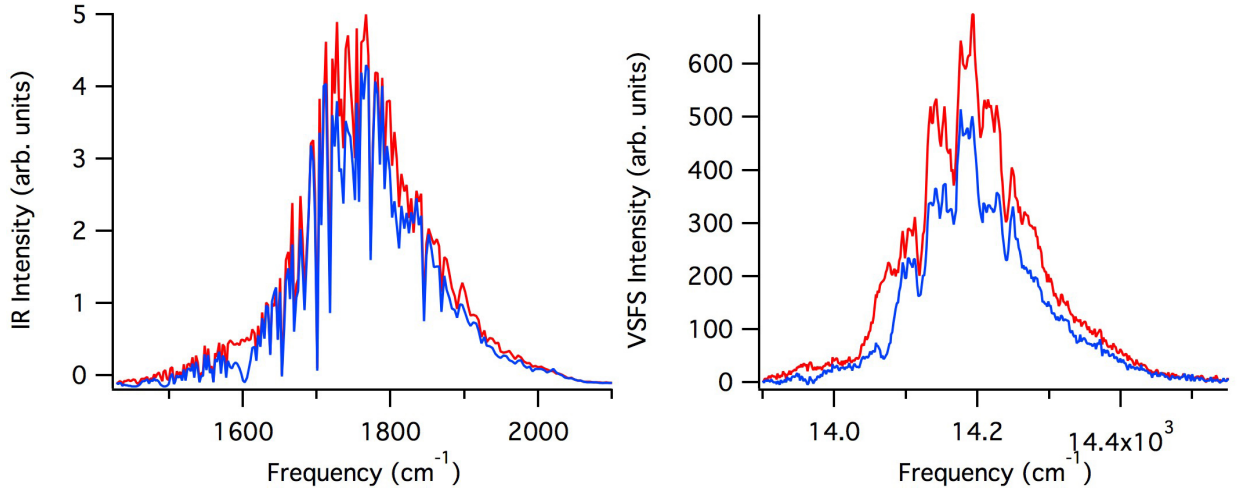
Figure 3.5. IR and VSFS gold spectra used for calibration of wavelengths. Spectra without polystyrene are shown in red and with polystyrene in blue.

Spectral Fitting

The final component to interpreting the VSFS data is spectral fitting. As mentioned in the previous chapter, the intensity of the sum frequency signal is a function of the square of the nonlinear susceptibility. This nonlinear susceptibility is a complex term containing an amplitude and respective phase,

$$I_{sfg} \propto \left| \chi_{NR}^{(2)} + \chi_{1R}^{(2)} + \chi_{2R}^{(2)} + \chi_{3R}^{(2)} + \cdots \right|^2 \tag{3.2}$$

$$I_{sfg} \propto \left| A_{NR} e^{i\varphi_{NR}} + A_{1R} e^{i\phi_1} + A_{2R} e^{i\phi_2} + A_{3R} e^{i\phi_3} + \cdots \right|^2 \tag{3.3}$$

Since the non-resonant and all the resonant terms are summed, and subsequently squared, interferences between the resonant terms (as well as between a given resonant term and the non-resonant term) can occur which complicate the interpretation. These interferences can result in distorted lineshapes that require spectral deconvolution to ensure that the spectral information is interpreted correctly. While the non-resonant response is usually negligible for many VSFS experiments, the BBSFG spectra presented here for the mid IR region produce relatively large non-resonant responses. These

34

responses interfere with the relatively weak resonant responses from the C=O modes of the molecules studied here and thus spectral deconvolution is particularly relevant.

All of the spectra taken in this work are of the condensed phase (specifically the water surface of the air/water interface). It is therefore necessary to develop a lineshape that more accurately captures the myriad phases present in the condensed phase than a simple Lorentzian lineshape used to treat individual molecules. The spectral fitting routine used in our laboratory was first proposed by Bain[4] and employs a convolution of homogeneous (Lorentzian lineshape) and inhomogeneous broadening (Gaussian lineshape).

$$\chi^{(2)} = \chi_{NR}^{(2)} e^{i\psi} + \sum_{v} \int_{-\infty}^{\infty} \frac{A_v e^{i\phi_v} e^{-\left[\frac{\omega_L - \omega_v}{\Gamma_v^2}\right]^2}}{\omega_L - \omega_{IR} + i\Gamma_L} \qquad (3.4)$$

The first term in the equation is the non-resonant second-order susceptibility and is represented by amplitude, A_{NR}, and a phase, ψ. The second term is the resonant second-order susceptibility. A_v is the amplitude (representing the strength of the transition as detailed in the previous chapter) and has an associated phase, ϕ_v. ω_L is the Lorentzian frequency (over which the integral is evaluated), ω_v is the resonant frequency, and ω_{IR} is the IR frequency (independent variable). Γ_L is the homogeneous linewidth while Γ_v is the inhomogeneous linewidth.

The fitting routine uses 5 parameters for each resonant component and 2 parameters for the non-resonant component. The non-resonant component parameters are simply the amplitude and phase. The resonant components are the amplitude (A_v), the associated resonant phase (ϕ_v), the Lorentzian linewidth (Γ_L), the Gaussian linewidth (Γ_v), and the spectral frequency (ω_L). Since $\chi^{(2)}$ is far from any electronic resonances, the non-resonant portion is treated as real and its phase is set to π or 0. All of these

parameters may be adjusted in a fit to VSFS spectral data; obviously this procedure is not arbitrary and requires careful control of over these parameters.

Several methods are used to constrain the parameters in such a way to give confidence to the fits achieved. The spectral frequencies are initially constrained by examples from other vibrational techniques (IR, Raman) that are in the literature. Since these are almost universally bulk values, they are only approximate but yield good starting positions for the spectral frequency. Separation of the individual contributions to the linewidths can be difficult at best so certain approximations are made. The Lorentzian linewidth is held constant with a value of 2 cm^{-1} (based on its values for most surfactants) and so only the Gaussian width is allowed to vary. In addition the phase of the resonant component is set to either π or zero. This means that the only variable parameters are the amplitude and Gaussian width.

The final scheme used to provide further confidence in the fitting routine is the use of global parameters. In a global fit, several different spectra from related environments (e.g. concentration or pH dependence) are fit together simultaneously to find parameters which are global versus local. In general, peak positions and Gaussian widths are considered global for a given set while amplitudes are considered local. This provides further confidence that the peak positions as well as the Gaussian widths are interpreted correctly from the data. The spectra are fit to a nonlinear least squares fit (Levenburg-Marquardt) algorithm implemented in the IGOR program from Wavemetrics, Inc.

Surface Tension

Surface tension measurements were performed using the Wilhelmy plate method.[5] A force balance (KSV Instruments) was used to measure the surface tension. A Pt plate (KSV) attached with a Pt wire is used for all measurements. The perimeter was measured and input into the accompanying software. The solutions were placed in a clean glass dish and great care was taken to ensure that the plate was oriented correctly to the interface. The plate was carefully lowered to the sample via a micrometer stage and allowed to just touch the surface. The samples were allowed to equilibrate before the measurement was taken. The Pt plate was cleaned by being flamed until glowing orange and rinsed repeatedly in >18 $M\Omega{\bullet}cm$ water between measurements. Measurements of a pure water solution were taken everyday prior to experiments to ensure both the viability of the instrument as well as provide a value of water for surface pressure measurements.

Sample Preparation

Malonic acid was purchased from Sigma-Aldrich (ReagentPlus 99%). Succinic acid (SigmaUltra, $\geq$99%) was purchased from Sigma-Aldrich. Glutaric acid (99%) was purchased from Sigma-Aldrich. Adipic acid (puriss, p.a.) acid was purchased from Sigma-Aldrich. NaOH was purchased from Mallinckrodt Chemicals (AR). All solutions were prepared fresh with >18 $M\Omega{\bullet}cm$ water and used within 72 hours.

All samples are placed into custom-made glass dishes (~2.5 ml). All glassware is cleaned stringently using concentrated sulfuric acid and NOCHROMIX (strong oxidizer). Glassware is immersed for 24 hours in the acid/oxidizer solution and then removed and immersed in Nanopure water (>18 $M\Omega{\bullet}cm$) for 24 hours. Finally, the glassware is

removed and copiously rinsed with more Nanopure water. After rinsing, the glassware is dried in a clean oven and then stored until use. For all experiments, the sample dish is placed in a custom made KEL-F cell which can be completely sealed. There are four windows; a CaF_2 entrance window to allow the visible and IR into the cell, a BK7 exit window that is AR-coated for SF wavelengths, and two BK7 windows used to visually monitor the interior of the cell. Samples are injected into the custom glass dishes placed in the cell by a gas-tight glass syringe (Hamilton, 10 μl) with a teflon needle. The cell can be deconstructed and cleaned in the acid/oxidizer solution. After cleaning the cell is rinsed with copious amounts of Nanopure water and allowed to briefly dry in a clean oven.

pH adjusted solutions were prepared in such a manner as to keep the overall concentration of acid constant, regardless of the amount of based added. A pH calculator, BATEpH,[6] was used for each acid with the corresponding pK_a values provided either by the software or through manual entry. The solutions were then prepared as calculated and double-checked with litmus paper (colorpHast, E.Merck) in the appropriate pH range and through a pH meter (110 series, Oakton).

Computational Methods

The computational methods used for Chapter IV (Malonic acid) is presented below. This work was performed by Eric Shamay. Classical molecular dynamics (MD) simulations were performed using the Amber 11 suite of simulation programs.[7,8] A single system of water and malonic acid was initialized for simulation by creating a cubic unit cell with side lengths of 30 Å. The unit cell was then randomly packed with 900 water

molecules, and 17 malonic acid molecules using the PACKMOL program created to simplify construction of MD starting configurations.[9] This resulted in a malonic acid concentration of 1M, purposefully set to be similar to that of the VSFS experimental conditions.

The initial system was energy minimized by a combination of steepest descent and conjugate gradient methods to reach a geometry optimization. The z-axis of the system was then expanded to 100 Å creating a large vacuum region adjacent to the aqueous cube. Periodic boundary conditions were then employed resulting in an infinite slab configuration with two aqueous-vacuum interfaces. This configuration was then evolved through MD simulation for 500 ps to equilibrate the system. The system was then evolved for 50 ns of data-collection, recording atomic coordinates every 100 fs for a total of 500,000 data points.

The simulations were performed using a timestep of 1 fs. Fully polarizable models were used for both the water and malonic acid molecules. Water was simulated using the POL3 model,[10] and the malonic acids were constructed using a fully atomistic model based on the Amber FF02EP force field.[11] The system temperature was set at 298K, and Langevin dynamics were used to propagate dynamics via a leapfrog integrator. The particle mesh ewald technique was used for calculating long-range electrostatic interactions with a force cutoff set to 10 Å. Waters were held rigid by means of the SHAKE algorithm to increase computational throughput and speed of data collection.

In all following analyses, the results obtained for molecular orientation are averaged between both of the water slab surfaces. The distance to each aqueous surface was determined for every malonic acid at each timestep using the method developed in a

computational study to determine water surface locations.[12] The closer surface was always used to analyze acid orientation, and the reference axis was always set to point from the aqueous bulk outwards towards the vacuum phase, normal to the plane of the water surface.

The computational methods used for Chapter V, VI, and VII (succinic, glutaric, and adipic) are shown below. This work was performed by Nicholas Valley. Classical molecular dynamics (MD) calculations were performed using the Amber 12 suite of programs.[13] Starting configurations were created using the PACKMOL[9] program. Succinic acid configurations consisted of 900 water molecules and 2, 4, or 8 succinic acid molecules in a 30 Å cube. These configurations correspond to concentrations of approximately 0.12 M, 0.25 M, and 0.5 M respectively. Glutaric acid configurations consisted of 900 water molecules and 2, 8, 16, or 48 glutaric acid molecules in a 30 Å cube. These configurations correspond to concentrations of approximately 0.12 M, 0.5 M, 1M, and 3 M respectively. Adipic acid configurations consisted of 900 water molecules and 1 or 2 adipic acid molecules in a 30 Å cube. These configurations correspond to concentrations of approximately 0.6M and 0.12M, respectively. A water slab with two surfaces was created by expansion of one of the box dimensions to 120 Å and applying periodic boundary conditions.

Energy minimization of the initial system was performed using a combination of steepest descent and conjugate gradient methods. Minimized structures were equilibrated by evolution through 2 ns of MD simulation. Each system was further evolved for 50 ns, with atomic coordinates recorded every 100 fs for a total of 500,000 data points. The simulations were performed using a timestep of 1 fs. Fully polarizable models were used

for both the water and acid molecules. Water was simulated using the POL3 model,[10] and the acid molecules were constructed using a fully atomistic model based on the Amber FF02EP force field.[11] The system temperature was set at 298K, and Langevin dynamics were used to propagate dynamics via a leapfrog integrator. The particle mesh ewald technique was used for calculating long-range electrostatic interactions with a force cutoff set to 10 Å. Waters were held rigid by means of the SHAKE algorithm to increase computational throughput and speed of data collection.

Distances from the water surface are calculated using the Gibbs dividing surface determined from a hyperbolic tangent fit to the water density profile. To correct for possible drift of the water surface over the length of the simulation, the coordinates of each data point are shifted so that the center of mass of the water system remains constant. Data is collected using both water/vacuum interfaces, and angles relative to the surface are measured from the surface normal pointing into the vacuum phase.

CHAPTER IV

MALONIC ACID AT THE VAPOR/WATER INTERFACE

The adsorption of malonic acid $((COOH)_2CH_2)$ to the air/water interface was investigated via VSFS, surface tension, and computational calculations and characterized by concentration dependence and pH dependence. Careful correlation of concentration dependent experiments using polzarized VSFS as well as macroscopic surface tension measurements revealed that malonic acid has exceptionally weak hydrogen bonding to the water molecules at the air water interface. The orientation of malonic acid was determined through molecular dynamics and confirms the spectral interpretation. Finally, VSFS and surface tension experiments demonstrated that the surface-active species of malonic acid at the air/water interface is the fully protonated species. The computational work was performed by Eric Shamay. The VSFS water region was taken by Stephanie Ota. Some surface tension data was taken by Loni Kringle.

Introduction

Malonic acid is one of the most highly detected dicarboxylic acid species and anthropogenic as well as biogenic sources have been identified for malonic acid.[1,2] The fact that malonic acid (as well as other dicarboxylic acids) has been found in urban, rural, and remote locations[3-12] indicates that they are persistent in the atmosphere. The presence in remote locations points to the production via secondary organic aerosol (SOA) processes. Since malonic acid is known to be surface active and persistent in the atmosphere, the behavior at aerosol surfaces requires further investigation.

This chapter seeks to characterize the surface adsorption of malonic acid at an air/water interface, which is a model for an aerosol surface. The behavior of malonic acid at an interface cannot be simply predicted by invoking typical surfactant (hydrophilic head group and hydrophobic tail) behavior since the molecule contains two hydrophilic groups separated by a hydrophobic group. Thus, the aqueous surface behavior of malonic acid is investigated through changes to concentration and pH. The carbonyl (C=O) mode of the carboxylic acid groups is interrogated via VSFS. This mode is sensitive to hydrogen bonding and provides a measure of the solvation environment at the surface. Additionally, polarized VSFS measurements of the C=O mode offer orientation information on the carboxylic head groups. VSFS experiments in the OH region give information about the solvent itself and how the surface structure is changed as malonic acid adsorbs to the surface. Surface tension measurements will provide adsorption parameters such as the area per molecule at the surface, which is an indication of surface packing. Computational modeling on these systems provides conformation in the spectral analyses, elucidates ambiguities in the spectral interpretation, and provides molecular specific geometries. These experiments fully describe the orientation, concentration and pH dependence, and solvation environment of malonic acid at an air/water interface.

Concentration Dependent Vibrational Spectroscopy

Shown in Figure 4.1a are the SSP spectra along with the fitted curves of aqueous malonic acid at four concentrations. The intensity of the signal from the carboxylic C=O modes in the SSP polarization scheme increases with bulk malonic acid. The intensity

shows a progressive increase from the lowest concentration at 100mM to 3M, the highest concentration investigated here. Malonic acid is clearly at the water surface with increasing population as the bulk solution concentration increases. The signal observed under SSP polarization further indicates that there is a net orientation of the dipole moment of one or both carboxylic acid groups on the diacid that is perpendicular to the surface plane. According to the global fits of the spectra, there is one peak centrally located at 1740 ± 2 cm^{-1} with a Gaussian width of 28 ± 1 cm^{-1}. Fits to the spectra are required due to overlapping interferences that can occur for VSFS between both resonant and non resonant signals. No shift in the frequency in the VSFS signal is observed with increasing bulk solution concentration.

The carboxylic C=O modes were also probed in the SPS polarization scheme and are shown in Figure 4.1b. The signal intensity in SPS was less than SSP. It should be noted that due to the angles used for these VSFS experiments (and hence the corresponding Fresnel factors), the signal intensity for SSP and SPS are comparable. This may not always be the case for VSFS experiments due to the dependence on the local field as a function of input angles of the visible and IR beams. As stated earlier, the SPS scheme interrogates modes that are in the plane of the interface. Since there is a rotational degeneracy for modes in the plane of the interface, signal intensity can appear weaker due to partial canceling of the VSFS signal. As was seen with SSP, the signal intensity increases as the bulk concentration of malonic acid increases. However, the fits to the spectra reveal a peak centrally located at 1730 ± 1 cm^{-1} (versus 1740 cm^{-1} for SSP) with a slightly larger Gaussian width of 37 ± 1 cm^{-1} (versus 28 cm^{-1} for SSP). This C=O frequency is closer to bulk aqueous values. The larger Gaussian width is consistent with

44

a more heterogeneous environment which supports the assertion that the SPS-active carboxylic C=O modes are in a slightly different environment than their SSP-active counterparts.
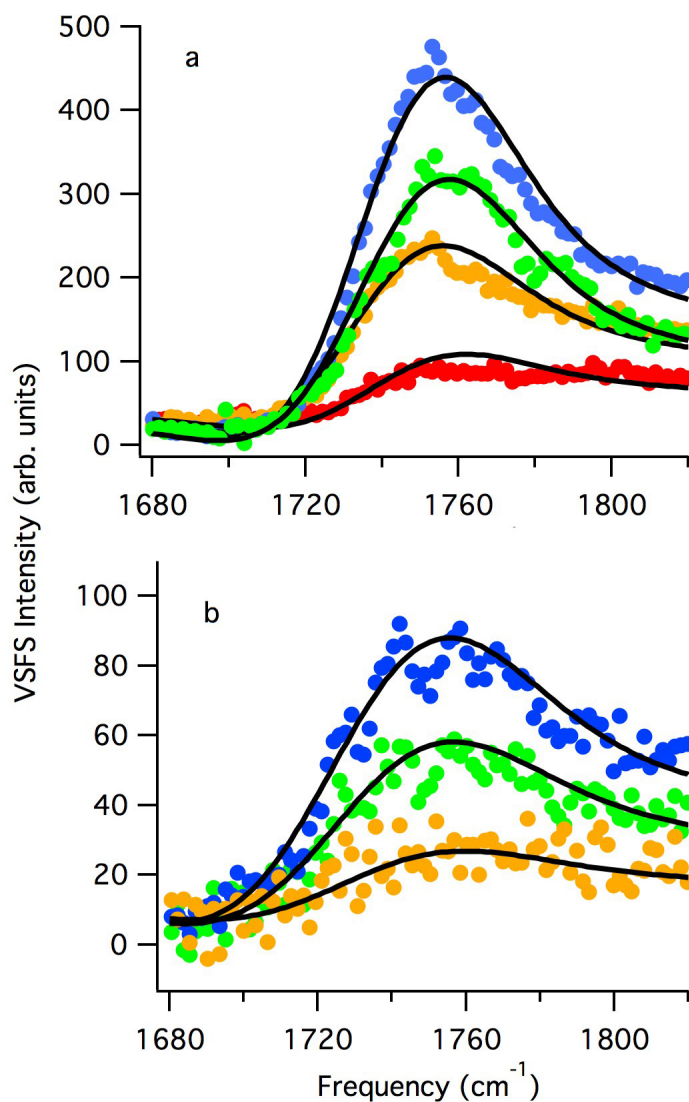
Figure 4.1. VSFS spectra of the carboxylic C=O of aqueous malonic acid a) for SSP at concentrations of 0.1M (red), 0.5M (gold), 1M (green), and 3M (blue) and b) for SPS at concentrations of 0.5M (gold), 1M (green), 3M (blue). Fits are shown in black. The intensity of the C=O signal increases monotonically as the concentration increases.

Infrared studies of malonic acid in bulk aqueous solution have shown that the carboxylic C=O modes appear at 1719 cm^{-1} for the fully protonated (H_2A) form and 1713 cm^{-1} for the singly protonated (HA^-) form.[13] In addition, this mode is also sensitive to the degree of water solvation, with monomers in the vapor phase measured as high as 1760 cm^{-1}.[14] Surface IR studies[15,16] have shown that distinct regimes of hydrogen bonding exist for long-chain fatty acid monolayers adsorbed to the air/water interface. The region from ~1735-1739 cm^{-1}, ~1715-1720 cm^{-1}, and 1700-1704 cm^{-1} are assigned as having non H-bonded, singly H-bonded, and doubly H-bonded character, respectively. While long-chain fatty acids and malonic acid will have different solvation properties, the trend will be similar for both. Therefore, since surface adsorbed malonic acid has values ~1730-1740 cm^{-1}, this indicates weak hydrogen bonding with surrounding water molecules to the carbonyl moiety.

There have been spectroscopic studies that have shown frequencies of the carboxylic C=O mode of malonic acid up to 1740 cm^{-1} but these samples were either crystalline malonic acid[17] or deliquesced samples.[18] It has been established that for these samples, the splitting of the carboxylic C=O is due to intermolecular hydrogen bonding (cyclic dimerization). There is a subsequent splitting of the C=O spectral features into an out of phase mode that is IR active located at higher wavenumbers (~1740 cm^{-1}) and an in phase Raman active mode that is located at lower wavenumbers (~1685 cm^{-1}).[17] In our raw spectra (before normalization), there is evidence of a very weak signal appearing around 1690 cm^{-1}, which was only seen in SSP. While this signal may be evidence of dimerization, the extremely weak signal makes any analysis very difficult and is therefore not pursued here. In addition, if there were symmetric cyclic dimers being formed, the

signal would disappear due to an inversion center being sum frequency inactive.[19] It should be noted that all VSFS spectra taken in this study are of relatively weak signals; consequently the normally negligible non-resonant signal interferes with the resonant signal on the blue-side of the spectra resulting in the VSFS signal not returning to zero on the blue-side of the spectra. This interference has been seen before in VSFS studies of carboxylic C=O modes[20] and nitrate modes[21] at aqueous interfaces.

Based on the SSP and SPS spectra, it is evident that there are C=O oscillators from malonic acid that have frequencies which are blue-shifted when compared to both bulk dicarboxylic acid as well as surface carboxylic acid (e.g. hexanoic acid).[22] This is consistent with weak hydrogen bonding of the C=O mode to water. In addition, the response from SSP and SPS are not equivalent, implying that these experiments are sampling two different hydrogen-bonding environments. These results indicate that the adsorption of malonic acid is more complex than simple alkyl carboxylate surfactant adsorption and requires further exploration to fully understand its adsorption on a water surface.

In addition to probing the carboxylic C=O modes of malonic acid, the spectral region associated with the CH modes of malonic acid ($\sim$2900 cm^{-1})[23] has been investigated to develop a more comprehensive picture of the adsorbate structure. Also investigated were the OH stretch modes of water as a means of determining how the presence of the adsorbate alters the surface water structure and bonding in three spectral regions. A simple picture that has evolved from many VSFS studies of water is that the free OH region ($\sim$3700 cm^{-1}) corresponds to the response of water OH oscillators that have minimal interaction with nearby water molecules and in fact are vibrationally

47

decoupled from the hydrogen-bonding network of bulk water. These modes are most affected by adsorbates at the top most layer of the interface (nearest the vapor phase). At much lower frequencies reside the OH oscillators corresponding to the most highly coordinated surface water molecules ($\sim$3200 cm^{-1}). These water molecules lie deeper in the interfacial region and are consequently more sensitive to the presence of interfacial ions. Oscillators residing in the region correspond to intermediate degrees of hydrogen bonding and interfacial depths are located between these two regions ($\sim$3400 cm^{-1}).[24-29]

Figure 4.2 shows 6 SSP spectra of the water/CH region for three different concentrations of malonic acid along with the neat water spectrum in gray as comparison. Looking first in the CH stretch region, as the malonic acid solution concentration increases, there is a corresponding increase in intensity in the CH (2800-3000 cm^{-1}) region. Unfortunately, the overlap between the OH modes and the CH modes makes distinct spectral characterization difficult in this region. Nevertheless, the broad region between 2800 and 3000 cm^{-1} is attributed to the carboxylic OH stretching of malonic acid. This attribution is based on isotopic VSFS studies done on selectively deuterated succinic acid, $(COOH)_2(CD_2)_2$ in D_2O and H_2O.[30] This carboxylic OH stretch is attributed to hydrogen bonding interactions between the OH and water[31] and is consistent with IR studies of aqueous dicarboxylic acids.[32]

The overall trend observed is that with increasing malonic acid concentration, there is a corresponding increase in signal in the CH region. A sharp peak appearing at 2945 cm^{-1} was assigned to the CH_2 stretch mode for succinic acid at the air/water interface for VSFS experiments in both SSP and SPS polarization schemes.[30] However, there is no evidence of a sharp peak indicative of CH_2 modes at the surface even at the
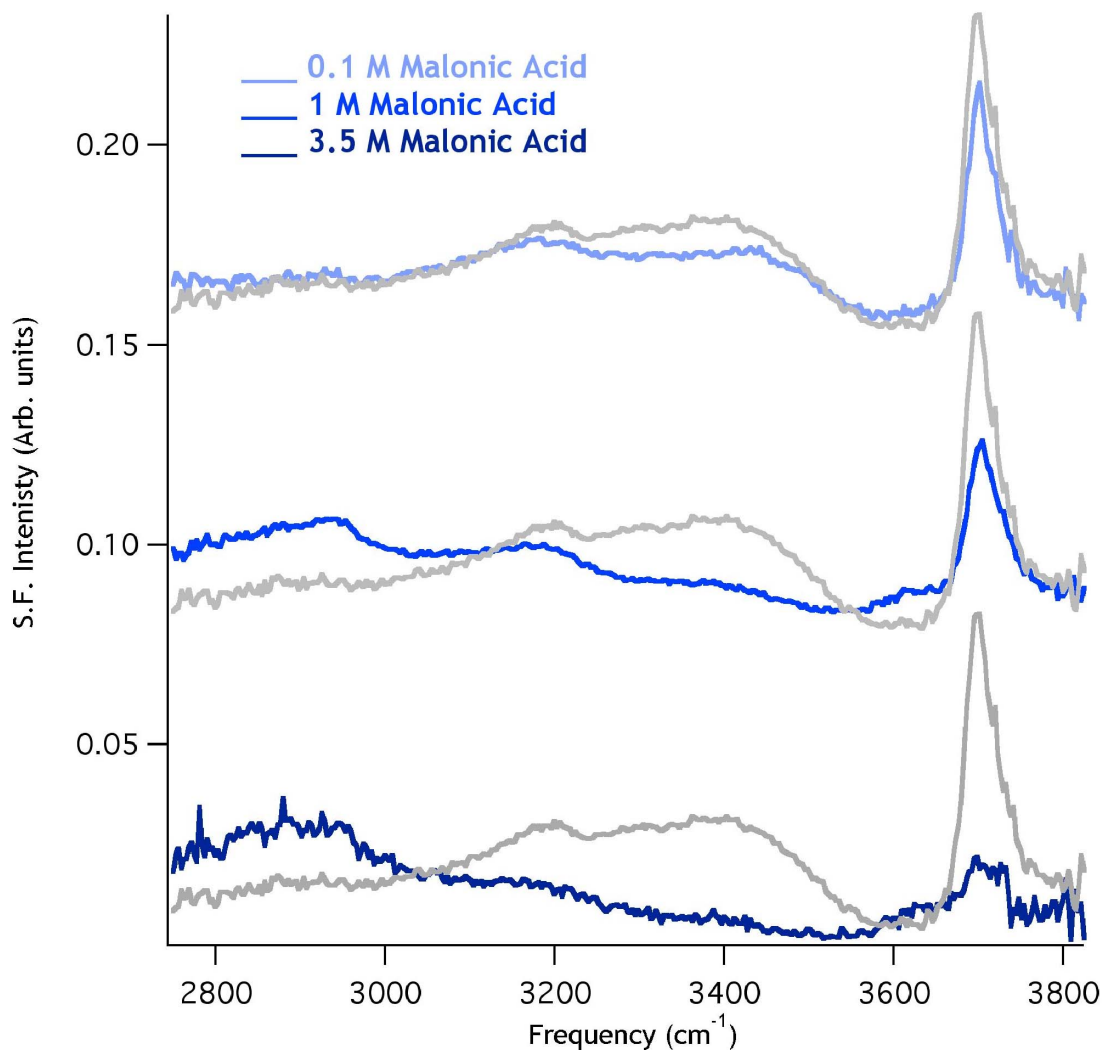
Figure 4.2. VSFS of water/CH region for 0.1M, 1M, and 3.5M aqueous malonic acid. The gray spectra are neat water.

highest concentration. The increase in this region thus most likely reflects the hydrogen bonding of the OH of the dicarboxylic acid. It is concluded that the absence of any observation of CH_2 modes is due to an orientational averaging effect. This will be addressed further in the computational section.

49

Looking next at the region corresponding to the response of water OH modes, upon adsorption of malonic acid there is a corresponding decrease in the free OH signal with increased malonic acid in bulk solution. This decrease is also observed in the 3400 cm^{-1} region corresponding to somewhat stronger but still relatively weakly bonded surface water molecules. A new peak forms above 3600 cm^{-1} that increases in intensity as the bulk concentration is increased. This peak has been attributed to solvation of ions[33] and would result from the presence of hydronium ions, H_3O^+. Interestingly, the free OH signal does not fully disappear even at concentrations of 3.5M indicating that the water surface is not completely covered by the malonic acid. This is unlike alkyl nonionic surfactants (e.g. long chain alcohol, sugar surfactants, alkyl poly(ethylene oxide) surfactants), where the free OH signal is virtually absent once complete surface coverage is reached.[34] These results then suggest that malonic acid adsorption is not completely disrupting water at the top most layer and must not pack tightly enough to fully cover the surface. This will be addressed further in the next section. The spectral characteristics of water at longer wavelengths are consistent with increased presence of malonic acid at the surface. The increase in the OH response around 3200 cm^{-1} is consistent with progressively stronger surface OH bonding with the increased concentration of malonic acid. However, as noted above, the signal from overlapping modes complicate further interpretation in this region.

Concentration Dependent Surface Tension

Surface tension, being a macroscopic technique, measures the overall surface concentration whereas VSFS simultaneously measures both surface concentration

(number density at the surface) as well as molecular orientation.[19] By combining the results of these two complementary techniques, the surface density and orientation can be decoupled. This allows for a more complete picture of the adsorption of malonic acid from either technique alone.

The surface tension of malonic acid on H_2O has been investigated[35,36] in previous studies. The surface pressure results are in excellent agreement with these earlier works and can be seen plotted in Figure 4.3. The Gibbs adsorption equation is employed,[37] to obtain the maximum surface excess. Activity coefficients were obtained from Clegg and Seinfeld.[38] The value of a^s_1 calculated from this data is 191 $Å^2$/molecule. This
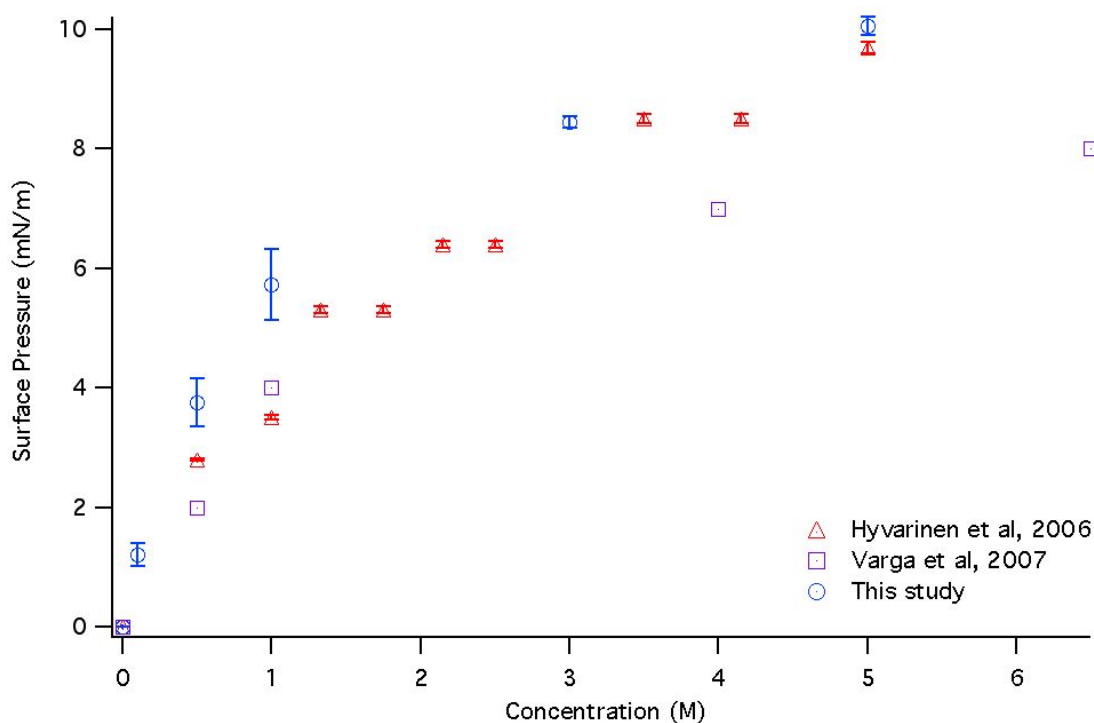
Figure 4.3. Plot of malonic acid concentration versus surface pressure. Shown are data from Ref 35, Ref 36, and this study.

comparatively large molecular area corroborates the VSFS data from the water region where the free OH signal did not disappear at high concentrations (3.5M) and confirms that malonic acid does not pack tightly at the air/water interface.

Figure 4.4 shows the comparison between trends in the surface pressure data and the changes in the square root of the VSFS amplitude (the concentration dependence of the sum frequency field is the square root of the intensity)[39] of the C=O mode (SSP and SPS) data with malonic acid concentration. As the bulk concentration of malonic acid increases from 0M to 3M, the surface pressure increases; further increases in concentration do not affect the surface pressure substantially and at higher concentrations the measurement is limited due to eventually reaching the solubility limit of malonic acid
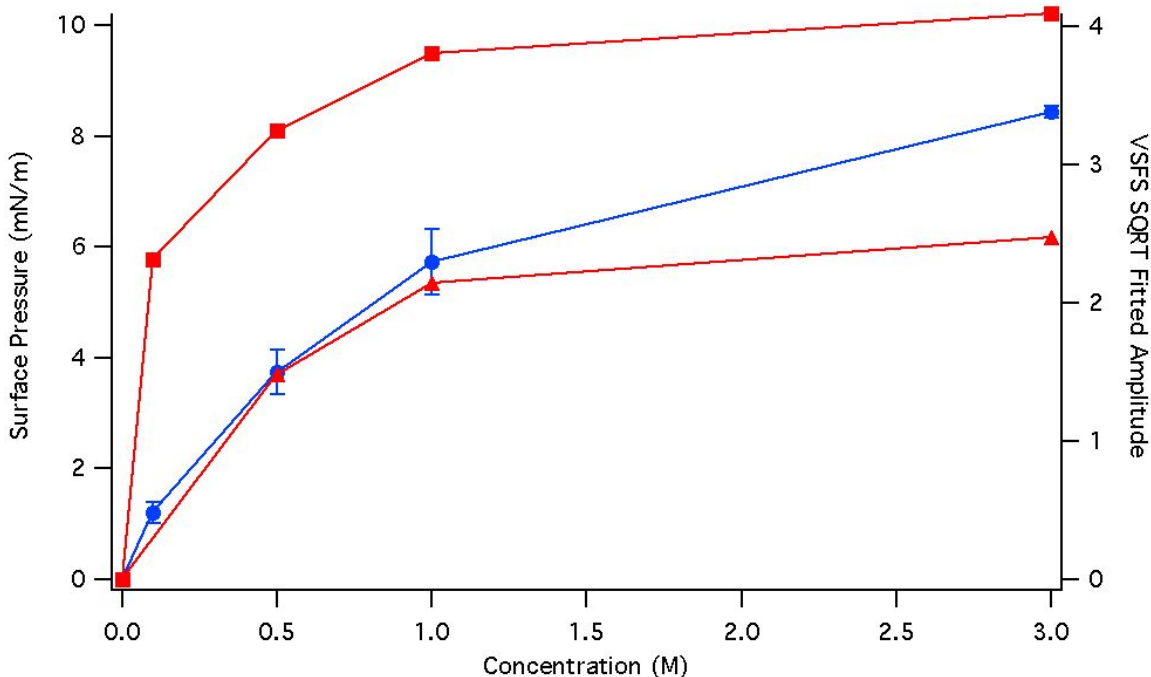
Figure 4.4. Plot of surface pressure (blue trace) versus square root of fitted VSFS amplitudes for SSP (red squares) and SPS (red triangles) C=O modes of malonic acid.

in water.[35] There is an analogous rise in the square root of the VSFS intensity of the VSFS C=O (SSP and SPS) signal over the same concentration range. This indicates that the adsorption of malonic acid to the air/water interface does not change orientation as a function of concentration. In order to confirm this, the surface coverage as a function of concentration is calculated. To determine the surface concentration at any bulk concentration, the Frumkin equation was employed.[37]

In Figure 4.5 the surface coverage as a function of bulk concentration of malonic acid is plotted versus the square root of the SSP VSFS fitted intensities. The linear dependence of the data as well as the unchanging frequency response in the C=O VSFS (SSP and SPS) confirms that additional adsorption that occurs at the surface as a function of concentration does not significantly change the orientation of the carboxylic C=O modes, but merely increases the total number of oscillators at the surface.
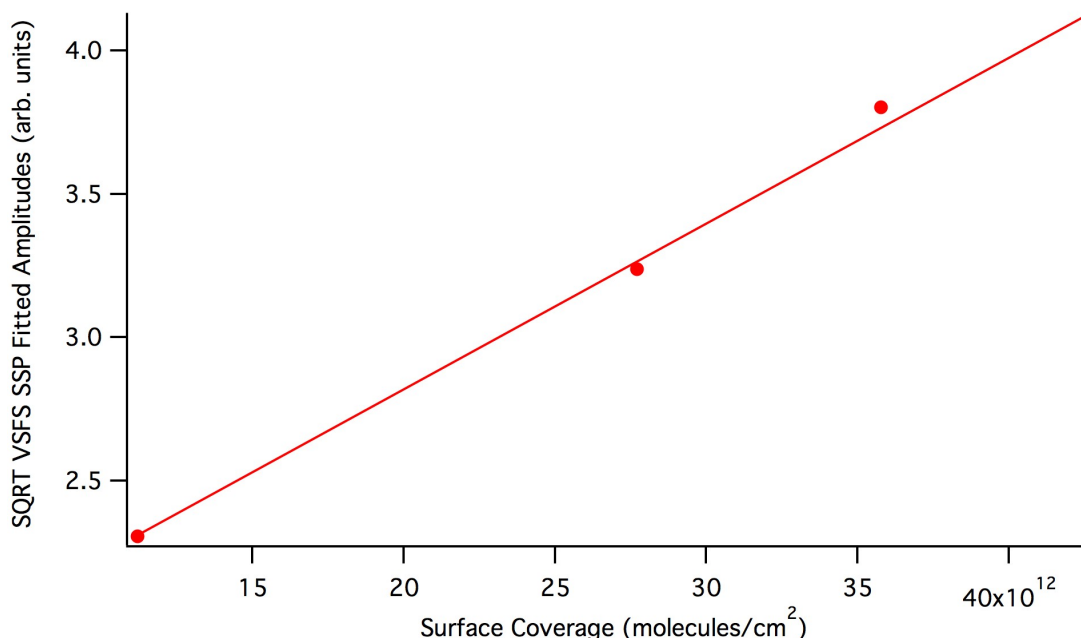
Figure 4.5. Plot of surface coverage versus fitted VSFS amplitudes for SSP modes.

By combining the VSFS spectra and the surface tension data, a rudimentary picture of malonic acid adsorption at an aqueous interface can be drawn. According to the SSP data, there are carboxylic C=O oscillators oriented normal to the surface. According to the SPS data, there are also carboxylic C=O oscillators in the plane of the interface. This latter signal is less intense, potentially due to orientational averaging. These carboxylic C=O frequencies are indicative of very weak solvation. As the concentration of malonic acid is increased in the bulk, the surface concentration also increases but in a fashion that does not alter the overall orientation of the C=O oscillators. This is supported by the surface tension data as well as the lack of changes in both the frequency and Gaussian width of the malonic acid C=O spectra as a function of concentration. The H_2O/CH region provides further evidence of adsorption that does not fully disrupt the top-most surface layer and that the adsorption more strongly affects the hydrogen bonding coordination. The lack of CH_2 signal is most likely due to an orientational averaging effect. These results therefore indicate isolated malonic acid molecules adsorbed to the very top of the air/water interface.

VSFS does provide orientation information, however, because the VSFS studies here are not phase sensitive, it is not possible to determine whether the dipole oscillators probed by the SSP polarization scheme are pointing into the vapor phase or into the aqueous phase. Phase-sensitive sum frequency generation[40] has been demonstrated to be capable of determining both the real and imaginary components of $\chi^{(2)}$ and therefore the unique phase associated with a resonance. By knowing the phase, the absolute orientation of a particular mode can be determined experimentally. However, the material of choice to create the local oscillator necessary for these experiments has traditionally been quartz.

The use of this material is prohibitive in the carbonyl wavelength regions (~6 μm) due to the lack of transmission of z-cut quartz. While these experimental challenges may be remedied soon, the use of phase-sensitive sum frequency measurements is not possible for these experiments at this time. By probing the behavior of these molecules using computational methods, further information about the most likely geometries of malonic acid adsorption can be obtained, compared with the VSFS data, and obtain a more complete picture of the bonding environment at the surface without requiring phase-sensitive measurements.

Computational Modeling

Angle Descriptions of Chemical Moieties

The discussion of the molecular orientation of malonic acid begins with a description of the angles used in the following analyses. Because the carbon atoms form the backbone of the malonic acid molecular structure, determining the orientation of the three atoms is the first step in understanding the overall orientation of the molecule in space with respect to a water surface. The orientation of the carbon chain backbone is described using two angles, and the molecule is oriented internally using two dihedral angles. All the angle definitions described below are depicted in Figure 4.6.

The group of three carbon atoms forms a moiety with a C_{2v} symmetry. The two C-C bond vectors have a bisector between them. In this work, the bisector is always referred to as a vector pointing out from the central carbon in the direction of the other two carbon atoms. The first angle defined, θ, describes the "tilt" of the triatomic carbon chain that forms the acid's backbone. The angle θ is calculated as the angle formed between the
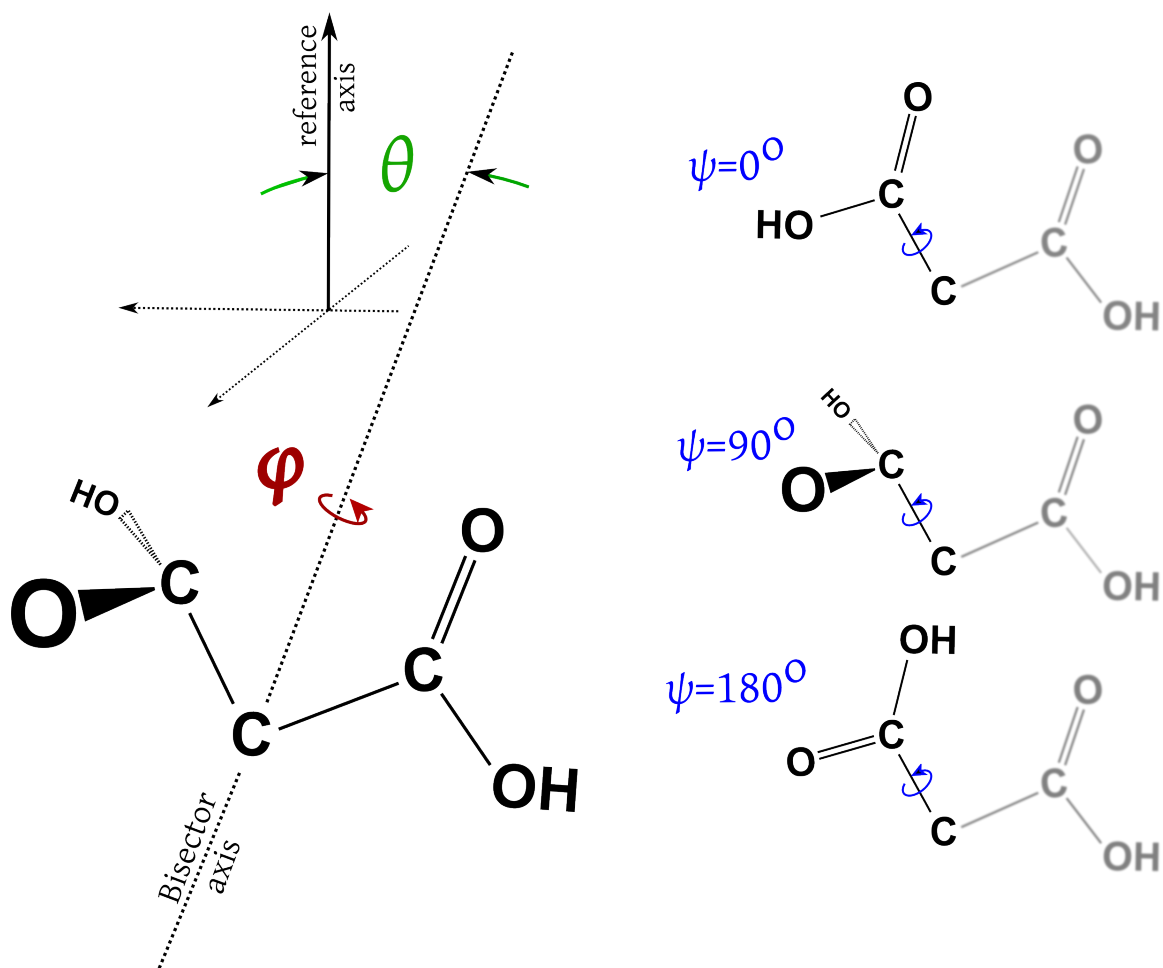
Figure 4.6. Description of angles that are used to orient a malonic acid molecule both in the space-fixed frame and internally in the molecular frame. θ (green) is the "tilt", φ (red) is the "twist", and ψ (blue) two dihedral angles. Three values of ψ are depicted (right).

carbon group bisector vector and a reference axis oriented perpendicularly to the water surface, pointing out of the water bulk towards the gas phase side of the water interface. When $\theta = 0°$, the bisector vector aligns with the reference axis. A value of $\theta = 90°$ places the bisector vector in the plane of the water surface, perpendicular to the reference axis. Rotating the bisector to $\theta = 180°$ makes the bisector anti-aligned with the reference axis, pointing in towards the water side of the interface.

The second angle used to orient the malonic acid carbon backbone, φ, describes a molecular "twist" of the malonic acid. This twist angle is defined as a rotation of the plane formed by the three carbon atoms around the bisector axis. For different orientations of the angle φ, the distribution of φ will necessarily become isotropic because of the symmetries of the plane of the aqueous slab surface. However, the value of φ is necessary to describe the overall molecular orientation for θ values near 90°. When $\theta = $ 90°, the bisector of the carbon atom group lies parallel to the water surface. In such a configuration, $\varphi = 0°$ means the plane of the carbon atoms orients perpendicularly to the plane of the water surface. Likewise, $\varphi = 90°$ lays the plane of the carbon atom group at on the surface, parallel to the plane of the water interface.

The planes formed by the atoms of the carboxylic acid groups orient by rotation of two dihedral angles, collectively referred to as ψ because they are not uniquely identified, referenced to the plane of the three backbone carbon atoms. The dihedral angle is the angle of rotation of the C-C bond between the central methylene carbon, and a carbonyl carbon of a carboxylic acid moiety. The reference orientation that sets $\psi = 0°$ is defined by two conditions: 1) the plane of the atoms of the carboxylic acid orients parallel to the plane of the three carbon atoms, and 2) the carbonyl C=O bond vector (pointing from the C to the O) points to the same side as the C-C-C bisector vector (i.e. the inner product of the bisector vector and the carbonyl bond vector has a positive value: C=O * bisector > 0). A dihedral angle of $\psi = 90°$ rotates the O=C-O plane perpendicular to the C-C-C plane. Lastly, $\psi = 180°$ rotates the carboxylic acid such that the carbonyl is anti-aligned with the C-C-C bisector. The various orientations of the dihedral angles are depicted in Figure 4.6, and characterize the internal orientation of malonic acid. By

combining all three of the described angles with information about the acid position within the simulation box, a complete picture is developed of the orientational behavior of malonic acid relative to a nearby water surface.

Carbon Backbone Orientation

Bivariate angle distributions of θ and φ were calculated for the three carbon backbone atoms, and are shown in Figure 4.7. The set of plots represents slices through the interface parallel to the water surface. Each slice is located at the distance labeled in the top-right of the respective plot. Positive positions are further into the vacuum phase, and negative positions are further into the aqueous phase of the interface. A distance of 0 Å is located at the water surface location. The location of the surface, and all calculations performed to relate interfacial position are done using a method of averaging top-most water molecule positions.[41] The molecular center of mass determined the position of each malonic acid.

In each set of axes of Figure 4.7, the values of θ and φ are plotted along the horizontal and vertical, respectively. The plots are two-dimensional histograms colored by the intensity (i.e. population) of the location in the angle space. Higher intensity is colored in dark red, and lower intensity is dark blue. Areas in the plots characterized by uniform coloration indicate an isotropic distribution of angles. A concentrated region of uniform coloration indicates an orientational preference in one or both of the angular degrees of freedom.
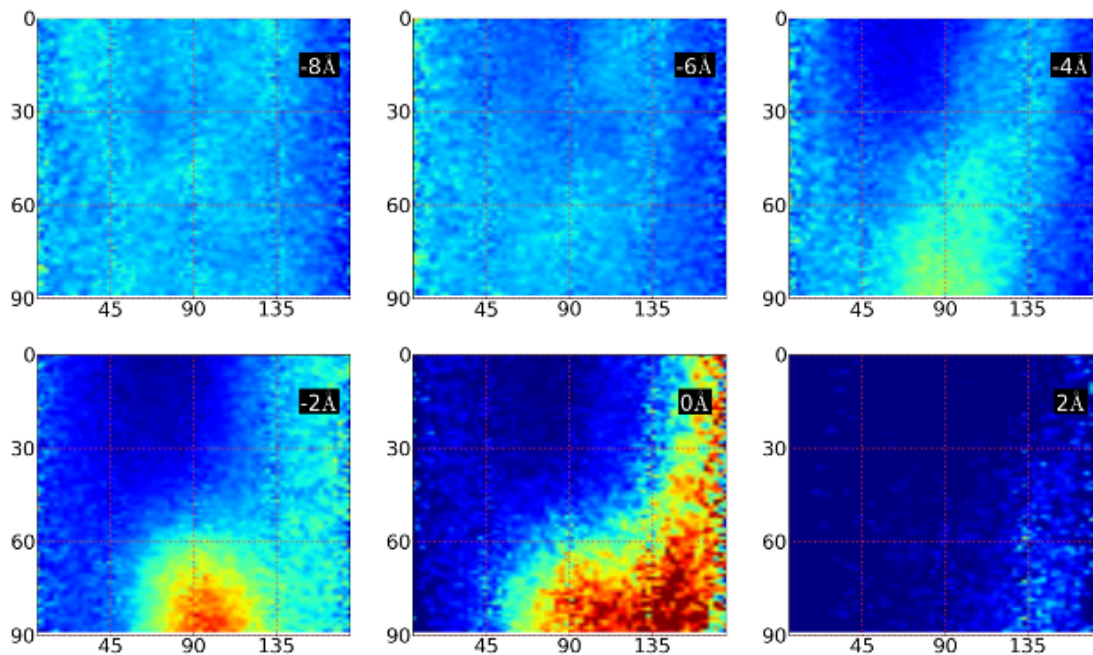
Figure 4.7.   Bivariate distribution plot of the tilt (θ) and twist (φ) of the malonic acid carbon chain with each plot representing a 2 Å slice of the simulated aqueous slab at the depth listed in the inset.

The plots for interface positions of 2 Å in Figure 4.7 show the orientation of the acid carbon backbones just above the water surface. The plot intensities at these positions of the interface indicate the presence of malonic acid, and correspond to the surface adsorption behavior found in the VSFS experiments. These acid molecules are most likely less solvated than those further into the water bulk. The most distinguishing feature is the vertically running band of intensity to the right of the plot centered between 135° and 180°. This results from a population of acid molecules with their three carbon atoms oriented with the carbon-group bisector vector pointed more than 45° into the water bulk. φ is spread nearly isotropically in this distribution. However, due to the symmetry of the θ angle as a spherical coordinate (i.e. a single θ value describes a cone in space) φ will necessarily become more isotropic relative to the interface, or spread out across the two-

59

dimensional plots, as θ takes values near its extrema. Values of θ closer to 90° require φ to fully describe the orientation.

At 0 Å and below, acid carbon backbone orientations are more complex. A second population of orientations forms at 0 Å, manifested in the plots as a region of intensity centered at $\theta = 90°$, with φ also concentrated towards 90°. This indicates a carbon atom group lying flat in the plane of the water surface. Additionally, as the depth of the molecules increases from 0 Å to -4 Å, the population above $\theta = 135°$ decreases, shifting intensity to the peak at $\theta = 90°$. The distribution spreads out both in θ and in φ. For acid molecules deeper into the water bulk, likely more solvated by waters, the orientational freedom expands in θ and φ until at -6 Å there is a loss of orientational preference, resulting in a flat (evenly colored) distribution, and isotropy of the carbon backbone group orientation.

At -4 Å the distribution expands below $\theta = 45°$. This is due to a population of submerged malonic acid molecules with their bisectors aimed slightly up towards the water surface. Thus, it is established that the influence of the interface on molecular orientation extends both above and below the water surface, and extends to a depth of at least 4 Å into the bulk water.

CH$_2$ Orientation

For each acid molecule, the orientation θ of the carbon backbone affects the position and orientation of the molecule's methylene hydrogens. For an orientation of $\theta = 90°$, and for all φ values, there are two hydrogens (one from each methylene) in a rather symmetrical configuration with one above and one below the backbone's plane, which is

itself parallel to the plane of the water interface. With $\theta = 90°$, variation in φ results in the plane formed by each H-C-H rotating from perpendicular ($\varphi = 0°$) to parallel ($\theta = 90°$) to that of the water surface. Consider acid orientations near $\theta = 90°$ and further consider the vector defined by each methylene's C-H bond. The geometry of the acid is such that each of these C-H bond vectors has a component perpendicular to the plane of the interface and the magnitude of each vector's perpendicular component is identical. Effectively, these 'perpendicular to the water interface' components are mirrors of each other.

Furthermore, if the θ distribution is symmetric around $\theta = 90°$ (as in the -2 Å plot of Figure 4.7), then the perpendicular components of the two methylene C-H bonds negate each other. The carbon group θ - φ distributions at or below the water surface (≤ 0 Å) exhibit this quality. The VSFS experiments failed to produce any spectral features related to the methylene CH_2 modes of malonic acid. Thus, it is proposed that the aforementioned orientational symmetry of the methylene C-H bonds about the water surface and the low population of malonic acids above the surface location, manifests spectrally in the polarized VSFS experiments as a lack of intensity where the C-H bond features are expected.

Carbon Backbone Dihedral Angles

Having established the orientation of the carbon backbone atom group from the distributions of Figure 4.7, the analysis of the internal geometry of carboxylic acid moieties near the water surface is explored. The two carboxylic acid groups rotate around the two C-C bonds, quantified by their dihedral angles. The magnitudes of the dihedral angles fall in the range $0° \leq \psi \leq 180°$. The O=C-O atomic plane is parallel to the C-C-C

61

plane at $\psi = 0°$ and $\psi = 180°$, and the two planes are perpendicular at $\psi = 90°$, as discussed above and depicted in Figure 4.9. The two dihedral angles are plotted in a set of bivariate distributions in Figure 4.8. The arrangement of the axes in the figure is identical to that of Figure 4.7, but with each axis representing one of the two ψ angles.

Figure 4.8 shows that the dihedral orientations are strongly related with a preferred rotation of 90° apart from each other. The two very concentrated peaks in the plots are located at $\psi = 0°$ and $\psi = 90°$. This results from the carboxylic O=C-O atomic planes of the two carboxylic acids aligning perpendicularly to each other. The topmost plot at 2 Å is not symmetric between the two dihedral angles with only a single peak in the distribution (located at the left-center of the axis). This is an artifact of how the carboxylic acid groups were enumerated computationally, and indicates that the top-most malonic acids above the water surface take on a fixed dihedral orientation, rarely switching values (i.e. rotating the molecule to flip the alignment of both carboxylic acid groups).

One of the carbonyl C=O bonds is preferentially aligned in the same direction as the carbon group bisector ($\psi = 0°$), and in the plane of the three carbons. The other carbonyl C=O bond points perpendicular to the plane of the carbon group atoms. The strong orientational preference is observed both in the bulk of the water and at the water surface location. This difference between the two carboxylic group orientations likely manifests spectrally as a shifting of the carbonyl peak frequencies. Each end of the molecule is configured differently and likely located in different solvation environments.
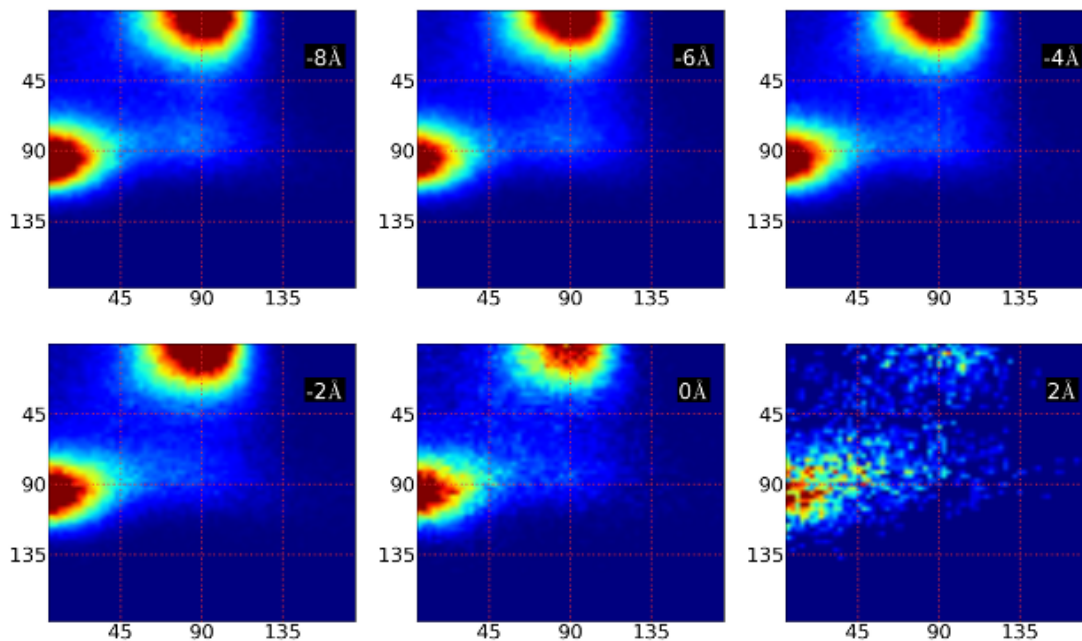
Figure 4.8. Internal orientation of malonic acid as a function of dihedral angles, ψ, describing the angle formed between the plane of the O=C-O atoms of the carboxylic acid group and the plane of the three carbon atoms. Each plot represents a 2 Å slice of the simulated aqueous slab at the depth listed in the inset.

The spectral peak shifting of the two polarization schemes of the VSFS experiments results directly from the orientational preferences of the two carboxylic acid groups of the malonic acid molecule.

There remains one final set of orientational data necessary to fully characterize the interfacial malonic acid. The θ - φ distributions of the carbon atoms show that the acid carbon chain lies flat when at the water surface (0 Å), and tilts with the bisector pointing further into the water bulk when the malonic acid is slightly above the water surface. The ψ - ψ dihedral distributions show one C=O carbonyl bond mostly aligned with the carbon group bisector and the other carbonyl aligned normal to the plane of the carbon atoms. The question remains as to which direction does the latter carbonyl C=O

63

bond vector point? Is it pointed into the aqueous phase of the interface, or does it point out towards the gas phase away from the water bulk?

The carbonyl orientation is determined by calculating the tilt angle of the C=O bond, $\theta_{C=O}$. Like the carbon group bisector tilt angle, $\theta_{C=O}$ is referenced to the axis normal to the plane of the water surface, pointing out towards the gas phase side of the interface. Figure 4.9 shows the angle distribution of $\theta_{C=O}$ plotted as a function of the malonic acid molecular center of mass position. Most of the distribution is isotropic in the tilt angle up to positions several Å beneath the water surface location.
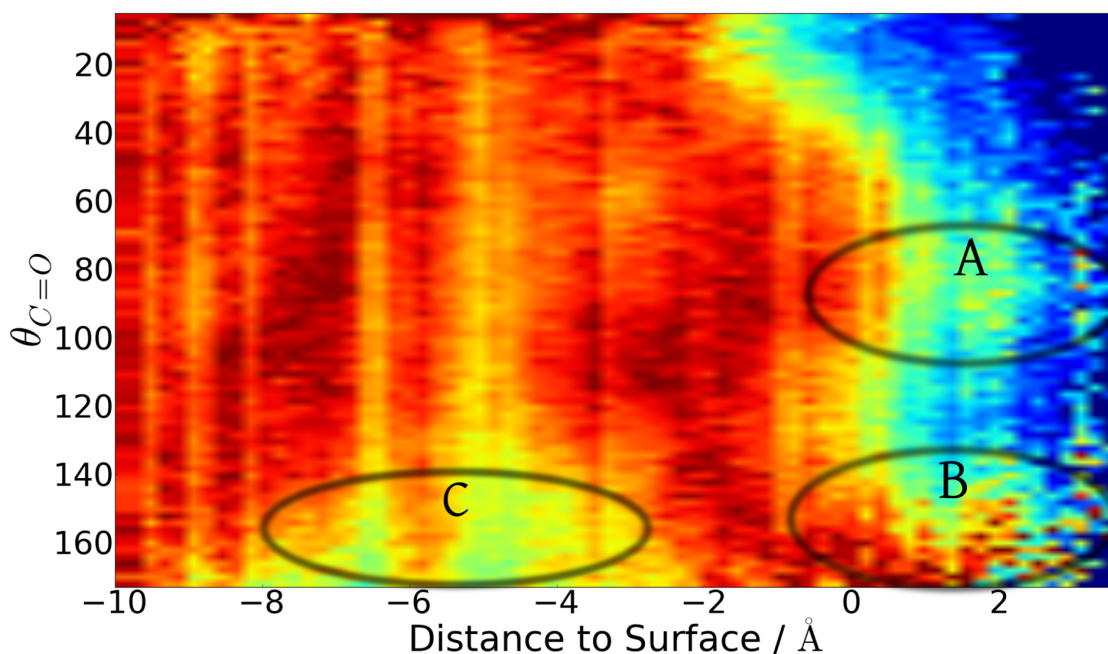
Figure 4.9. Two-dimensional histogram of the carbonyl bond tilt angle $\theta_{C=O}$ plotted against molecular center of mass position.

Starting above the surface (positions > 0 Å), the distribution bifurcates into two distinct angle regions. There is a protrusion in the distribution (region 'A' in Figure 4.9) beginning just below 0 Å and extending above the surface, centered at $\theta_{C=O} = 90°$. A

second peak in the distribution (region 'B') is concentrated towards the bottom of the plot near $\theta_{C=O}$ = 180°. At this position slightly above the water surface, it is more clear that one of the C=O bonds points into the water (the bond oriented near $\theta_{C=O}$ = 180°), and the other points more out into the plane of the surface and often slightly angled out from the water phase. When an acid molecule located at, or just above, the water interface exhibits this internal orientation, it means that one carbonyl bond is oriented pointing more towards bulk water while the other is oriented towards the gas phase.

Further down into the water surface, the angle distribution spreads over a much larger range until becoming isotropic near -2 Å. However, a feature appears at -3 Å and extends down slightly past -8 Å into the water phase (region 'C' in Figure 4.9). In this region there is a decreased intensity in the histogram for $\theta_{C=O}$ > 120°. This shows a population of malonic acid carbonyl C=O bonds pointing less into the bulk water. At this depth, the carbon backbone orientation distribution becomes relatively more isotropic, but there remains a population of acids with θ_{CCC} < 90° (i.e. the carbon group bisector aims further towards the water surface), in agreement with the carbonyl bond behavior, and the carboxylic dihedral orientations.

These orientational distributions paint the following picture of malonic acid orientation broken into interfacial depth regions: 1) Above the water surface the carbon group bisector tilts down towards the water, and the carbonyl bonds orient with one bond pointing towards the water phase, and the other carbonyl bond pointed out of the water either parallel to the plane of the surface, or slightly out towards the gas phase. 2) At the water surface location (0 Å) the carbon group lies mostly flat in the plane of the surface. The methylene C-H bonds align symmetrically above and below the surface. Also, the

carboxylic C=O bonds have a similar orientation to those further out of the water, but the carbonyl bond tilt distribution quickly becomes isotropic just a few Å under the surface location. 3) At -4 Å and down to approximately -6 Å, the carbon group θ - φ distributions broaden and quickly become isotropic. The distribution of the carbonyl bond tilt, $\theta_{C=O}$, shifts intensity at this lower depth leaving a low-intensity region at approximately $120° \leq \theta_{C=O}$. Both carbonyls orient to point more towards the water surface at this depth than slightly above or below. 4) Further down in the water bulk, below -8 Å, the distributions become isotropic and malonic acid assumes bulk-like behavior. The outstanding correlation between the MD results and the experimental results provide confidence in the spectral assignments. The combined use of MD and experiments therefore build a complete picture of the adsorption of malonic acid to the air/water interface.

The results from this study point to a unique geometry at the air/water interface for malonic acid: an intramolecularly bonded ring structure. In this ring structure, which has been seen before in computational studies of gas phase malonic acid,[42,43] the OH mode associated with SSP active C=O is hydrogen bonded to the SPS active C=O to form a stable 6-membered ring. This structure provides an explanation of the frequency differences in the SSP and SPS VSFS spectra of C=O, the strong OH bonding seen in the SSP VSFS spectra of the OH/CH region and the weak solvation at the interface. Preliminary MD evidence has shown this structure to be stable at the air/water interface and calculations are currently being performed to confirm this structure.

pH Dependent Vibrational Spectroscopy

The previous section investigates the adsorption characteristics of malonic acid as a function of concentration. Since malonic acid is a diprotic acid, the protonation state of the adsorbed species is necessary to fully describe the adsorption characteristics. By adjusting the pH, the protonated carboxylic acid will turn into a resonance-stabilized carboxylate ion that completely removes the carboxylic C=O spectral response in this region. Since there are two carboxylic moieties, there are correspondingly two pK_a values. Based on IR bulk studies,[13] the frequency of the singly protonated carbonyl should red-shift as compared to the fully protonated species. Therefore, as the bulk pH is adjusted, malonic acid adsorbed at the interface can be examined for spectral changes indicating deprotonation. This will in turn provide more insight into the bonding environment at the interface.

The pK_a values for malonic acid are 2.85 and 5.70.[44] The percentages of protonated species for the bulk are plotted in Figure 4.10. At a pH of 3, the bulk percentage of the fully protonated malonic acid approaches 40% with the singly protonated form near 60%. At a pH of 4, the fully protonated form should be about 7%, with the singly protonated form at 91% and the completely dissociated form near 2%. At a pH of 6, the fully protonated form should not exist, with a third of the acid molecules being singly protonated and the remaining two thirds completely dissociated.
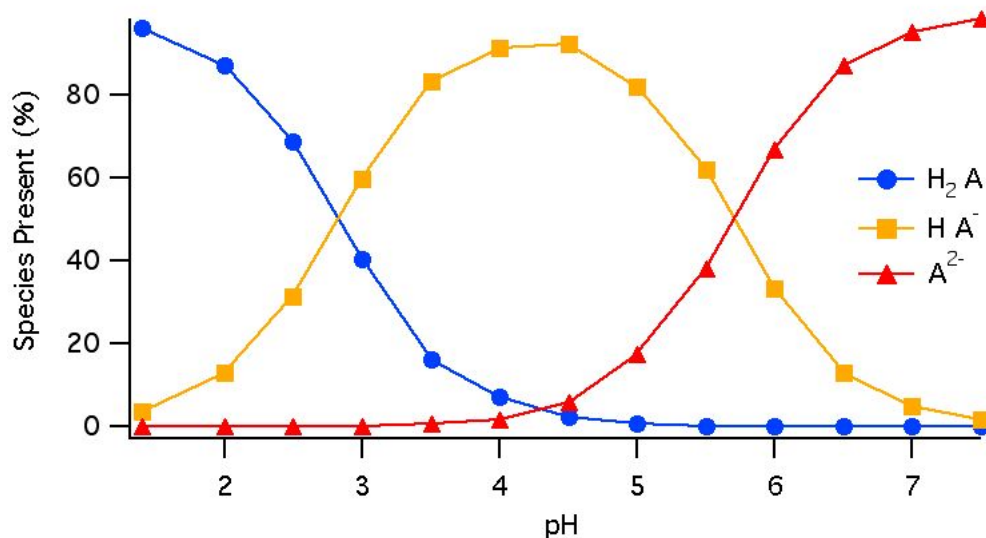
Figure 4.10. Plot of bulk percentages of fully protonated, singly protonated, and fully deprotonated species of malonic acid.

At a constant concentration of acid (1M), the bulk pH was adjusted and fitted spectra of the C=O region were taken in both SSP and SPS schemes. Figure 4.11 shows the spectral response of the malonic acid in the C=O region as a function of bulk adjusted pH as well as spectral fits. The SSP active C=O mode is located at 1741 ± 2 cm^{-1} with a Gaussian width of 28 ± 1 cm^{-1} while the SPS active C=O mode is located at 1731 ± 2 cm^{-1} with a Gaussian width of 35 ± 1 cm^{-1}. The VSFS signal of the C=O mode decreases as the bulk-adjusted pH is increased but does not track the bulk pK_a values closely. At a bulk pH value of 3, the SSP scheme (Figure 4.11a) shows signal with fitted amplitude that, while decreased, compared to the non-pH adjusted solutions, is still clearly present. In the SPS scheme (Figure 4.11b), the signal at pH 3 is very low and is difficult to obtain. The SSP VSFS amplitudes continue to decrease and by a pH of 6, the signal is nearly undetectable.
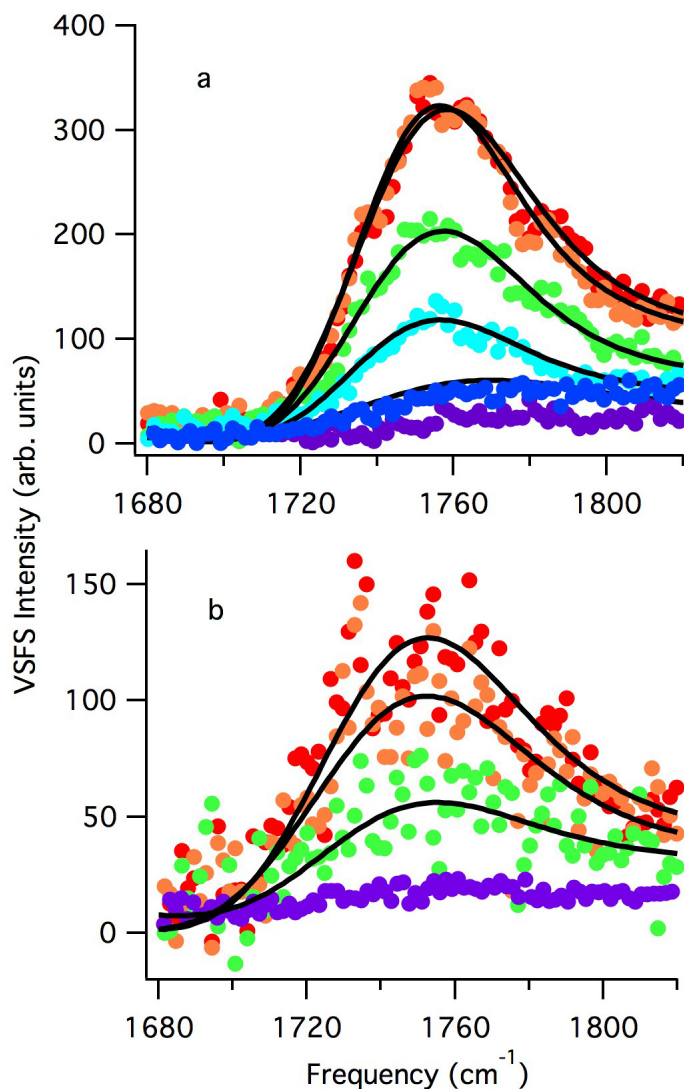
Figure 4.11. VSFS spectra of carboxylic C=O of aqueous malonic acid a) for SSP at 1M with bulk adjusted pH values from native (top) to 6 (bottom) and b) for SPS at 1M with bulk adjusted pH values from native (top) to 6 (bottom).

Attempts were made to probe the COO- region of malonic acid (~1400 cm^{-1}) but no signal could be found for native pH, pH 4, or pH 7 solutions. It would be unlikely to detect signal for a native pH solution since it is dominated by the fully protonated species and thus very little carboxylate exist. Likewise, signal for pH 7 is unlikely since although it is dominated by doubly deprotonated species, the surface tension shows no adsorption

to the interface. According to surface tension measurements addressed in the next section and C=O SSP VSFS measurements, malonic acid is still present at the interface at pH 4. At this pH, over 90% of the molecules (in the bulk) should be in the singly protonated state and therefore signal at pH 4 should be present if there are molecules at the interface. A lack of signal leads to two possibilities: 1) there is no orientational order for a singly or doubly deprotonated species at the interface or 2) that desorption occurs when malonic acid loses a proton. While it is difficult to distinguish between these two options, the invariant frequency in the C=O region as a function of pH would suggest that there is no change to the adsorbed species and therefore the lack of signal is due to the inability of the mono- or di- anion to remain at the interface. This would then indicate that the surface active species is fully protonated malonic acid.

<u>pH Dependent Surface Tension</u>

Surface pressure (left axis) values and the square root of VSFS fitted amplitudes (right axis) versus bulk pH are plotted in Figure 4.12. It is known that NaOH can increase the surface pressure at the air/water interface,[45] so the surface pressure values plotted are corrected by not pure H_2O, but H_2O with the equivalent NaOH added for each corresponding pH value. As the bulk pH is increased, the corrected surface pressure decreases. The surface pressure values follow the square root of the VSFS fitted amplitudes indicating that as the bulk pH is adjusted to higher pH values, malonic acid is desorbing from the surface. If one recalls the bulk pK_a values and the corresponding percentages of species (Figure 4.10), it is clearly evident that both the VSFS and surface pressure values closely follow the percentage of the fully protonated species. When

70

combined with unchanging frequencies of the SSP and SPS active modes and the lack of a detectable COO⁻ signal, these results demonstrate that the surface-active species of malonic acid is the fully protonated form.
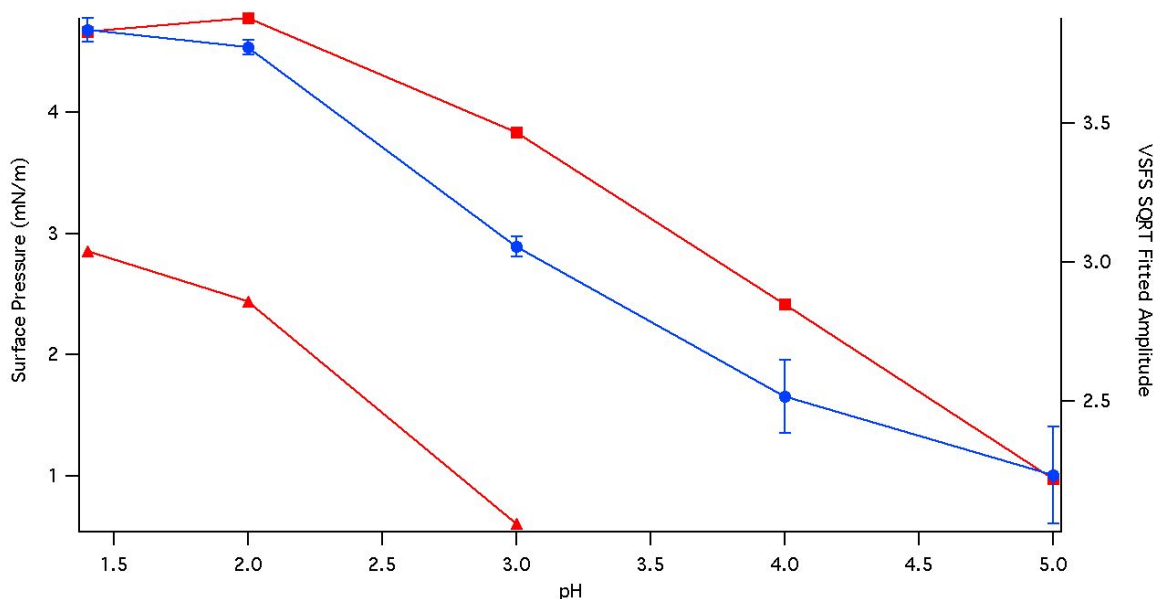
Figure 4.12. Plot of surface pressure in blue (left axis) and square root of fitted VSFS amplitudes for SSP (squares) and SPS (triangles) C=O modes in red (right axis) versus pH for bulk adjusted pH 1M malonic acid.

The results of the concentration and pH dependent spectroscopic and surface tension studies provide an almost complete picture of the adsorption of malonic acid at the air/water interface. As the bulk concentration is increased, malonic acid does not change its orientation due to increased adsorption at the interface. There are two carboxylic acid moieties present at the interface with the higher energy moiety having its dipole pointing perpendicular to the interface and the lower energy moiety oriented in the plane of the bulk. It has been shown that probing these two distinct moieties by adjusting the bulk pH of the solutions results in no observed red-shift of the C=O mode for either

71

polarization scheme. In addition, the fully protonated species has been shown to be the surface-active species, indicating that the surface has only one pK_a value.

Conclusions

By using vibrational sum frequency spectroscopy, surface tension measurements, and MD calculations, the adsorption and orientation of malonic acid to the air/water interface has been fully described. VSFS results in the C=O region demonstrate that carboxylic C=O oscillators have frequencies representative of weak solvation at the air/water interface while VSFS results in the OH region confirm results from surface pressure experiments that malonic acid does not fully saturate the surface. The VSFS and surface tension studies also clearly show that the orientation of the adsorbed malonic acid molecules does not change as a function of concentration. pH studies of malonic acid adsorption demonstrate that the surface-active species of malonic acid is the fully protonated species. Computational results confirm and enhance the conclusions from the VSFS results and provide quantifiable distributions of malonic acid orientation as a function of depth into the water surface.

These results paint a picture of an isolated malonic acid molecule that lies mostly flat on the surface of an aqueous solution and displays no acid-acid interactions at the surface. There is a competition at the interface for the hydrophobic alkane spacer between the two carboxylic ends to remove itself from the water while still allowing the hydrophilic carboxylic ends to be solvated by aqueous phase water molecules. As a result, surface malonic acid is not well solvated and the surface-active species are located in the first layer of water molecules. Malonic acid molecules just a few Ångstroms

deeper into the aqueous phase assume bulk-like behavior. The weak solvation is also apparent due to the fact that the aqueous surface cannot accommodate malonic acid that is partially or completely deprotonated. The rather surprising result of weak solvation and pH dependence invite questions about the surface behavior of succinic acid. Does the addition of a methylene unit along the alkyl backbone cause changes to the solvation of the carbonyls or is there evidence of a ring structure as well? Is succinic also an isolated molecule at the surface or is there evidence of acid-acid surface interactions? Does the additional methylene provide different pH dependencies? This will be explored fully in the next chapter.

CHAPTER V

SUCCINIC ACID AT THE VAPOR/WATER INTERFACE

The adsorption of succinic acid $((COOH)_2(CH_2)_2)$ to the air/water interface was investigated via VSFS, surface tension, and computational calculations. Aqueous succinic acid systems were characterized by varying concentration and pH. Concentration dependent VSFS experiments were corroborated with macroscopic surface tension measurements and demonstrate that succinic acid has weak hydrogen bonding to the water molecules at the air/water interface. The orientation of succinic acid conformations was determined through molecular dynamics and confirms the spectral interpretation. Finally, VSFS and surface tension experiments demonstrate that the surface-active species of succinic acid at the air/water interface is the fully protonated species. The computational work was performed by Nicholas Valley. Deuterated CH spectra were obtained by Stephanie Ota. Some surface tension was performed by Suzzanah Wood.

Introduction

Succinic acid is one methylene unit longer than malonic acid. In terms of atmospheric aerosols, succinic acid is often the most highly concentrated dicarboxylic acid detected in atmospheric aerosols, second only to oxalic acid. It is detected in a variety of urban, rural, and remote locations.[1-10] Sources of succinic acid are both anthropogenic and biogenic in nature, but succinic acid is mainly implicated in secondary organic aerosol formation.

The results from malonic acid demonstrated that the adsorption of a dicarboxylic acid to an air/water interface is not as straightforward as that of a simple surfactant. The

VSFS data indicated very weak solvation at the interface, far from bulk solvation values. Surface tension measurements and VSFS data showed that malonic acid is also isolated at the interface and does not pack tightly enough to cover the surface. Malonic acid was shown to have pH dependent surface adsorption with only the fully protonated species surface active. Although the only difference between malonic and succinic acid is the addition of a methylene unit along the alkyl backbone, these two molecules have drastically different solubilites (along with other differences such as melting point).[11-13] Exploring the C=O response via VSFS provides information about the solvation around the head group as well as orientation. Are there drastic differences between bulk and surface solvation like what was seen for malonic acid? The results of surface tension measurements can corroborate and enhance the spectral analyses. Does succinic acid have a large surface area per molecule or does it pack tightly at the interface? Computational modeling can give depth specific, molecular geometries of aqueous succinic acid. Will succinic acid be "locked" into a specific surface orientation or are there multiple conformations at the surface? It is, therefore, necessary to explore the surface adsorption behavior of succinic acid to determine how this atmospherically relevant molecule behaves at the air/water interface.

<center>Concentration Dependent Vibrational Spectroscopy</center>

VSFS spectra, shown in Figure 5.1 along with the fitted curves in black, of aqueous succinic acid were measured from 1680-1720 cm^{-1} using a SSP polarization scheme in order to measure the C=O mode. The intensity of the signal from the carboxylic C=O modes rises monotonically as the concentration increases from 0.1M to

<center>75</center>

0.5M.   Due to the limited solubility of succinic acid in water (~0.7 M at room temperature),[14] the highest concentration studied here is 0.5M. The presence of signal under the SSP polarization indicates that one or both of the C=O carboxylic modes have a net orientation of its dipole moment components normal to the interface. According to the global spectral fits, there is one peak centrally located at 1722 cm^{-1} +/- 2 cm^{-1} with a Gaussian width of 30 cm^{-1} +/- 2cm^{-1}. There is no observed shift in the frequency of the VSFS signal when bulk concentration is increased.
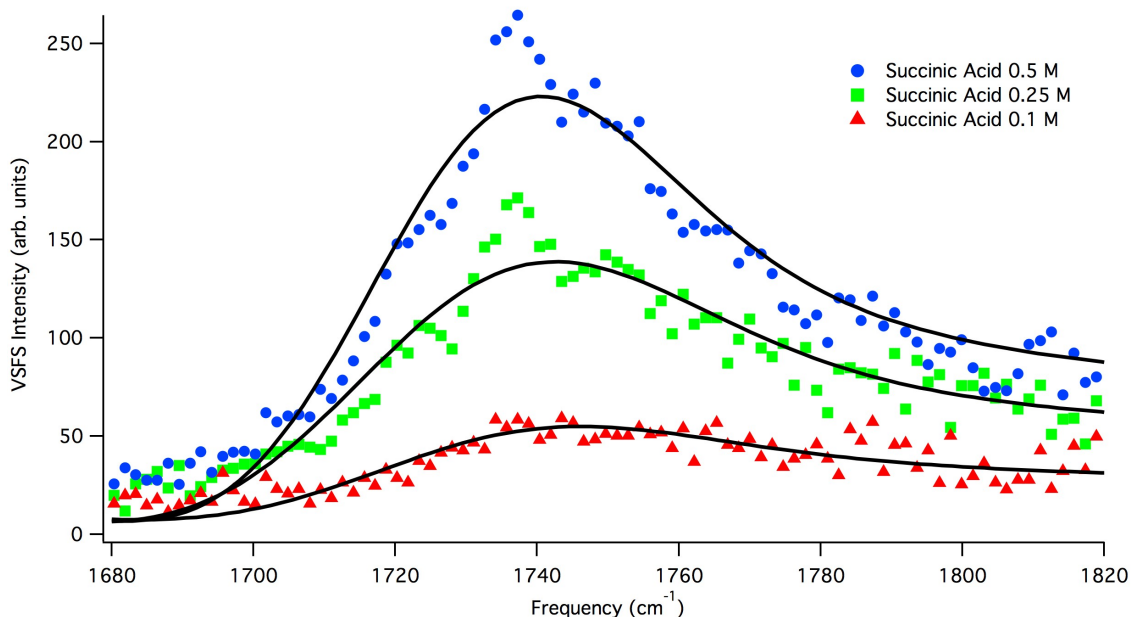
Figure 5.1. VSFS SSP of the C=O region for aqueous succinic acid at 0.1M, 0.25M, and 0.5M. Fits are shown in black.

The carboxylic C=O mode was also probed in the SPS polarization scheme which interrogates the molecular dipole moments parallel to the plane of the interface. Two different concentrations (0.5M and 0.25M) with their corresponding fitted curves are

shown in Figure 5.2. The signal intensity for these modes was less than that probed in SSP. It is important to note that for the VSFS experiments done in the C=O region, the angles used for the visible and infrared beams (and hence the corresponding Fresnel factors) are such that the intensities for the SSP and SPS polarization schemes are comparable. This may not always be the case for VSFS experiments. The presence of signal under the SPS polarization scheme indicates that one or both of the C=O carboxylic acid modes have a net orientation of its molecular dipole moment component parallel to the plane of the surface. The spectra reveal a peak centrally located at 1722 +/- 3 cm^{-1} with a Gaussian width of 30 +/- 1 cm^{-1}. The VSFS intensity increases as the bulk concentration of succinic acid increases, as was seen with the SSP signal. VSFS SPS spectra taken at a concentration of 0.1M did not have strong enough intensity to permit analysis.
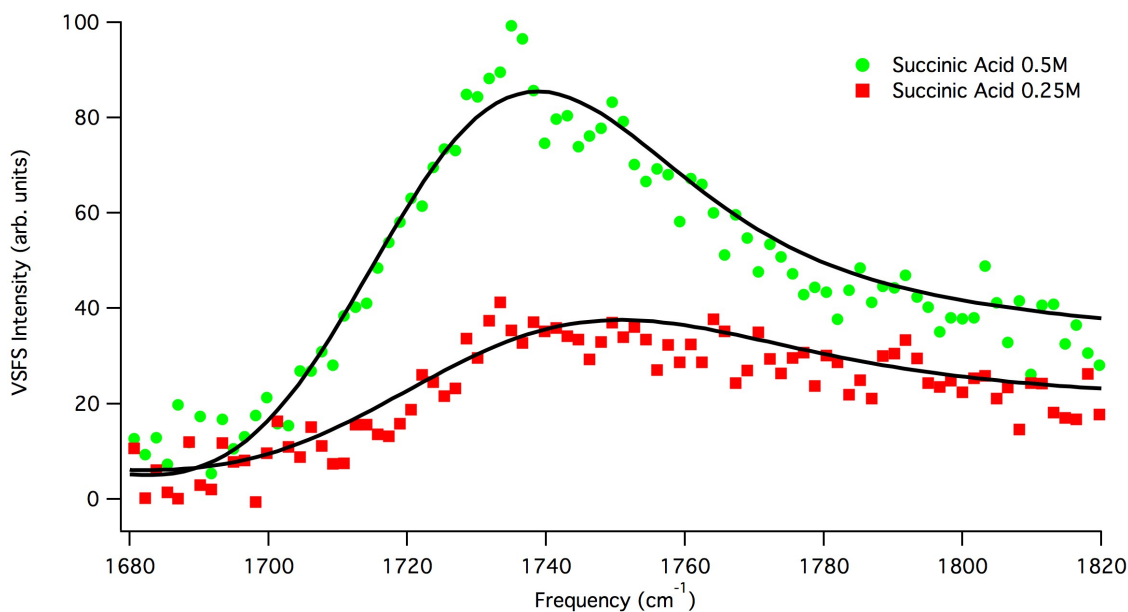
Figure 5.2. VSFS SPS of the C=O region for aqueous succinic acid at 0.25M and 0.5M. Fits are shown in black.

Both the SSP and SPS polarization schemes show a peak located at 1722 cm^{-1} with comparable Gaussian widths. This indicates that the C=O modes for the carboxylic group are experiencing similar solvation environments. It should be noted that the signals detected here are relatively weak so that the normally negligible non-resonant interferes with the resonant signal. This manifests itself spectrally by the signal not returning to zero on the blue side of the spectra. This has been seen before in previous VSFS experiments probing C=O modes[15,16] (including Chapter IV) as well as NO$_2$[17] modes at the air/water interface. It has been postulated[18] that since the non-resonant signal is not spectrally flat over this spectral region, it may be due to the presence of libration overtones and the bending modes of water, similar to IR and Raman spectra of bulk water over the same region.[19-21]

Examining the bulk IR and Raman vibrational responses for aqueous succinic acid can provide information about the solvation of these species at the interface. Infrared studies of aqueous succinic acid have shown the C=O mode for the fully protonated form is located at 1717 cm^{-1} and the C=O mode for the singly protonated form at 1715 cm^{-1}.[22] Raman spectra of saturated succinic solutions show the C=O mode located at 1717 cm^{1} as well.[23] The VSFS results presented here yield slightly higher frequencies at 1722 cm^{-1}. This is not surprising due to the weaker solvation that is typical for an air/water interface. However, the difference in frequencies is only ~5 cm^{-1} indicating that the solvation of the C=O carboxylic mode is only slightly less well solvated than that of a bulk solvated succinic acid molecule.

Surface IR studies[24-26] have shown that specific ranges of C=O frequencies correspond to different hydrogen bonding for long-chain fatty acid monolayers at an

air/water interface. The region from ~1735-1739 cm^{-1}, ~1715-1720 cm^{-1}, and 1700-1704 cm^{-1} are assigned as having non H-bonded, singly H-bonded, and doubly H-bonded character, respectively. Even though it is obvious that long-chain fatty acids and short-chain dicarboxylic acids will have different solvation properties, the trend will be similar for both. VSFS experiments done on other carboxylic containing molecules have shown a range of frequencies as well. The monocarboxylic acids, acetic[15] and hexanoic,[16] were determined to have a central frequency of 1720 cm^{-1}. As was seen in Chapter V, malonic acid was found to have frequencies in the 1730-1740 cm^{-1} range and was shown to be weakly solvated at the air/water interface. Succinic acid has frequencies at ~1722 cm^{-1}, indicating that it would fall into the singly H-bonded region and is indicative of weak solvation at the air/water interface. However, the C=O mode for succinic acid is more solvated than its slightly smaller counterpart, malonic acid.

Succinic acid has been studied previously via VSFS in the infrared region probing the OH and CH$_2$ stretching modes.[27] The results of these studies as pertaining to the work here are briefly reviewed. VSFS spectra were taken in both SSP and SPS polarization schemes. In addition, isotopic substitution of hydrogen for deuterium was used extensively for unambiguous peak assignment. Spectral fitting in this region is greatly complicated by overlapping resonances and therefore deuteration of the solvent, the methlyenes, and the carboxylic acid acidic proton were varied to confirm spectral assignment. A peak located at 2945 cm^{-1} with a Gaussian width of 12 cm^{-1} corresponds to the CH$_2$ mode seen in both SSP and SPS in both H$_2$O and D$_2$O . There is a broad response at 2940 cm^{-1}, which is attributed to the interaction between the carboxylic OH and water or other OH acid groups. Exchange of carboxylic acid protons in D$_2$O revealed

the removal of the   broad response at 2940 cm^{-1}. Deuteration of only the methylenes in H$_2$O removed the sharp peak at 2945 cm^{-1} but retained the broad 2940 cm^{-1} response. These three experiments therefore unambiguously determine the methylene response at the vapor/water interface for succinic acid.

There were changes to the VSFS air/water spectrum in the H$_2$O region for solutions of succinic acid indicating adsorption to the interface. There was minor suppression of the free OH at 3700 cm^{-1}, which are uncoupled OH oscillators residing at the top most layer as well as the appearance of a new peak at 3660 cm^{-1}. When a molecule has complete coverage at the interface, significant suppression of the free OH is expected. The suppression of the free OH is very minor and indicates that succinic acid is not packing tightly at the interface.[28] The presence of the intensity at ~3660 cm^{-1} is due to the solvation of ions and small molecules[29-31] at the interface and arises from the increased pH of these solutions in comparison to neat water. There is also suppression of intensity for the strongly coordinated modes at 3200, 3335, and 3460 cm^{-1}. This drop in intensity results from the adsorption of succinic acid disrupting the hydrogen-bonding network and is another indication of adsorption at the interface. Finally, increased intensity also develops at 3080 cm^{-1} which has been attributed to a highly coordinated hydrogen bonding environment and has been seen for strongly acidic solutions.[32,33]

The VSFS experiments, therefore, unambiguously show that succinic acid adsorbs to the air/water interface. The solvation of the head groups is in line with monocarboxylic acid studies and indicates that while succinic acid is weakly solvated at the interface, the solvation is stronger than that of malonic acid. The presence of new peaks associated with acidic adsorption (3660 cm^{-1} and 3080 cm^{-1}), as well as

suppression of the coordinated OH region, further demonstrate adsorption of succinic acid. The free OH response is only slightly diminished signifying that the surface of these aqueous solutions do not become fully packed. Finally, intensity arising from the CH_2 and COOH hydroxyl modes are identified using isotopic substitution.

<u>Concentration Dependent Surface Tension</u>

Surface tension of succinic acid was measured for concentrations of 0.1, 0.25, and 0.5M and is in good agreement with previous experiments.[34-36] The surface area per molecule was determined to be ~191 $Å^2$/molecule via the surface excess calculated from the Gibbs adsorption equation.[37] The area per molecule gives an idea of how tightly the molecules are packed at an interface. This comparatively large molecular area of 191 $Å^2$/molecule for succinic acid corroborates the VSFS data in the water region where there was a small decrease in the free OH signal and confirms that succinic acid does not pack tightly at the air/water interface.

The surface pressure values are plotted with the square root of VSFS fitted amplitudes (the concentration dependence of the sum frequency field is the square root of the intensity)[38] for SSP and SPS experiments in the C=O region in Figure 5.3. As the bulk concentration of succinic acid is increased, there is an increase in the surface pressure as well as both SSP and SPS C=O VSFS signals. Due to the limited solubility of succinic acid in aqueous media (~0.7M),[14] it is impossible to attain bulk concentrations in the molar range. In addition, solutions higher than 0.5M were close enough to the solubility limit that issues with crystallization became apparent in samples prepared for both VSFS experiments as well as surface tension measurements. The plots indicate that

the orientation of succinic acid does not undergo large changes to the orientation as a function of concentration.
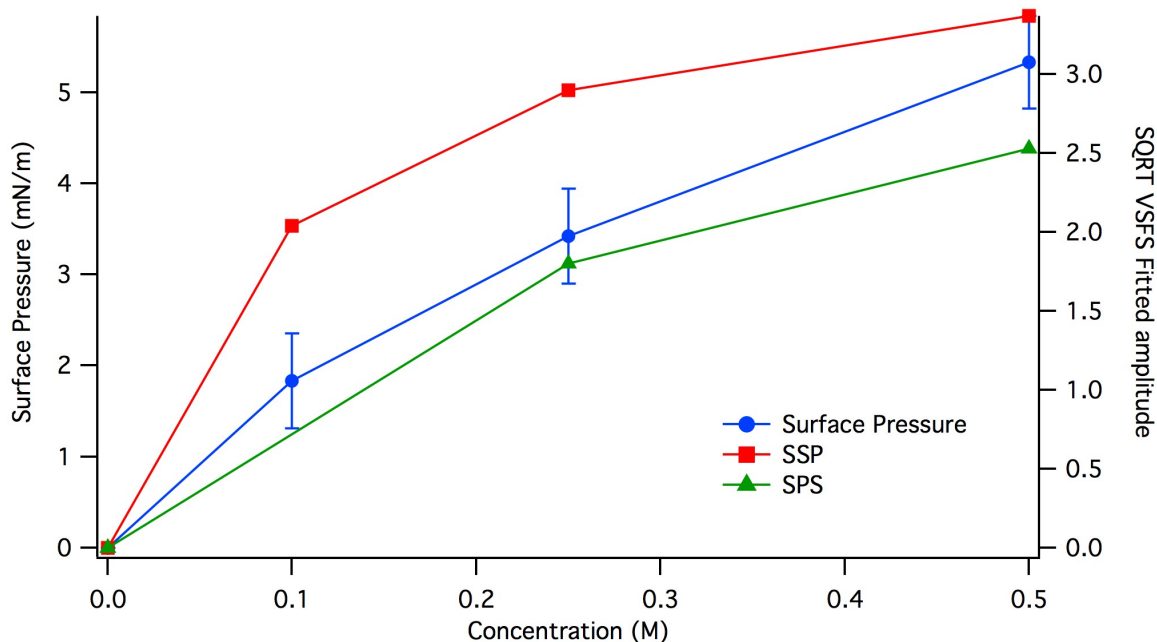
Figure 5.3. Plot of Surface pressure and square root of VSFS fitted amplitudes for SSP and SPS versus aqueous succinic acid concentrations.

To confirm the invariance of orientation as a function of concentration, the Frumkin equation was used to determine the surface excess concentrations for each bulk concentration.[37]   The surface excess concentrations are plotted against the fitted VSFS amplitudes for the C=O SSP and SPS spectral data in Figure 5.4. The linear dependence of the data for both polarizations suggests that there are no large changes in orientation of succinic acid at the vapor/water interface as the bulk concentration is increased. Claims made about linear changes in orientation from 0.1M (which there was insufficient signal

to permit analysis for SPS) to 0.25M are not possible except through extrapolation. This
will be examined in further detail in the computational section.
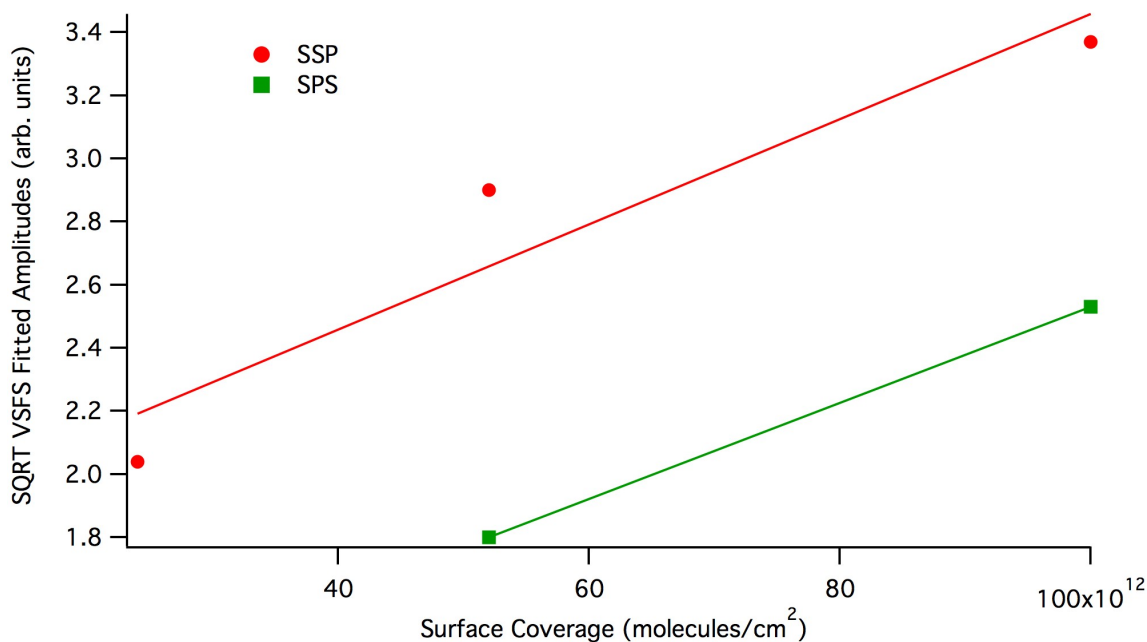
Figure 5.4. Square root of VSFS fitted amplitudes versus surface coverage of succinic
acid.

The surface tension experiments performed as a function of concentration on
succinic acid adsorption at the air/water interface confirm and enhance the results from
VSFS experiments. The area per molecule is quite large for such a small molecule
indicating that it is isolated at the surface. This corroborates the VSFS frequencies
indicating weak solvation at the interface. The constant frequency and Gaussian width
for the various concentrations support the assertion that the orientation at the interface
does not change dramatically as a function of concentration for succinic acid. In

addition, the presence of a clear free OH signal indicates that succinic acid doesn't pack tightly at the interface resulting in destruction of the free OH signal.[28]

<div align="center">Computational Calculations</div>

Confirmation of experimentally observed VSFS signal from succinic acid molecules through MD and DFT calculations require an understanding of both the conformation of the molecules and their orientation relative to the water surface. A density profile was computed for the system as an initial check of the robustness of the MD trajectory. Analysis of the computed density profile for succinic acid in water shows an increase in concentration of acid molecules at the water/vacuum interface (located from ~5Å below the interface to directly at the interface), which after a small dip in concentration, levels off to a moderate concentration in the bulk. Only a small percentage of succinic acid molecules appear above the water surface. Stability of the calculations is confirmed by fitting the water density profile to a hyperbolic tangent function as can be seen in Figure 5.5. These results confirm that the simulations are behaving similarly to experimental observations.

Unlike malonic acid, the torsional freedom from an additional methylene unit along the carbon backbone results in a much larger sample of structures. Thus, it is more difficult to classify the orientations of these molecules. In order to appreciate the results, molecular conformations were studied using both density functional theory and MD calculations. Geometries of stationary point structures from the DFT calculations were used as a set of structures to represent those found in the MD trajectory. This fitting was
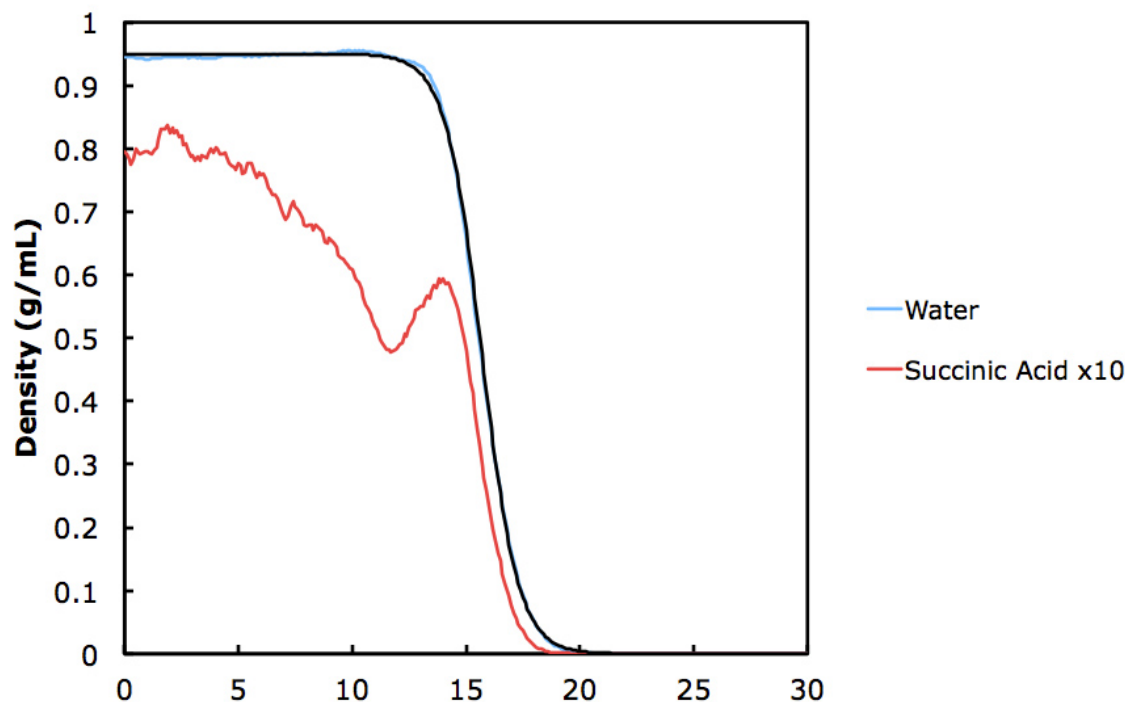
Figure 5.5. Density profile of 0.5M succinic acid from the MD trajectory.

performed through examination of numerous torsions and dihedral angles in the
molecules. A range was defined around the values of each angle obtained from the DFT
calculations. Only conformations that substantially contribute (>2% of total) to the
average state of the molecule are discussed here. Ignored structures account for
approximately 3 percent of all structures in the molecular dynamics calculations. Figure
5.6 displays structures of 6 of the stationary points found for succinic acid in the DFT
calculations. All geometries shown correspond to local minima on the gas-phase
potential energy surface. The conformations in Figure 5.6 are identified first by whether
the carbon backbone is anti or gauche (A or G) and then by whether a carboxylic unit is
eclipsed (e). The eclipsed form is defined as the plane of the carboxylic moiety lying in
the same plane as a CH bond from the methylenes. Therefore, the conformation Ae is in

anti conformation with one carboxylic eclipsed, while the conformation Gee has a gauche

backbone with both carboxylic moieties eclipsed.
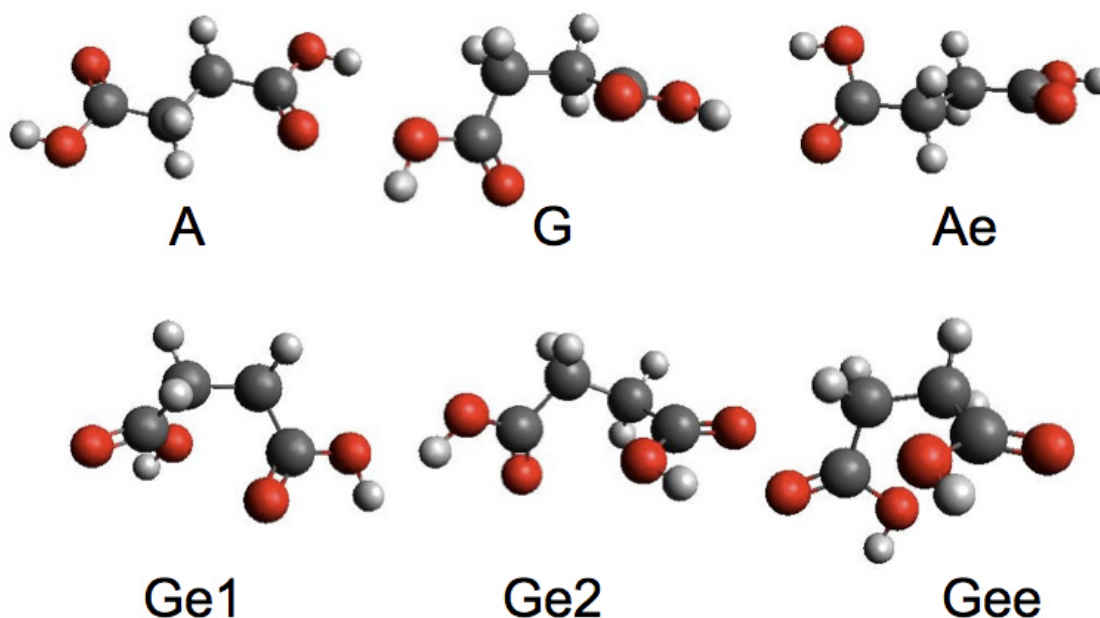
Figure 5.6. DFT stationary structures representative of MD geometries.

After each conformation in the MD trajectory is matched with one of the representative DFT structures, the contribution at different depths relative to the surface in the MD calculations was analyzed. The results for each concentration are shown in Figure 5.7. At almost all depths at 0.12 M, structure A is the most common, followed by G and Ae. At 2 Å below the water surface, structure A sees an increase from the bulk. Conformation G is always the most common structure at the higher concentrations (0.25 M and 0.5 M). This increase occurs mainly at the expense of the A and Ae conformers.
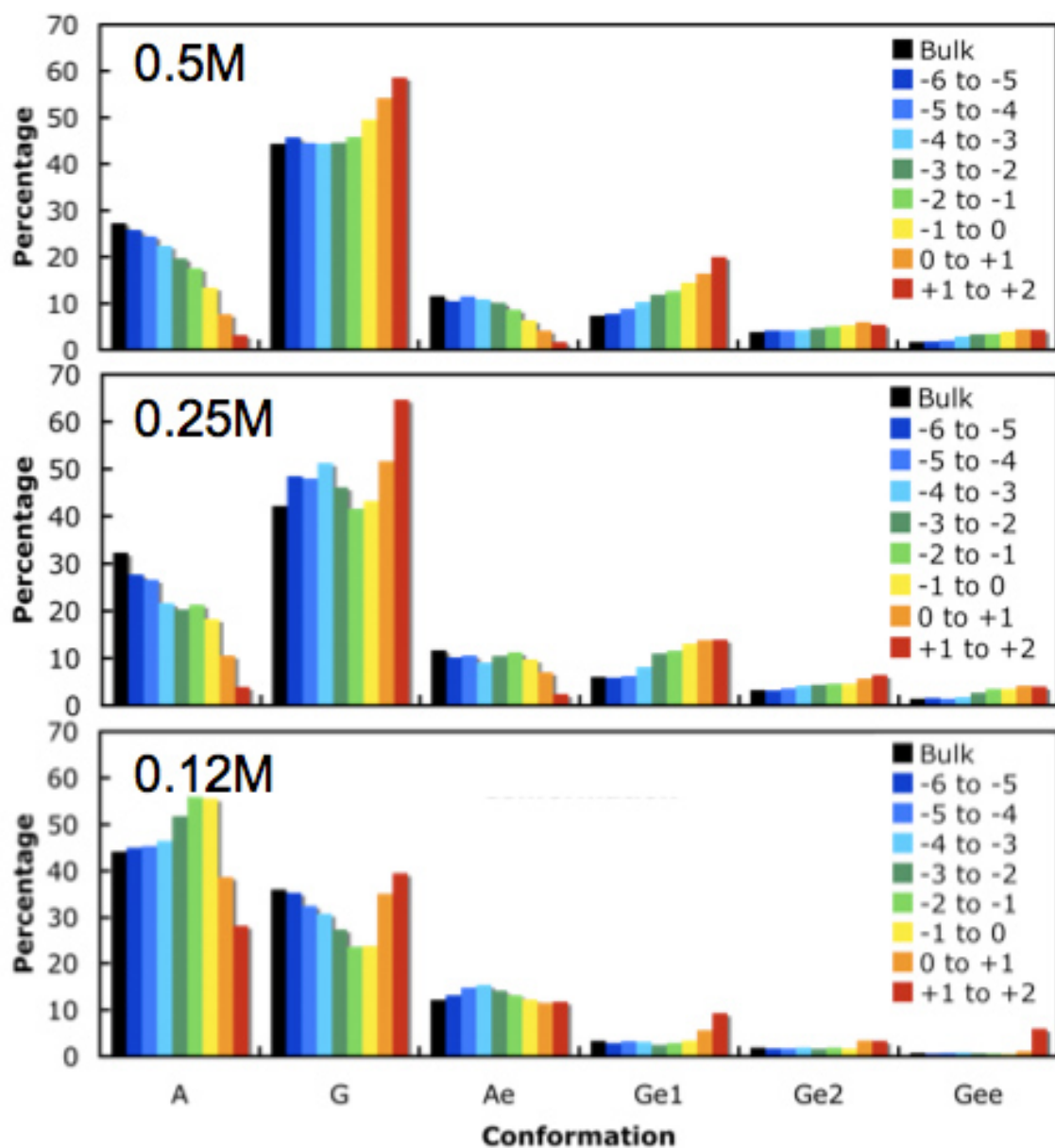
Figure 5.7. Percentage of conformations as a function of depth for representative structures of succinic acid at 0.12M, 0.25M and 0.5M concentrations.

As the concentration of succinic acid is increased, the population percentage of the family of G structures increases while the population percentage of the family of A structures decreases as these molecules approach the interface. The G family of structures have the methylene backbone twisted so that there will be a net orientation of their dipoles active in SSP or SPS. This is unlike the A family which would have the net

dipole from the methylene backbone either weak or negligible due to oppositely oriented dipoles. This indicates that the orientation of succinic acid molecules at the interface prefer a gauche conformation over an anti conformation in the carbon backbone. The spectral analysis of the VSFS signal in the CH region did show the presence of a CH_2 signal (albeit weak). The MD trajectory corroborates the assertion that gauche twists along the carbon backbone provide CH_2 dipoles that would be SSP and SPS active in the VSFS spectra.

The next step necessary to describe the orientation of succinic acid molecules is the C=O pointing direction for the different conformations. The depth specific orientations of the C=O for the G conformation are shown in Figure 5.8. These plots show an angle range from 0° to 180°. 0° is defined as normal to the surface, pointing away from the bulk and 180° as normal to the surface, pointing towards the bulk. An angle of 90° therefore describes a carbonyl pointing in the plane of the surface.

As can be seen in Figure 5.8, there is no preferred orientation of the carbonyls at and near the bulk (-6 to -5Å). This stands in contrast to malonic acid. In that study, the carboxylic acid planes are "locked" in an orientation about 90º apart. This reflects the torsional freedom resulting from an extra methylene along the alkyl backbone. Upon approach to the interface, the succinic acid molecules begin to orient the carbonyls in a preferred direction with one carbonyl tilted in the plane with the other carbonyl tilted downward towards the bulk. At the interface, this distribution becomes even more narrowed and it is clear that there is an anisotropic orientation of the carbonyls.
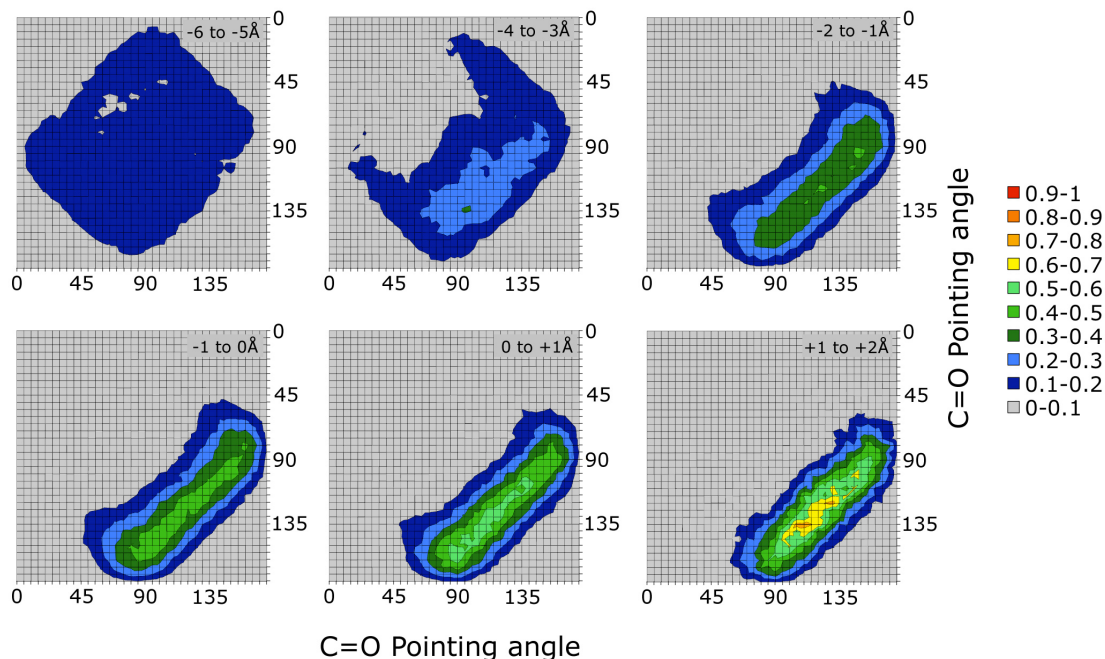
Figure 5.8. Carbonyl pointing direction angles for G conformation of 0.5M succinic acid. Depths are in the top right corner of each plot. The percentages are shown at the right.

In Figure 5.9, the C=O pointing direction of the Ge1 conformation is shown. At depths of -6 to -5Å, there are C=O directions spanning from near 0º to 180º, but for all angles, the two C=O pointing directions are roughly in the same direction. For example, if one carbonyl is pointing at 45º, the other carbonyl is pointing in a range from around 30º to 60º with the highest distribution near 45º. This is due to the orientation of the carbon backbone, which sterically forces the two carbonyl moieties to point in the same direction. However, there is no clear orientation of the carbonyl group. As succinic approaches the interface, a change occurs where the carbonyl pointing direction becomes more oriented, adopting an orientation that is between the plane of the interface and pointing directly down. This reflects the desire for the hydrophobic methylene groups to reside away from the aqueous phase while simultaneously allowing the hydrophilic

carboxyl groups to stay solvated. This conformation once again shows that there are gauche defects in the carbon backbone and that the carboxyl groups orient at the surface in a manner that is consistent with the spectral analysis from VSFS spectra.
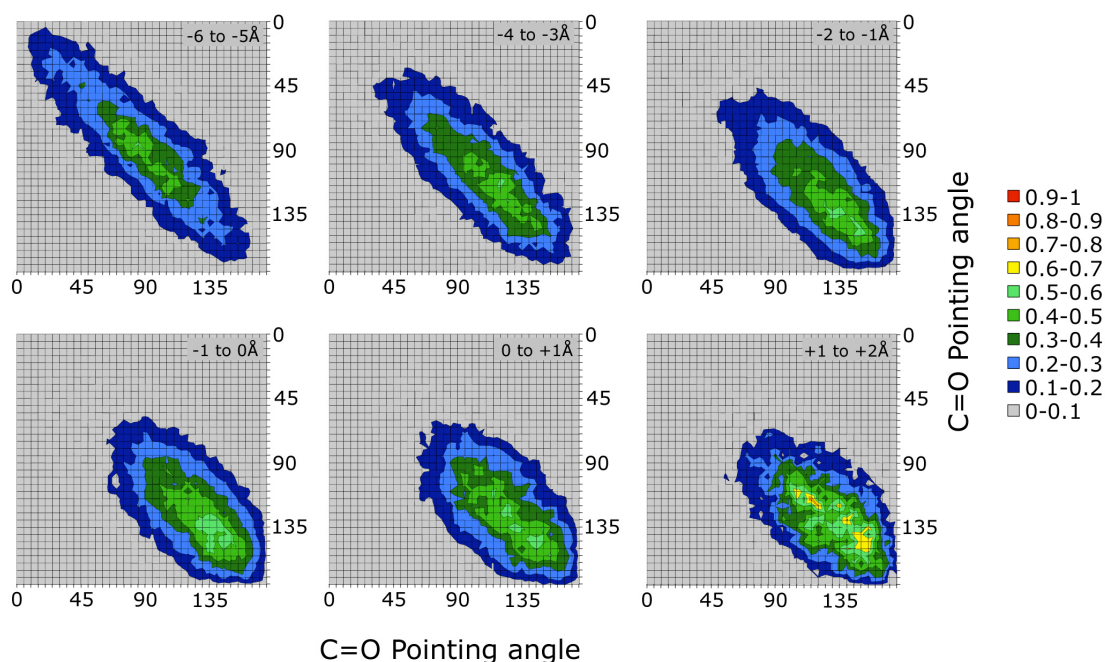
Figure 5.9. Carbonyl pointing direction angles for Ge1 conformation of 0.5M succinic acid. Depths are in the top right corner of each plot. The percentages are shown at the right.

These results confirm the experimental conclusions derived from VSFS spectra. The C=O signal intensity for succinic acid was shown to be equivalent for SSP and SPS active modes. The peak frequency (~1722 cm^{-1}) showed a C=O mode that was less solvated than bulk succinic acid (~1717 cm^{-1}). A weak but detectable CH$_2$ signal was found in VSFS and the structures that would contribute to this were found to increase at the interface. Additionally, the depth specific percentages of conformations for the different concentrations confirm and elucidate the surface tension results.

<u>pH Dependent Vibrational Spectroscopy</u>

Since succinic acid is a diprotic acid, the protonation state of the adsorbed species is necessary to fully characterize the adsorption characteristics. When the pH of these solutions is adjusted to higher pH values, the carboxylic acid will turn into a resonance stabilized carboxylate ion thus removing any response from VSFS experiments in the carbonyl region. There are two carboxylic moieties and therefore two different pK_a values. According to bulk IR studies,[22] there are frequency differences between the fully and singly protonated species. By adjusting the bulk pH of the solutions and monitoring the adsorption of succinic acid through VSFS and surface tension measurements, the adsorption behavior can be fully understood.

The pK_a values for succinic acid are 4.19 and 5.48.[39] At a pH of 4, the fully protonated species represent about 60% with the remaining species being singly prononated. At a pH of 5, the fully protonated species only makes up about 12%, with the singly protonated species dominating the solution at around 72% and the fully dissociated species making up about 16%. At a pH of 6, there is virtually no doubly protonated species left (0.5%), with a third of the species being singly protonated and the remaining two-thirds completely dissociated.

At a constant concentration (0.5M), the bulk pH was adjusted and VSFS data was taken in both SSP and SPS schemes. Figure 5.10 shows the spectral response of succinic acid in the C=O region for SSP as a function of bulk adjusted pH as well as the respective fits. The spectral fits reveal a peak centrally located at 1724 +/- 2 cm^{-1} with a Gaussian
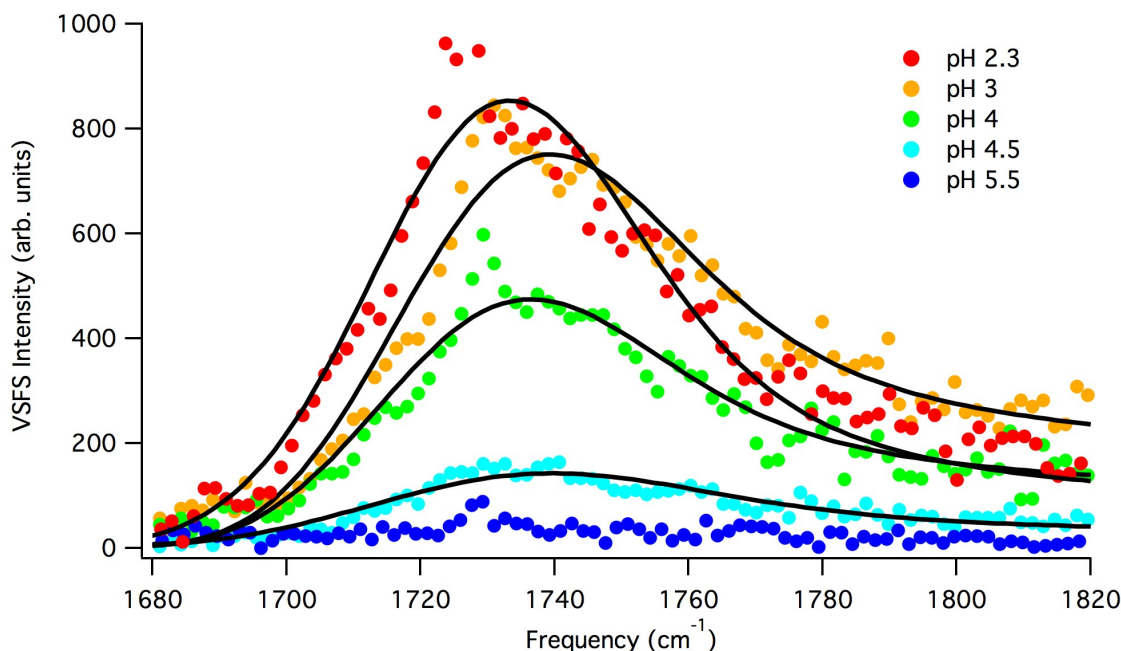
Figure 5.10. VSFS SSP of bulk pH adjusted 0.5M succinic acid in the C=O region. Fits are shown in black.

width of 35 +/- 2 cm^{-1}. There is little to no change in intensity for pH of 3 and the intensity decreases monotonically as the pH increases. At a pH of 5.5, there is essentially no VSFS signal remaining in the C=O region.

Figure 5.11 shows the spectral response of succinic acid in the C=O region for SPS as a function of bulk adjusted pH as well as the respective fits. The spectral fits reveal a peak centrally located at 1722 +/- 2 cm^{-1} with a Gaussian width of 35 +/- 2 cm^{-1}. As was seen for SSP, the change in intensity for pH of 3 is negligible and the intensity decreases monotonically as the pH increases. At a pH of 5.5, there is once again no VSFS signal remaining in the C=O region. Attempts were made to probe the carboxylate region (~1400 cm^{-1}) for succinic acid solutions of a high pH (4 and above) but no VSFS signal was found. The VSFS results in the C=O region therefore provide evidence that the surface-active species of succinic acid is the fully protonated moiety.
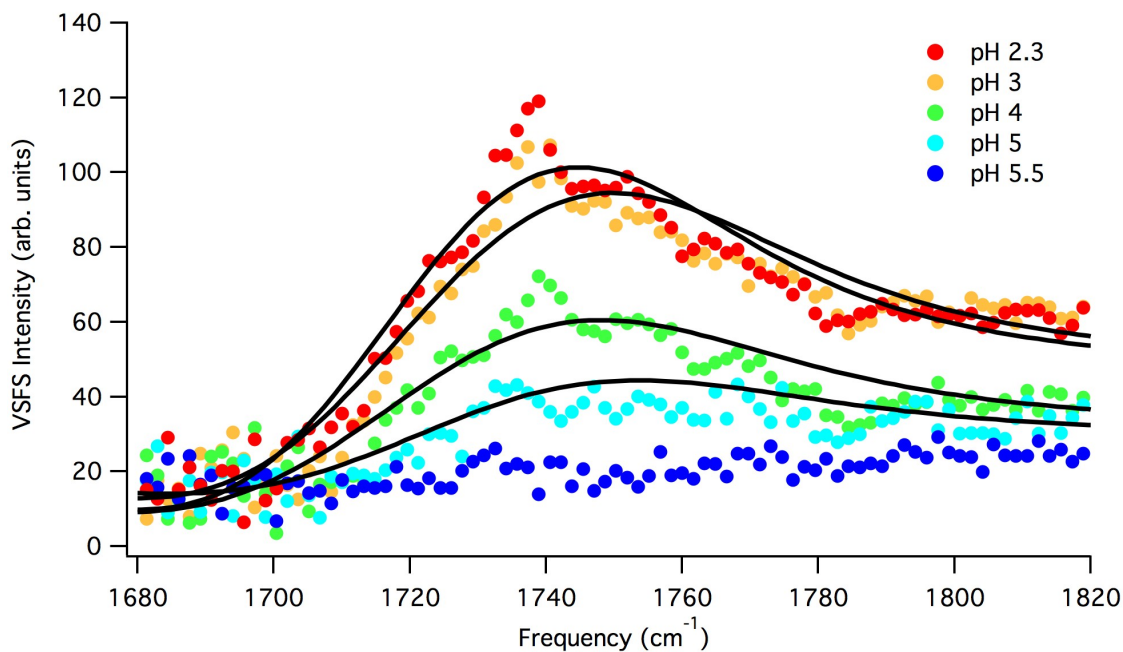
Figure 5.11. VSFS SPS of bulk pH adjusted 0.5M succinic acid in the C=O region. Fits are shown in black.

By using another mode that is does not undergo changes as a function of pH, the surface dependence can be elucidated further. Malonic acid (Chapter IV) displayed no discernible signal arising from CH modes in the region between 2700 and 3000 cm^{-1}. However, there is a small peak arising from the methylenes in the alkane backbone of succinic acid. Therefore, it is possible to interrogate the pH dependence of succinic acid using the CH region. The VSFS SSP response in D_2O was taken between 2700 and 3200 cm^{-1} (CH region) and is shown in Fig 5.12. There are four traces overlaid with each other. The black trace shows the response to D_2O only and the red trace shows the response of succinic acid (0.25M) in D_2O. The pH of succinic acid was adjusted by
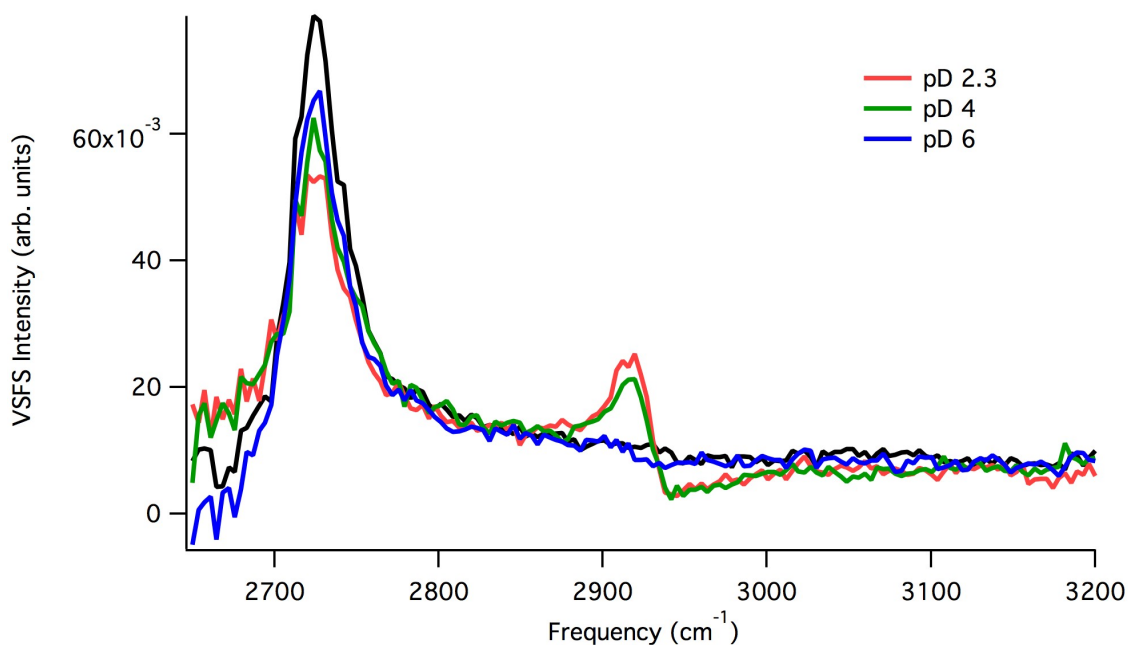
Figure 5.12. VSFS SSP of bulk pD adjusted 0.5M succinic acid in D_2O in the CH region.

NaOD with the green trace adjusted to pD of 4 and the blue trace adjusted to pD of 6. As the pD is adjusted from native to pD 4, there is a decrease in the CH signal as was seen with the C=O experiments. When the pD was further adjusted to pD 6, the response from succinic acid disappears. These results provide further evidence that the surface-active species is the fully protonated succinic acid moiety.

pH Dependent Surface Tension

The pH adjusted VSFS experiments provide convincing evidence that the surface-active species of succinic acid is the fully protonated moiety, although, this can be confirmed by employing surface tension measurements. The surface pressure is the difference in the surface tension of the sample from the neat water value. The surface pressure as a function of pH is displayed as well as the percentage of protonated species

in the bulk (based off pK$_a$ values) are shown in Figure 5.13. The decrease in surface

pressure as the bulk pH is increased follows the percentage of fully protonated species
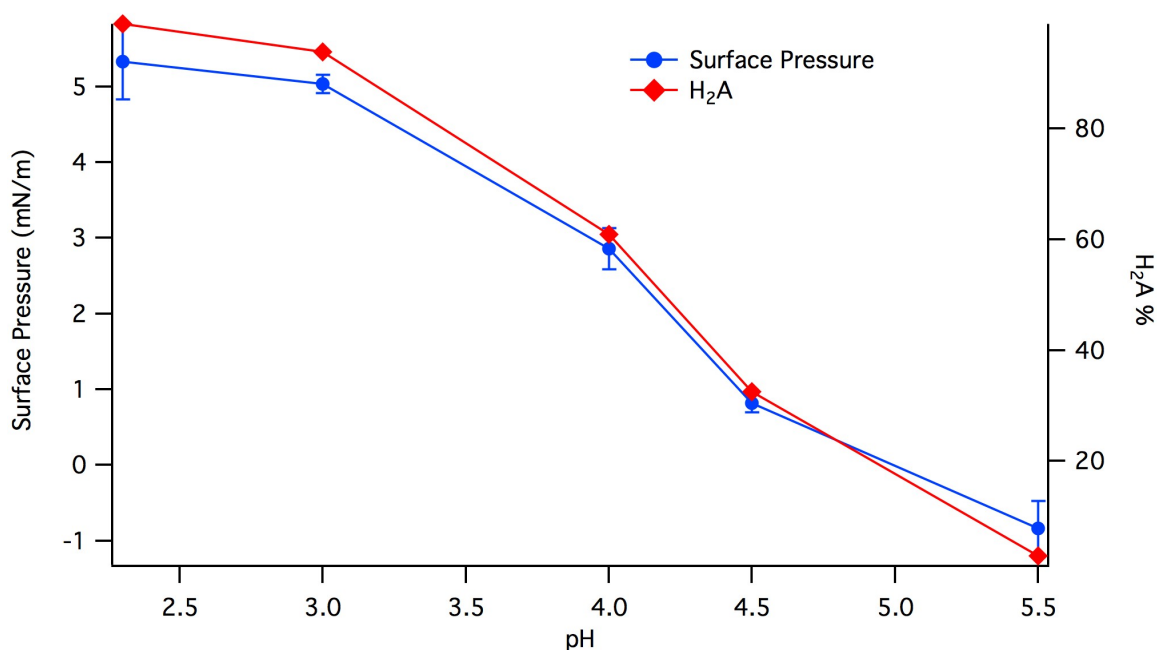
Figure 5.13. Surface pressure of 0.5M succinic acid and percentage of fully protonated species versus bulk pH values.

closely. The surface pressure decreases as the pH increases indicating that succinic acid

is desorbing from the interface as the bulk pH of the solutions is adjusted. Shown in

Figure 5.14 is surface pressure of bulk pH adjusted succinic acid (left axis) as well as the

square root of the fitted amplitudes for both SSP and SPS C=O VSFS (right axis). The

square root of the fitted amplitudes from the VSFS C=O experiments follow the decrease

in surface pressure as the bulk pH is increased as well, finally attaining values indicative

of no organic adsorption for both experiments. By using VSFS in the C=O and CH region

as well as surface tension measurements, it is now clear that the surface-active species of succinic acid is the fully protonated species.
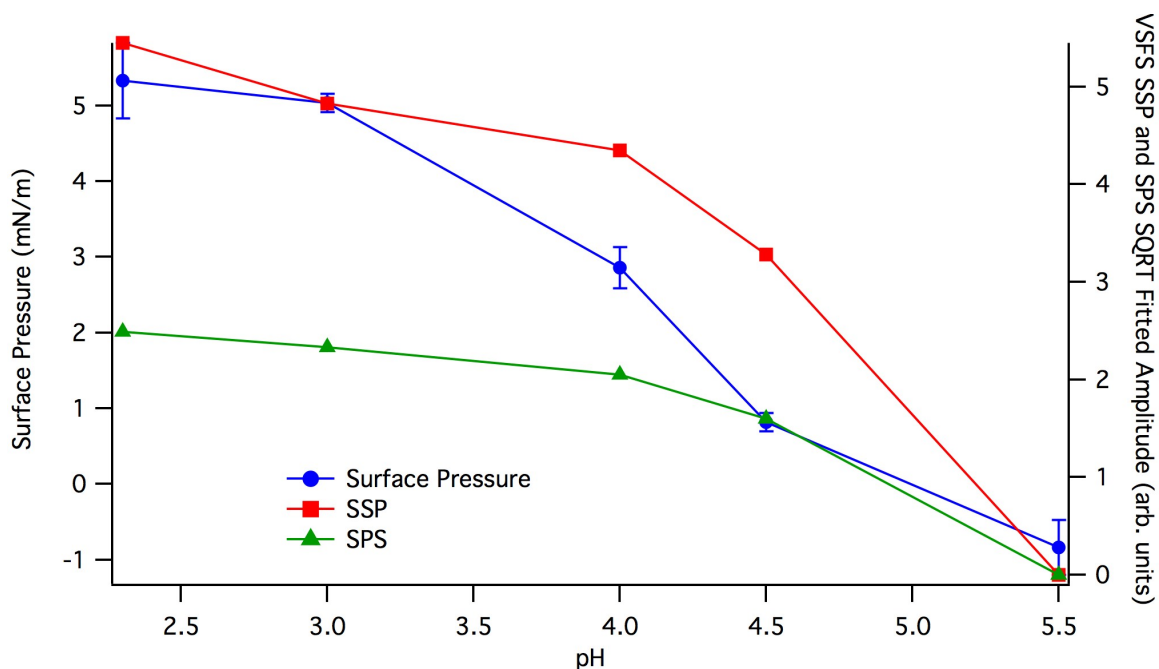
Figure 5.14. Surface pressure and square root of VSFS fitted amplitudes versus (SSP and SPS) bulk pH of succinic acid

Conclusions

Succinic acid is widely found in various aqueous forms throughout our environment and this study characterizes the surface adsorption via a combination of surface spectroscopy, thermodynamics, and computational modeling. By investigating the concentration and pH dependence of succinic acid through VSFS and surface pressure measurements, the adsorption of succinic acid is characterized. The VSFS concentration data reveals that both the SSP and SPS C=O signals yield similar frequency responses

indicating that the carboxylic C=O experience the same solvation environment whether it is pointing normal to the interface or parallel to it. By coupling the surface tension data to the VSFS data, it has been shown that the orientation of succinic acid doesn't change greatly as a function of concentration and is isolated at the interface. In addition, the adsorption of succinic acid disrupts the water network at the air/water interface and gives rise to a weak but detectable CH signal. The use of computational calculations confirms the experimental VSFS results and provides further illumination on molecular geometries responsible for VSFS signal. Finally, the pH dependence of succinic acid was explored and found that the surface-active species is the non-dissociated species.

Although the difference between malonic and succinic acid is seemingly small, the addition of a methylene unit along the alkyl chain induces changes in the adsorption of succinic acid at the air/water interface. This work naturally introduces the question of what happens as the carbon backbone is increased further? Does the solvation remain weak like that similar to a surfactant, or does it change? Does the increased hydrophobicity of the alkyl backbone change the pH dependency of the surface adsorption? These issues will be addressed in the next chapter.

CHAPTER VI

GLUTARIC ACID AT THE VAPOR/WATER INTERFACE

In this chapter, the adsorption of glutaric $((COOH)_2(CH_2)_3)$ acid to the air/water interface is investigated via VSFS, surface tension, and computational calculations. Characterization of the aqueous system is through concentration and pH dependence. Careful correlation of concentration dependent experiments using polzarized VSFS as well as macroscopic surface tension measurements reveal that glutaric acid has concentration dependent solvation to the water molecules at the air water interface. The orientation and conformations of surface adsorbed glutaric acid is determined through molecular dynamics and enhances the spectral interpretation. Finally, VSFS and surface tension experiments demonstrate that the surface-active species of glutaric acid at the air/water interface is not as strongly dependent upon pH as the shorter chain dicarboxylic acids. The computational work was performed by Nick Valley. The water spectra were taken by Katy Plath. Some surface tension data was taken by Suzzanah Wood.

Introduction

Glutaric acid is one methylene unit longer than succinic acid. Glutaric acid is not detected in as high concentrations in atmospheric aerosols as malonic or succinic acid yet it is still one of the most commonly detected aliphatic dicarboxylic acids. Glutaric acid is postulated to have direct sources (anthropogenic and biogenic),[1-4] but it is believed to form mainly in secondary organic aerosol reactions. These SOA reactions come from

precursors of both longer chain molecules (such as mono and di-carboxylic acids) but also from common atmospheric organic cyclic species such as cyclohexene.[5,6]

Through the investigations presented in Chapter IV and Chapter V on malonic acid and succinic acid, respectively, it is obvious that the behavior of short chain dicarboxylic acids at the air/water interface is more complex than simple adsorption. The results from those studies indicated that these molecules lie "flat" at the interface, with the carbon backbone generally along the plane of the surface. This orientation is a result of the balance between the hydrophilic carboxylic groups and the hydrophobic carbon backbone. The behavior of these acids stands in contrast to a typical surfactant, which has its carbon backbone pointing away from the interface. Results from surface tension measurements indicate that these molecules are isolated at the interface and do not pack tightly together.

There are also differences in the solvation of the head groups. The addition of a single methylene unit along the carbon backbone of malonic acid resulted in much better solvation of the carbonyl mode for succinic acid. However, the methylene addition did not change the pH dependence of surface adsorption for both dicarboxylic acids. In each case, the fully protonated species is the surface active one. By continuing to investigate the role an additional methylene units plays, more information on the class of low molecular weight, aliphatic dicarboxylic acids and their adsorption to the air/water interface can be determined. The combination of VSFS, surface tension, and computational modeling experiments, are used once again to investigate the surface adsorption of glutaric acid in molecular detail.

Concentration Dependent Vibrational Spectroscopy

VSFS spectra of the C=O carboxylic mode of aqueous glutaric acid measured in the SSP polarization scheme with fitted curves are shown in Figure 6.1. The intensity of the VSFS signal increases monotonically as the bulk concentration is increased from 0.1M to 1M but there is a noticeable decrease in signal for a bulk concentration of 3M. Because the intensity of a VSFS active mode is determined by number density and net orientation, the decrease in C=O intensity for 3M may be a result of lower number density, a change in orientation, or a combination of both. This will be addressed in depth in the surface tension section. Nonetheless, there clearly is adsorption of glutaric

Figure 6.1. VSFS SSP spectra of aqueous glutaric acid in the C=O region for 0.1, 0.5, 1, and 3M concentrations. Fits are shown in black.

acid to the air/water interface with a net orientation of C=O molecular dipole moments normal to the interface. Global fits of the VSFS spectra provide a central peak located at 1715 +/- 1 cm^{-1} with a Gaussian width of 34 +/- 1 cm^{-1} for concentrations up to 1M. The fits provide a peak for the 3M solution centrally located at 1712 +/-1 cm^{-1} with a Gaussian width of 35 cm^{-1}.

The SPS polarization scheme was also used to probe the adsorption of glutaric acid to the air/water interface. The spectra along with the respective fitted curves are plotted in Figure 6.2. The intensity of the signal is less than that of the corresponding SSP. The presence of signal under the SPS polarization scheme once again indicates that one or both of the C=O carboxylic acid modes has a molecular dipole moment with components parallel to the plane of the water/vapor interface. The global fits reveal a peak centrally located at 1718 +/- 2 cm^{-1} with a Gaussian width of 32 +/-1 cm^{-1}. The VSFS signal intensity increases with increasing concentration from 0.5M to 1M, but does not increase for concentrations above 1M. According to the global fits, the 3M solution has a slightly decreased amplitude (7.7 vs 7.4) that is between the amplitudes for the spectra taken at solution concentrations of 0.5M and 1M. The use of surface tension measurements will compliment both the SSP and SPS spectral data and aid in their interpretation. The combined approach will distinguish between changes in the number density and a change in orientation at the interface.

Similarly to the spectral data in the previous chapters, the non-resonant signal interferes with the resonant C=O mode. This manifests itself spectrally through interference with the blue-side of the spectra presented and results in the VSFS signal not
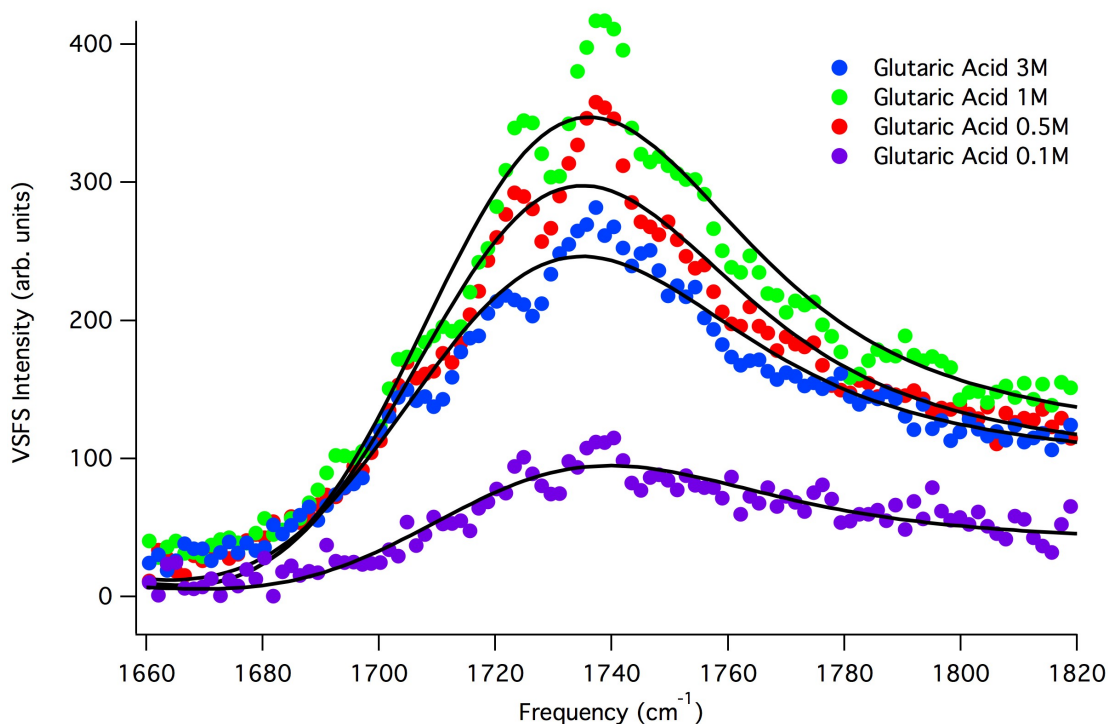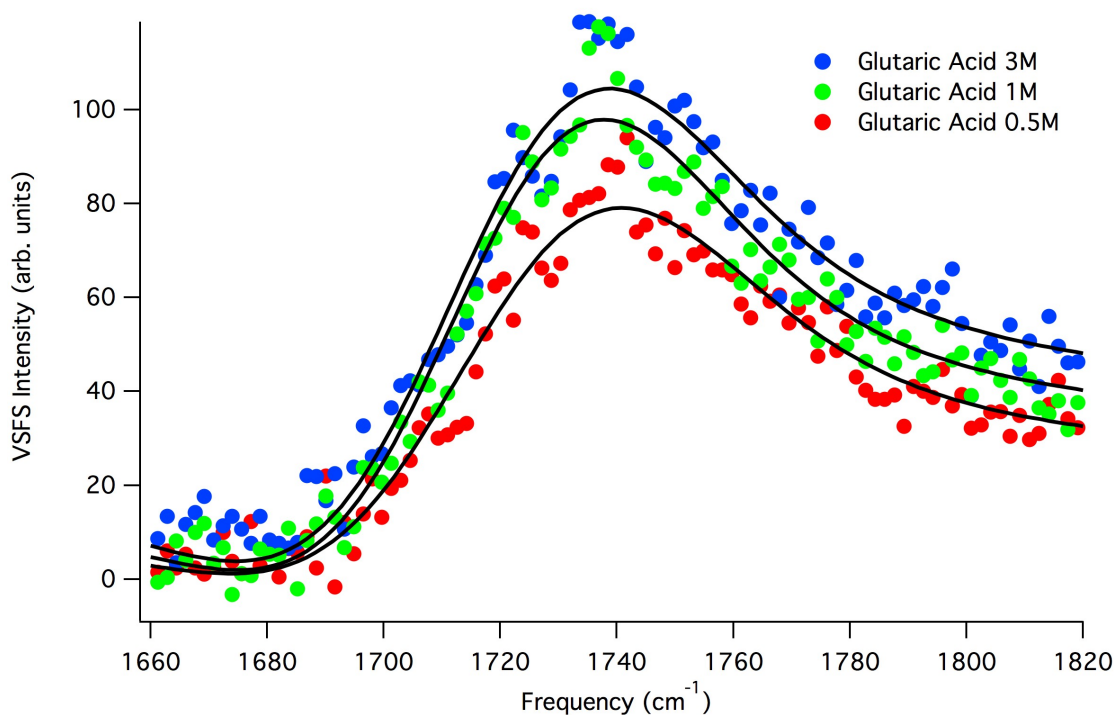
Figure 6.2. VSFS SPS spectra of aqueous glutaric acid in the C=O region for 0.5, 1, and 3M concentrations. Fits are shown in black.

returning to zero on the blue-side of the spectra. The interference with the non resonant signal does not change the spectral interpretations made; this phenomenon has been seen before in previous VSFS experiments at the air/water interface of both C=O modes[7] as well as NO_2 modes.[8]

The C=O mode has been shown to be sensitive to hydrogen bonding with different frequencies reflecting the solvation around the C=O. Bulk aqueous IR values for the C=O of fully protonated glutaric acid have been recorded at 1709 cm^{-1} and the C=O for a singly protonated glutaric acid located at 1707 cm^{-1}.[9] A Raman study on glutaric acid particles found an aqueous Raman transition for the C=O mode[10] located at 1710 cm^{-1}. A combined IR and Raman study found the C=O mode for aqueous glutaric acid at 1707 cm^{-1} for IR and 1715 cm^{-1} for Raman.[11]

102

Surface IR[12-14] studies have shown that specific ranges of C=O frequencies correspond to different hydrogen bonding for long-chain fatty acid monolayers at an air/water interface. The region from ~1735-1739 cm^{-1}, ~1715-1720 cm^{-1}, and 1700-1704 cm^{-1} are assigned as having non H-bonded, singly H-bonded, and doubly H-bonded character, respectively. While long-chain fatty acids and short-chain dicarboxylic acids will have different solvation properties, the trend will be similar for both. Glutaric acid would fall into the singly bonded character based on these assignments.

More detail about C=O solvation can be obtained when glutaric acid is compared to VSFS experiments on similar molecules. Hexanoic acid, a monocarboxylic acid, was investigated with VSFS and was found to have a C=O central frequency[15] at 1720 cm^{-1}. As seen in Chapter IV, surface adsorbed malonic acid has C=O frequencies higher than hexanoic acid (~1730-1740 cm^{-1}) while surface adsorbed succinic acid had C=O values very similar to hexanoic acid (~1722 cm^{-1}) as seen in Chapter V. Based on the frequency response of the C=O from glutaric acid, it appears that the carboxylic end groups have slightly stronger solvation (i.e. more bulk-like) than their monocarboxylic counterparts. In addition, the steric hindrances that led to the orientation and solvation of malonic and succinic acid at the air/water interface are alleviated by the carbon backbone torsion that is available for glutaric acid. This will be explored further in the computational section.

The VSFS SSP response of 1M glutaric acid with fitted curve in the OH region is plotted in 6.3. The VSFS spectrum of neat water is plotted in gray, glutaric acid in red, and spectral fit to glutaric acid in black. It is evident that there are dramatic changes to the water region with the addition of glutaric acid. The free OH response, while greatly diminished, does not completely disappear. This indicates that the water surface is not

completely covered by glutaric acid and that a small percentage of water molecules remain at the surface with decoupled OH oscillators. Above 3600 cm^{-1}, there is also a new peak formed at ~ 3630 cm^{-1}. This peak has been attributed to the solvation of ions and small molecules in previous VSFS investigations of the vapor/water interface.[16-18]
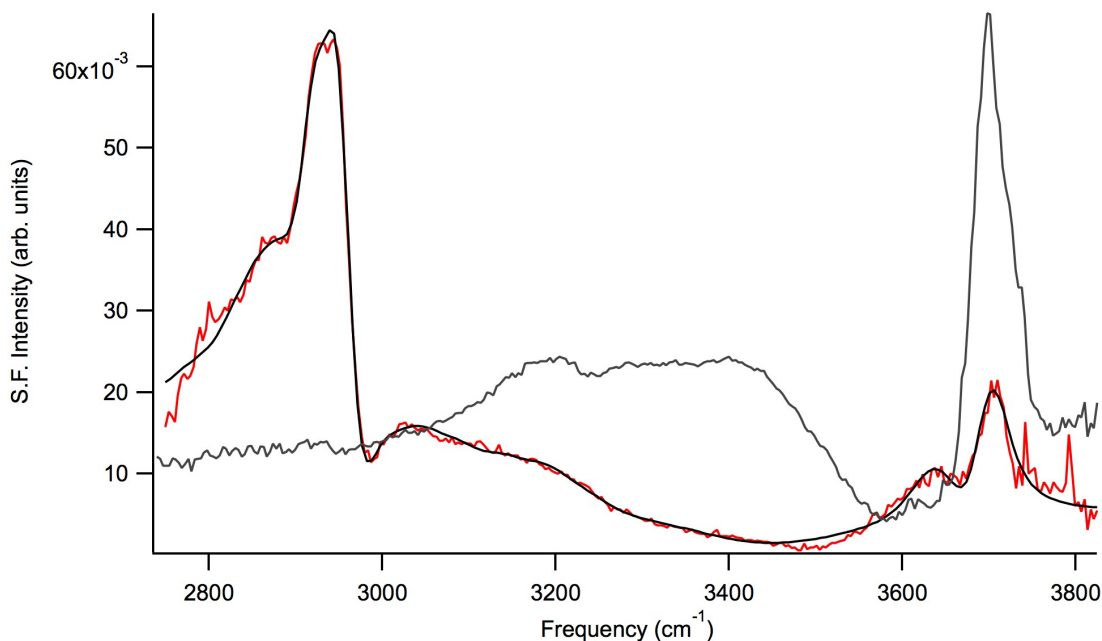
Figure 6.3. VSFS SSP spectra of 1M glutaric acid in the CH/OH region. The pure water spectrum is shown in black and the fit is shown in gray.

Below 3600 cm^{-1}, there is a large decrease in signal for the strongly coordinated OH region. The presence of glutaric acid clearly disrupts the coordination of water in this region. A new peak located at ~3060 cm^{-1} appears that has been attributed to strong hydrogen bonding and cooperative motions of hydrogen bonds. These have been seen for aqueous solutions of strong acids.[19,20] This spectral feature demonstrates that glutaric acid is adsorbing to the air/water interface with specific features indicative of hydrogen

bonding from acidic species. In addition, a broad peak centered at 2940 cm^{-1} gives intensity to the region between 2800 and 3200 cm^{-1}. This peak, which was seen and unambiguously identified with succinic acid, is assigned to the OH stretches of the carboxylic group of glutaric acid. While there is small intensity for the water peaks between 3200-3400 cm^{-1}, the two peaks at 3060 and 2900 cm^{-1} are mainly responsible for the intensity between 3400 and 2800 cm^{-1}, with the obvious exception of the CH$_2$ stretches.

The OH region gives another piece of the puzzle of the bonding environment of glutaric acid at the vapor/water interface by providing information about solvent structure changes. The presence of glutaric acid severely disrupts the strongly coordinated region and diminishes the free OH response. However, even at a bulk concentration of 1M, the free OH signal does not completely disappear indicating that glutaric acid does not completely cover the water surface. New peaks associated with acidic hydrogen bonding also appear due to the increased pH of the solutions in comparison to neat water.

While the changes to the OH region due to glutaric acid are similar to the other diacids studied (e.g. malonic and succinic acid), there are marked differences in the CH region. Intensity between 2800-3000 cm^{-1} results from CH$_2$ modes, with the exception of the broad OH response from the carboxylic OH. According to bulk IR and Raman studies, the CH$_2$ fundamental symmetric stretches (ss or d+) are assigned as the band near 2850 cm^{-1}, the antisymmetric CH$_2$ (as or d$^-$) are assigned as the band near 2890 cm^{-1}, and the Fermi resonance (FR) of the overtone state of the CH$_2$ bending mode with the fundamental ss mode as the band near 2940 cm^{-1}. The above frequencies can shift by a few wavenumbers depending upon their chemical environment.[21] While these bulk

spectroscopic studies provide a framework for the interpretation of VSFS active modes, the differences between bulk and surface solvation environments result in different assignments of the vibrational mode.

As can be seen in Figure 6.3, a large peak appears at ~2930 cm^{-1} with a shoulder ~2880 cm^{-1}. Overlapping resonances of OH modes interfere with CH modes making analysis more difficult. By eliminating the OH modes from water, better assignment of the CH_2 modes is possible. VSFS SSP spectra of glutaric acid was therefore taken in D_2O, as seen in Figure 6.4. In fitting the spectra seen in Figure G4, it becomes clear that there are three distinct spectral peaks. These peaks appear at 2877 cm^{-1} with a Gaussian width of 9 cm^{-1}, 2925 cm^{-1} with a Gaussian width of 10 cm^{-1}, and 2952 cm^{-1} with a Gaussian width of 16 cm^{-1}. The peak at ~2750 cm^{-1} is the uncoupled OD stretch, analogous to the free OH. Attempts to fit with more peaks in the CH_2 region did not improve the quality of the fits. The peak positions for the CH_2 modes were then used in the H_2O spectral fits. The peak positions determined in the D_2O data fit well to the H_2O CH_2 peaks, confirming their position. Additionally, these values are in general agreement with bulk aqueous glutaric acid Raman values for the CH_2 mode found at 2945 and 2912 cm^{-1}.[11]

The clear presence of CH_2 modes in the VSFS SSP spectra demonstrate and confirm the adsorption of glutaric acid to the interface. In addition there are more CH_2 peaks present for glutaric than succinic (one peak) or malonic (no peak). This may be due to the increase in the number of methylene units, an orientation of the methylene units, or a combination of both. Since there is intensity arising from the CH_2 modes, there is most
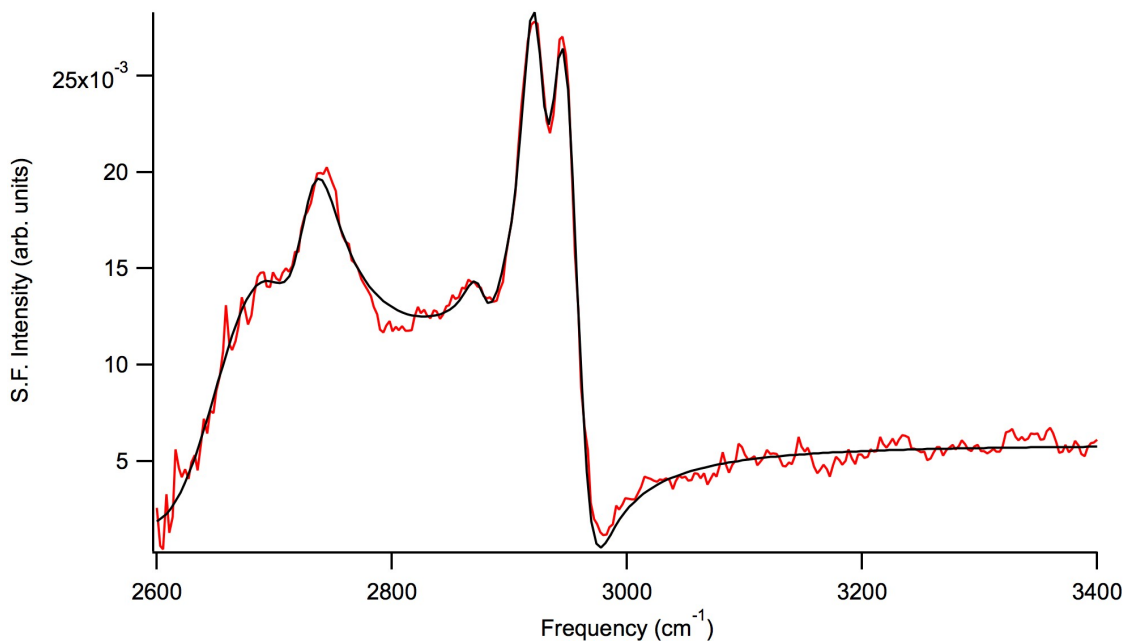
Figure 6.4. VSFS SSP spectra of glutaric acid in D_2O. Fit is shown in black.

likely some torsion along the carbon backbone resulting in gauche configurations. To accommodate the solvation of the C=O modes, the carbon backbone must twist in such a way to maximize this solvation while also allowing the hydrophobic CH_2 modes to orient away from the aqueous phase. This will be explored further in the computational section.

Concentration Dependent Surface Tension

The surface tension of glutaric acid was taken for bulk concentrations of 0.1, 0.5, 1, and 3M (shown in Figure 6.5). The surface tension results agree well with previous investigations by other laboratories.[22,23] The Gibbs adsorption equation is employed[24] (using the activity coefficient from Clegg and Seinfeld[25]) to obtain the surface excess concentration. From this, the area per molecule was calculated to be 117 $Å^2$/molecule.

This relatively large molecular area (for example, hexanoic acid is calculated to be ~60 $Å^2$/molecule)[15] corroborates the VSFS data from the water region where the free OH signal did not disappear at 1M and confirms that glutaric acid does not pack tightly at the air/water interface. However, in comparison to malonic and succinic acid, this area per molecule
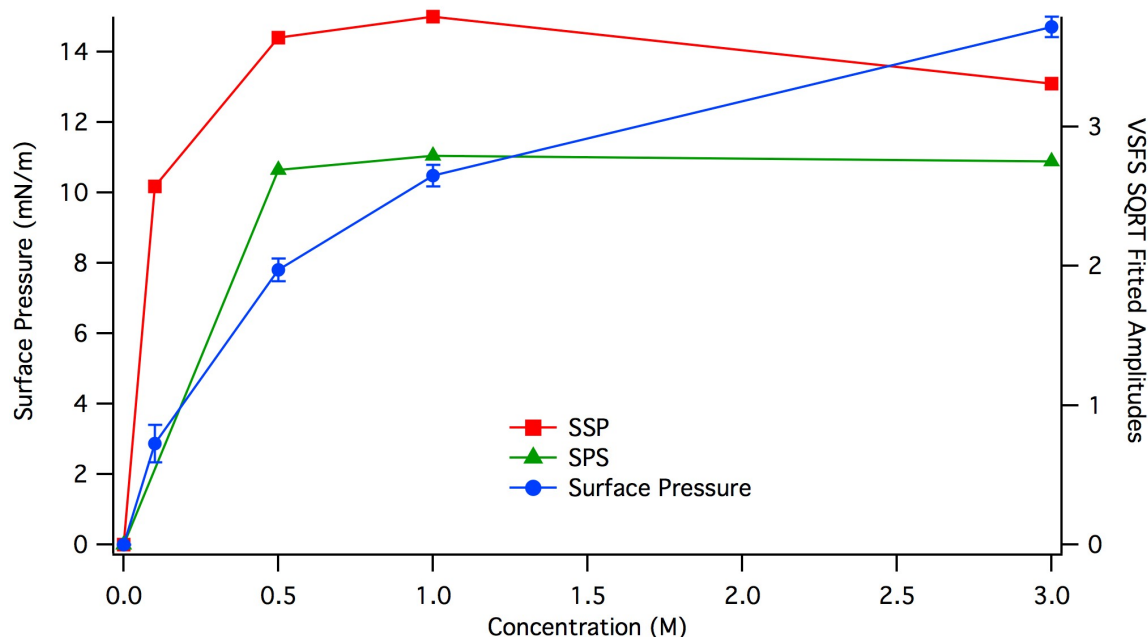
Figure 6.5. Surface pressure and square root of fitted VSFS amplitudes plotted versus concentration.

is much smaller (~190 $Å^2$/molecule vs ~120 $Å^2$/molecule) and indicates that glutaric acid molecules at the air/water interface are more likely to interact due a smaller area per molecule at the surface.

The surface pressure values and the square root of VSFS fitted amplitudes (both SSP and SPS) of the C=O region for glutaric acid are plotted in Figure 6.6. As the bulk concentration of glutaric acid is increased, there is an increase in the surface pressure.

108

The increases in the square root of the VSFS C=O signal (the concentration dependence of the sum frequency field is the square root of the intensity)[26] as a function of concentration for SSP and SPS show similar behavior and follow the changes in surface pressure over the same concentration range. This would then suggest that the adsorption of glutaric acid is invariant with concentration. In order to confirm this, the surface coverage as a function of concentration is calculated. The surface coverage was calculated via the Frumkin equation.[24] The surface excess concentrations are plotted against the VSFS fitted amplitudes for the C=O SSP and SPS spectral data in Figure 6.6. As can be seen in the figure, there is a noticeable decrease in the fitted amplitudes for the SSP and SPS at 3M. The surface excess concentrations (which are a reflection of the
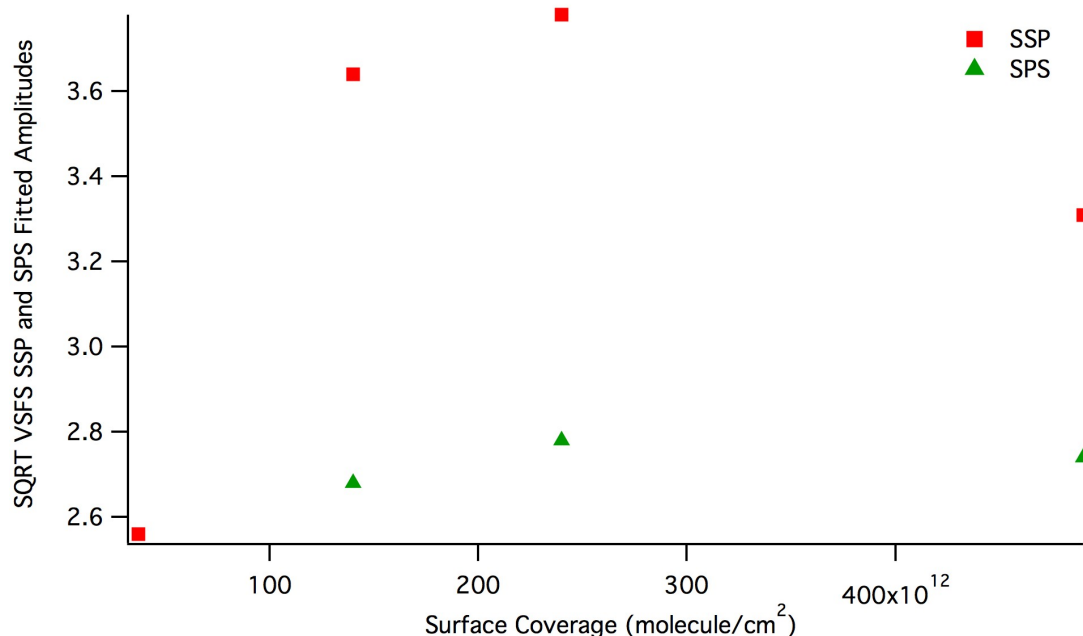
Figure 6.6. Square root of VSFS Fitted amplitudes versus surface coverage of glutaric acid.

surface pressure) do not decrease at a bulk concentration of 3M but rather increase, as would be expected based on increasing surface concentration. A linear fit to this data fails unlike what was seen for malonic and succinic acid. A considerate examination of the available data can provide a reasonable explanation for this phenomenon.

VSFS signal intensity arises from both the number density as well as the orientation at the interface, whereas surface tension measurements measure only number density. Careful correlation between the two techniques can illuminate the behavior of glutaric acid at the interface. The surface tension data (and correspondingly the surface excess concentrations) does not decrease for bulk concentrations of 3M. This rules out the potential explanation for the decrease in the VSFS signal from any desorption of glutaric acid at the interface i.e. loss of number density. If the decrease in VSFS intensity then arises from a change in orientation, it would be expected to see an increase in one polarization with a concurrent decrease in the other polarization. For example, if the C=O dipoles shifted orientation more towards the plane of the interface, a loss of signal from the SSP polarization and an increase in the signal for the SPS polarization would be seen and vice versa. For glutaric acid at 3M, there is a decrease in both SSP and SPS VSFS signals.

An explanation for this phenomenon can be found by considering that the VSFS signal can also destructively interfere in certain cases, such as when an anti-parallel layer adsorbs beneath the interfacial layer[27] or in dimerization events.[7,28] Dimerization of carboxylic acid groups in the gas phase and dilute aqueous media is well established. If the concentration at the interface can become sufficiently high that the carboxylic group can hydrogen bond to another carboxylic group to form a cyclic dimer which has a center

110

of symmetry, then the C=O mode will be cancelled due to the formation of an inversion center following VSFS selection rules.[7] This would explain the drop in VSFS signal intensity for both SSP and SPS modes and the increase in surface tension.

A dimerization event is also corroborated by the VSFS spectra in the OH region. At 1M glutaric acid, the signal from the strongly coordinated OH region is very weak. This indicates that the adsorption of glutaric acid at 1M is great enough to disrupt the subsurface layer and provides evidence that near surface glutaric acid is in a position to interact with surface adsorbed glutaric acid. At a higher bulk concentration, the possibility of dimerization events would be expected to be even more likely. Therefore, the dimerization of VSFS active C=O modes is most likely occurring for high concentrations of glutaric acid, resulting in a loss of VSFS signal. It should be noted that there is not a complete destruction of signal for either SSP or SPS and that these dimerization events are not the main species present at the interface but merely a transient species.

Computational Calculations

While the experimentally observed VSFS signal combined with surface tension measurements provide a thorough description of the adsorption behavior of glutaric acid to the air/water interface, further insight and confirmation can be gained by using molecular dynamics (MD) calculations. These MD calculations provide molecular specific geometries, which can be compared to the experimental results. The first step for the MD calculations begins with a computed density profile of glutaric acid in the water box. The density profile is used as an initial check for the stability and robustness of the

simulations. The water density profile is fit to a hyperbolic tangent function to confirm the stability of the calculations. A representative density plot of 0.5 M glutaric acid is shown in Figure 6.7. The plot shows a peak in concentration at the interface representative of surface adsorption of glutaric commensurate with what is seen both spectrally and through surface tension measurements. These results provide validation that the MD simulations are behaving similarly to experimental results.

The next step in the MD studies is to identify different molecular conformations of glutaric acid present in the simulations. Figure 6.8 displays structures of 4 of the stationary points found for glutaric acid in DFT calculations. All geometries shown
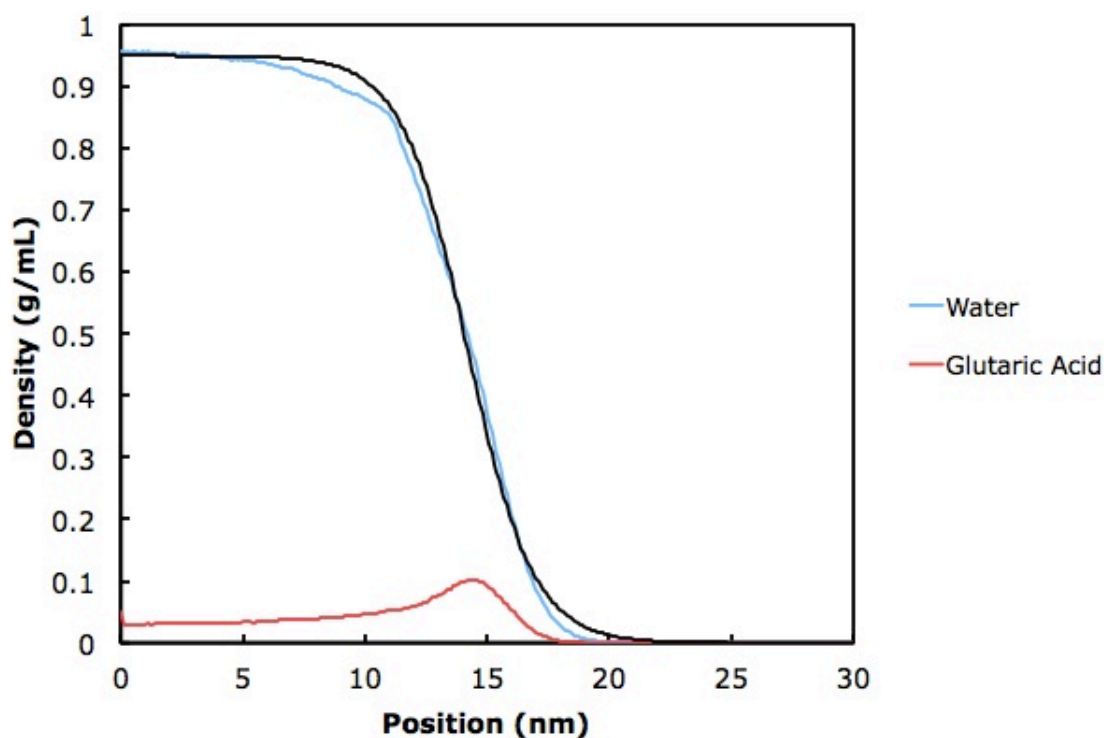
Figure 6.7. Representative density profile of 0.5 M glutaric acid MD trajectory.

correspond to local minima on the gas-phase potential energy surface. These DFT structures are visual representations of the families of conformations that correspond to the CH_2 backbone orientation. For example, there can be an anti structure (see AA in Figure 6.8) in which all the methylenes are positioned anti to each other or there can be a G structure (see AG in Figure 6.8) that contains a gauche rotation of one of the methlyenes in the backbone. The MD geometries are fit to the representative DFT structures by examining the torsion and dihedral angles with a range defined around the values of each angle found in the DFT calculations. Conformations that do not substantially contribute to the average state of the molecule are ignored.

Once the MD structures have been fit to the representative DFT families, the population of these conformations can be determined at different depths. As shown in
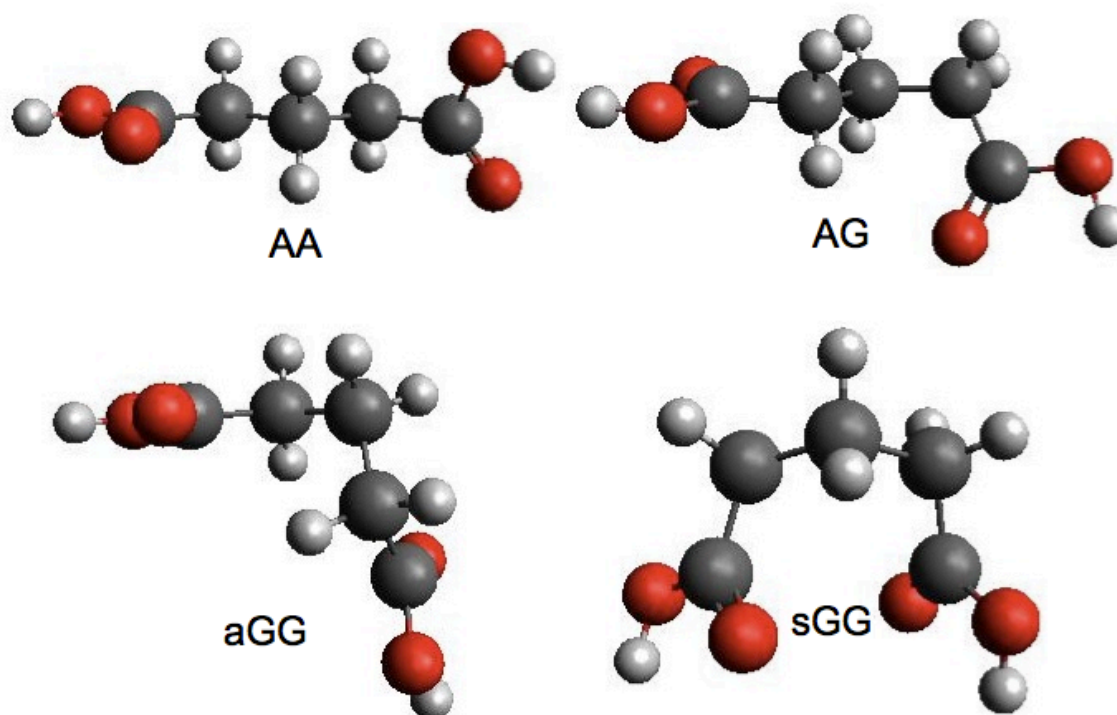
Figure 6.8. Stationary point DFT structures for representation of MD geometries.

Figure 6.9 the AA and AG structures contribute most while there is a smaller contribution

to from the doubly gauche conformations. However, as the acid molecules approach the

interface, there is an increase in the doubly gauche structures at the expense of the AA

structure. This shows that as a glutaric acid molecule approaches and resides at the

interface, more gauche conformations are favored. This confirms the spectral analysis in

the CH region where it was postulated that gauche defects were present. In addition, the

presence of signal in the SSP VSFS spectra indicated that there were CH dipole
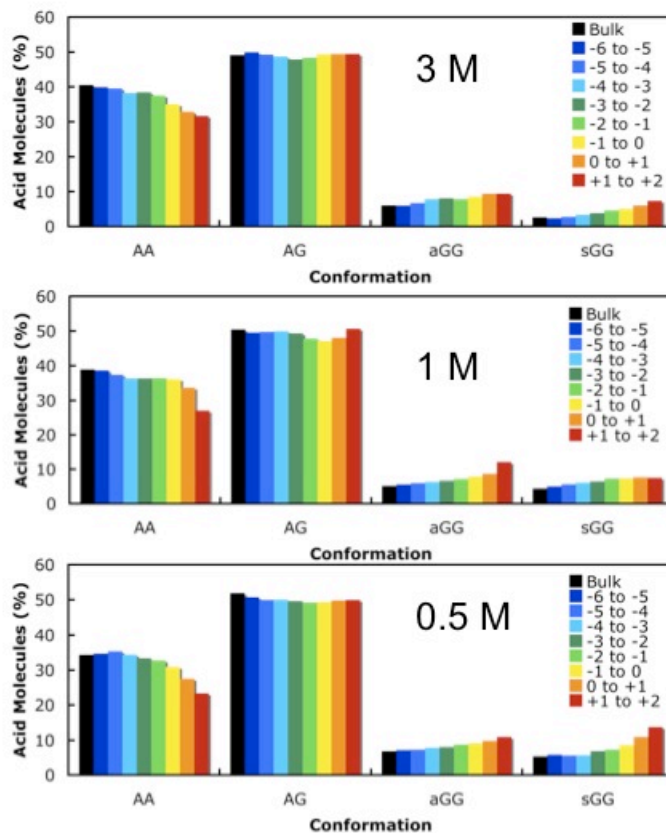
Figure 6.9. Percentages of conformations as function of depth for 0.5M, 1M, and 3M glutaric acid.

transitions normal to the plane of the interface. The MD simulations also captured this behavior as can be seen in the AG structure as well as the increase in the doubly gauche structures at the interface.

The MD simulations were performed at different concentrations corresponding to the experimental concentrations (Figure 6.9). There are no major changes in the distribution of conformations as the concentrations change, indicating that there are not large changes in the adsorption characteristics as a function of concentration. There is also similarity in the increase in the doubly gauche structures at the expense of the AA structure for the concentrations studied here. Both of these features confirm the spectral correlation to surface tension indicating that there is not a change in the orientation of the adsorption as a function of concentration. It should also be noted that the MD trajectory for the higher concentrations solution showed evidence of dimerization events, which is in accordance with the spectral analysis of the VSFS spectra.

The only remaining ambiguity is the direction of the carbonyl of the carboxylic acid. The carbonyl pointing directions for the AG conformation is shown for different depths in Figure 6.10. Each axis represents the C=O angle for one dicarboxylic end. A value of 0° would be normal to the surface, pointing away from the bulk, while a value of 180° would be normal to the surface but pointed towards the bulk. Therefore, a value of 90° would be in the plane of the interface. By choosing an angle on the bottom axis (which sets the angle of one carbonyl) and following the other axis through all angles, the population of carbonyl angles for an acid molecule can be determined. Figure 6.10 shows that away from the interface at bulk depths, there is no clear preference for the
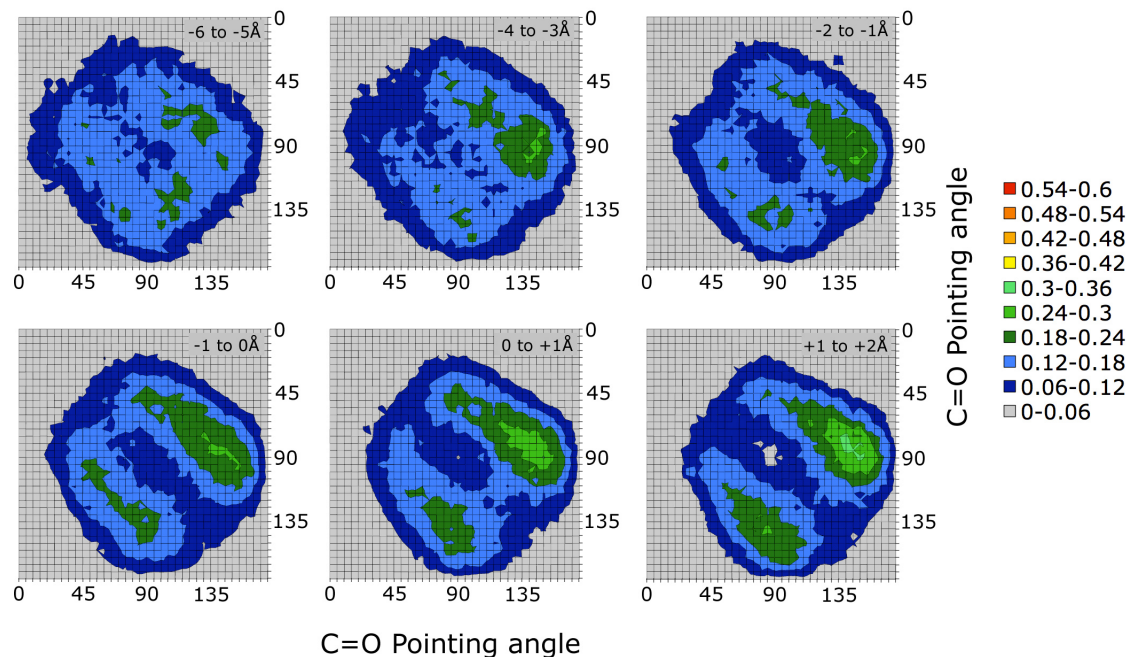
Figure 6.10. Orientational distributions of C=O pointing angles for the conformation AG at 0.5M.

carbonyl orientation. As the acid molecules approach the interface, the distribution of the carbonyl orientation becomes smaller until it is apparent that the carbonyls are adopting a preferred orientation pointing down into the bulk.

The orientational distribution of the carbonyl pointing angle for the sGG conformation is shown in Figure 6.11. Once again, as the glutaric acid molecules approach the interface, there is a change from bulk, isotropic behavior to directed orientation of the carbonyls. The carbonyls for the sGG show an even more pronounced preference for the carbonyls to point towards the bulk. Specifically, the sGG conformation shows that the carbonyls orient with one carbonyl more in the plane of the surface with the other carbonyl pointed towards the bulk, which corroborates the VSFS polarized spectra. This final piece confirms the VSFS spectral results for the carboxylic

116
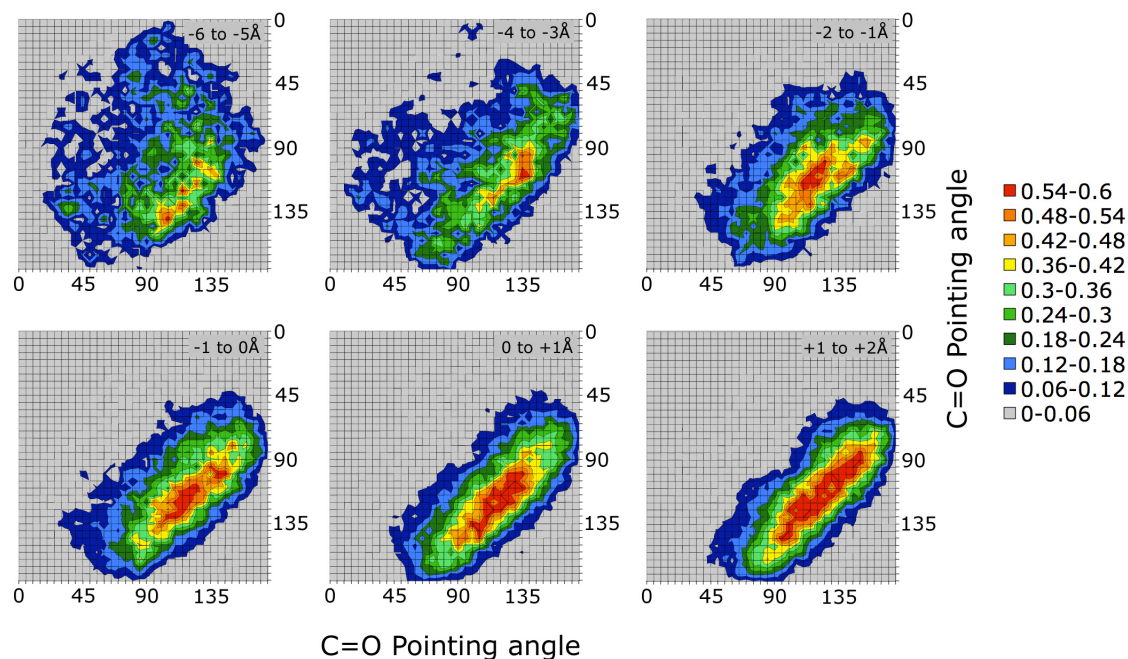
Figure 6.11. Orientational distribution of C=O pointing angles for the conformation sGG at 0.5M.

acid region. As shown earlier, the C=O frequencies were indicative of near bulk like solvation indicating that were most likely not pointing away from the bulk but instead participating in hydrogen bonding with the water network. The MD results therefore confirm the absolute direction of the SSP active modes as pointed towards the bulk while also showing that there should be SPS signal based on the carbonyl directions. The MD trajectory and analysis therefore provide confirmation of the VSFS spectral results while also allowing for a detailed, molecular level view of the conformations of surface adsorbed glutaric acid.

pH Dependent Vibrational Spectroscopy

The previous sections detail the adsorption of glutaric acid as a function of concentration. Since both acids are diprotic, it is also necessary to characterize the

adsorption as a function of pH. The adsorption of pH adjusted glutaric acid is achieved by changing the bulk pH of the solutions and monitoring changes via VSFS and surface tension measurements. The C=O signal arising from the carboxylic moiety will disappear as the pH is increased since the loss of a proton from a carboxylic unit results in a change to a resonance stabilized carboxylate ion. Glutaric acid has two carboxylic moieties and thus two distinct pK_a values. By monitoring the C=O signal using VSFS as well as changes to surface tension, the adsorption of glutaric acid under different pH conditions can be revealed and fully characterized.

The pK_a values of glutaric acid are 4.34 and 5.42.[29] The percentages of protonated species of glutaric acid are plotted in Figure 6.12. At a pH of 4, 67% of glutaric acid molecules are fully protonated, over 31% are singly protonated with the remaining small
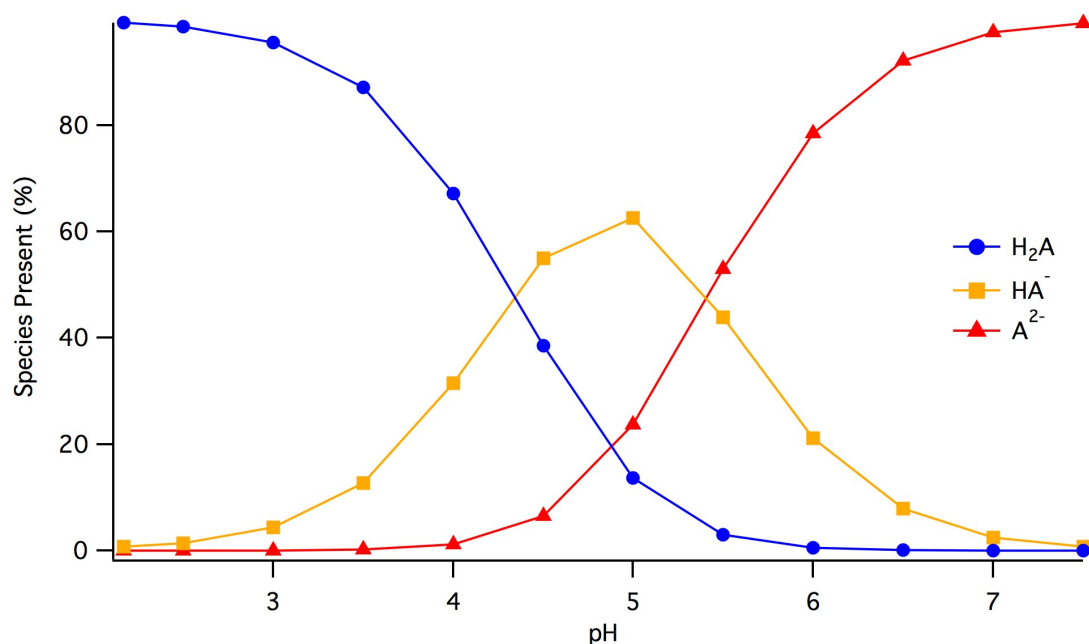
Figure 6.12. Percent of fully protonated, singly protonated, and fully deprotonated aqueous glutaric acid solutions based on pK_a values.

faction being fully deprotonated. At a pH of 5, only ~14% of glutaric acid molecules are fully protonated, with over 62% being singly protonated and the remaining ~24% are fully deprotonated. When the pH reaches 6, there is less than 1% fully protonated glutaric acid molecules and only ~21% singly protonated left.

At a constant concentration of 1M, the bulk pH of glutaric acid was adjusted by the addition of NaOH. Figure 6.13 shows the spectral response of glutaric acid in the C=O region for SSP as well as their respective fits. The fits to the spectra reveal a peak centrally located at 1717 cm-1 +/- 2.5 cm^{-1} with a Gaussian width of 36 +/- 4 cm^{-1}. There is a large decrease in signal (roughly half) going from an unadjusted solution to a pH of 4.5. The VSFS C=O signal further diminishes at a pH of 6 and completely disappears at pH values in excess of 6.5.
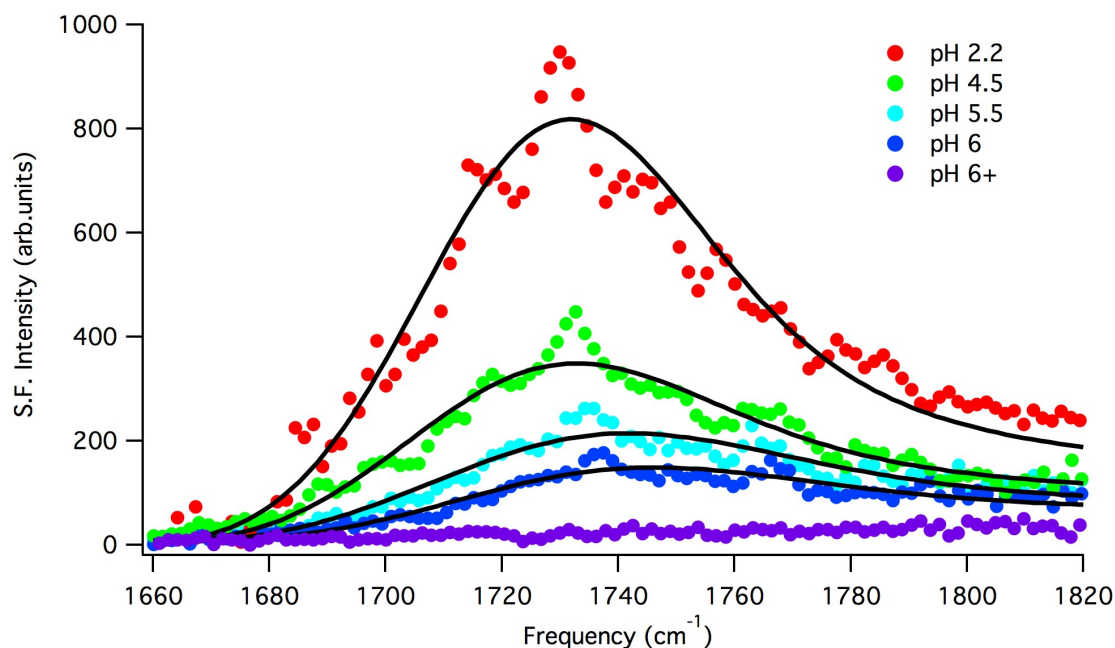
Figure 6.13. VSFS SSP in the C=O region of bulk pH adjusted 1M glutaric acid. Fits are shown in black.

Figure 6.14 shows the spectral response of glutaric acid in the C=O region for SPS as well as their respective fits. The fits to the spectra show a peak centrally located at 1716 +/- 2.5 cm^{-1} with a Gaussian width of 36 +/- 4 cm^{-1}. The changes to the C=O VSFS intensity at a pH of 3 are negligible. While there is a diminished intensity at a pH near 5, the signal is still clearly present. The signal quickly drops as the pH increases further. At a pH of 6, there is barely any detectable C=O signal and above pH values of 6, there is no detectable C=O signal. This trend follows the VSFS SSP data. Attempts were made to detect the glutaric carboxylate signal (~1400 cm^{-1}) but were unsuccessful in obtaining any VSFS signal.
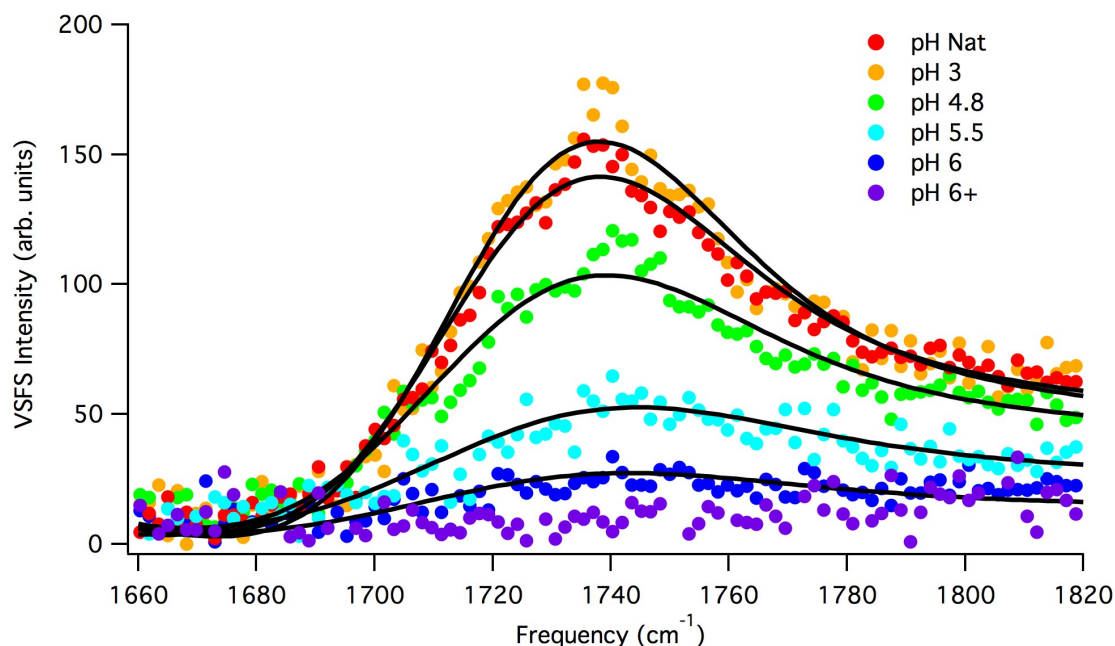
Figure 6.14. VSFS SPS in the C=O region of bulk pH adjusted 1M glutaric acid. Fits are shown in black.

In addition to the C=O modes, the presence of CH_2 modes permit pH analysis based on the CH region. The spectra taken in the CH/OH region for bulk pH adjusted glutaric solutions were difficult to resolve due to increased scattering from the interface. The visible energy was lowered to 60% of normal to allow for useable intensity, however this resulted in more noise at the far ends of the spectral region. Regardless, the results of these experiments demonstrate the surface dependence of glutaric acid based on changes to the pH. The CH_2 signals arising from 1M glutaric acid adsorbed to the air/water interface were investigated at native pH, pH 5, and pH 6. In all spectra, the signal from the CH region does not disappear. This is in contrast to succinic acid (see Chapter V) where the CH_2 signal decreased as the bulk pH was increased and was completely removed at a pH of 6. The spectral analysis resulting from this data indicates that there is still glutaric acid adsorbed at the interface at pH values of 6 although the C=O signal is almost or completely removed. Similar results are seen when looking at the OH region. The coordinated OH region is flat over all spectra indicating a disruption (i.e. glutaric acid adsorption) in the hydrogen-bonding network of water at the interface. Likewise, the intensity arising from the free OH vibrational mode does not change dramatically over all spectra, once again indicating that there is surface adsorption of glutaric acid that is not from only fully protonated species. This stands in contrast to the pH dependent results from malonic and succinic acid.

These experiments provide further detail to the pH dependent adsorption of glutaric acid to the air/water interface. The C=O signal from glutaric acid is shown to persist to a bulk pH value of 6, beyond what is expected if the surface species was only due to fully protonated glutaric acid. VSFS in the CH/OH region also show similar

results. The presence of glutaric acid at pH of 6 is confirmed by CH_2 signal and diminished spectral intensity in the coordinated water region and the free OH region. Surface tension measurements in the next section provide further proof that glutaric acid adsorption to the air/water interface has different pH dependencies than malonic and succinic acid.

pH Dependent Surface Tension

By measuring the number density at the air/water interface from surface tension measurements, the effect of bulk pH on the surface adsorption of glutaric acid can confirm and elucidate the spectral data. Since the addition of NaOH has been shown to increase the surface pressure at an air/water interface,[30] the surface pressure values here are those of water with an equivalent amount of NaOH added. Plotted in Figure 6.15 is the adjusted surface pressure (left axis) and fully protonated species present in the bulk based on the bulk pH (right axis). The decreases in the surface pressure based on the changes in the pH demonstrate desorption of glutaric acid molecules as the pH increases. There are small changes to the surface pressure as the pH is adjusted from native 1M solutions to pH values between 3 and 4. As the pH increases, decreases in the surface pressure become more pronounced. However, the surface pressure never reaches below 6 mN/m and therefore indicates that there is still glutaric acid adsorbed to the interface for these bulk adjusted pH values. The number of fully protonated species present in the bulk, based on the pK_a values, also follows the same trend illustrated by the surface pressure changes. This corroborates the data from the VSFS experiments. By combining

122
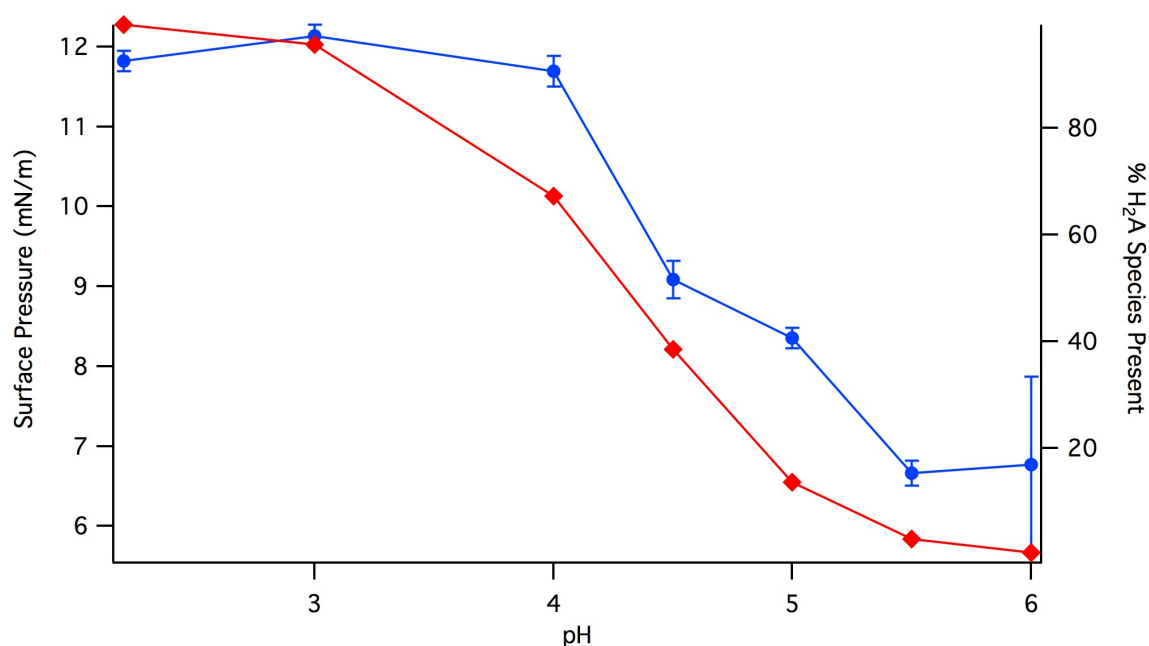
Figure 6.15. The surface pressure (blue trace) and percentage of fully protonated species (red trace) plotted versus the bulk adjusted pH value.

the surface pressure data and the square root of the VSFS SSP C=O amplitudes (Figure 6.16), a similar trend is seen. The VSFS signal arising from the C=O decreases as the pH increases and follows the commensurate decrease in surface pressure. However, there is still surface active glutaric acid based on surface tension and VSFS spectra in the CH/OH region.

As can be shown through the combination of VSFS spectral data and surface tension, the adsorption of glutaric acid at the air/water interface is dependent upon pH. However, unlike what has been shown for malonic and succinic acid, glutaric acid is still slightly surface active for a singly deprotonated species. These species are most likely disordered since no COO⁻ VSFS signal could be obtained.
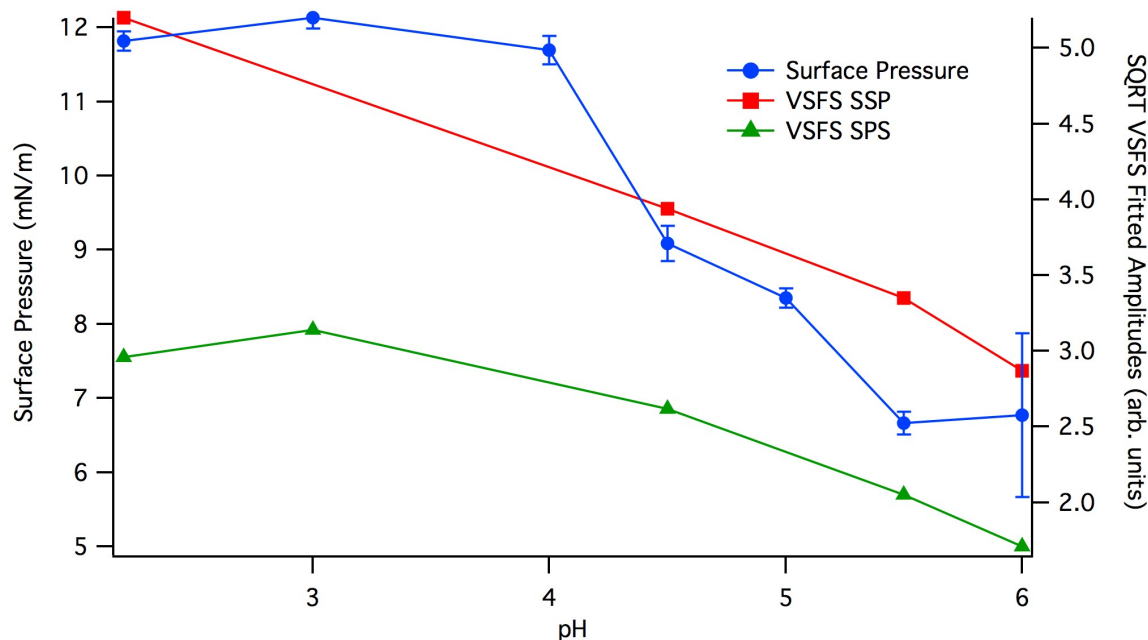
Figure 6.16. Surface pressure and square root of VSFS fitted amplitudes for SSP and SPS versus bulk pH values.

Conclusions

Although there is only an addition of one CH_2 to the carbon backbone when going from succinic to glutaric acid, there is a large change in the surface adsorption behavior of glutaric acid. The very soluble nature of glutaric acid allows for much more concentrated aqueous solutions when compared to succinic acid. At very high concentrations, intermolecular bonding between organic species becomes relevant. By correlating the VSFS spectral data with surface pressure data, evidence of cyclic dimerization between surface adsorbed glutaric acid molecules was demonstrated. In addition to the concentration dependent changes that arise from an additional CH_2 along the carbon backbone, there is also a change in the pH dependent surface adsorption. Glutaric acid is shown to be present at the air/water interface via VSFS as well as surface tension measurements at pH values of 6 and higher. Based on the bulk pKa values, this

124

indicates that singly protonated and, potentially fully deprotonated, glutaric acid molecules can be considered surface species. This somewhat surprising result from the addition of a CH_2 leads to interesting questions. Does the addition of another CH_2 moiety along the carbon back bone result in further increases in surface adsorption like for change from malonic and succinic acid to glutaric acid or does the behavior resemble the shorter carbon backbone dicarboxylic acids? Does an additional methylene change the pH dependence of surface adsorption as well? These questions will be addressed in the following chapter by investigating adipic acid, the longest and final dicarboxylic acid to be studied in this work.

CHAPTER VII

ADIPIC ACID AT THE VAPOR/WATER INTERFACE

In this chapter, the adsorption of adipic acid $((COOH)_2(CH_2)_4)$ to the air/water interface was investigated via VSFS, surface tension, and computational calculations. As has been done previously for the shorter chain acids, adipic acid was characterized by its concentration and pH dependence. Concentration dependent experiments using polzarized VSFS revealed that adipic acid has a range of solvation, from bulk like solvation to weaker solvation with water molecules at the air/water interface. Surface tension measurements demonstrated an isolated surface adsorption based on its area per molecule. The orientation of adipic acid was further determined through molecular dynamics and enhances the spectral analysis. In addition, VSFS and surface tension experiments demonstrated that the surface-active species of adipic acid at the air/water interface is the fully protonated species. The computational work was performed by Nick Valley. The water spectra were taken by Katy Plath. Some surface tension data was taken by Suzzanah Wood.

Introduction

Adipic acid is one methylene unit longer than glutaric acid and is the longest dicarboxylic acid studied in this work. While detected concentrations of adipic acid are not as high as malonic or succinic, adipic acid appears at atmospherically relevant concentrations. Much like glutaric acid, adipic acid is believed to have direct emission sources,[1-3] yet also form in secondary organic aerosol (SOA) reactions. The precursors

for the SOA reactions include common atmospheric organic species such as cyclohexene.[4,5]

As the behavior of the shorter chain dicarboxylic acids has been elucidated through the previous three chapters, it is obvious that there are subtle differences between these acids due to the addition of a methylene unit along the carbon backbone. This class of molecules has thus far shown that the preferred orientation involves a balance between the hydrophobic alkyl backbone and the hydrophilic carboxylic groups. This results in an orientation that is "flat" at the air/water interface. The solvation of the carbonyl local mode has shifted to lower frequencies as the carbon backbone length has increased. Malonic and succinic acid have shown a strong pH dependency that results from the fully protonated species being only surface active species. However, glutaric acid results demonstrated that the loss of an acidic proton does not result in desorption from the interface. In addition, malonic and succinic acid have much larger surface areas per molecule at the interface compared to glutaric acid. Since the hydrophobic backbone of glutaric acid is longer than both succinic and malonic, it may be that the difference in behavior at the surface is from the increasing length of the alkyl chain. The surface behavior of adipic acid can shed light on this question due to the longer alkyl chain. Does adipic acid fall into the malonic and succinic category, is it like glutaric acid, or does it display behavior that is completely unique? To answer these questions, this chapter explores the concentration and pH dependent surface adsorption of aqueous adipic acid through a combination of VSFS, surface tension, and computational modeling.

VSFS spectra of the C=O carboxylic mode of adipic acid was taken in SSP polarization scheme with fitted curves and is shown in Figure 7.1. The intensity of the VSFS C=O signal increases monotonically from bulk concentrations 0.025M to 0.1M. The global fits provide a central peak located at 1707 +/- 1 with a Gaussian width of 35 +/- 1 cm^{-1}. Since adipic acid has a limited solubility in aqueous media (~0.17M),[6] it is only studied up to a concentration of 0.1M. Even at these lower concentrations however, adipic acid is clearly adsorbing to the vapor/water interface with dipole components of C=O oscillators normal with respect to the water surface plane based on the observance of VSFS signal intensity present in the SSP experiments.
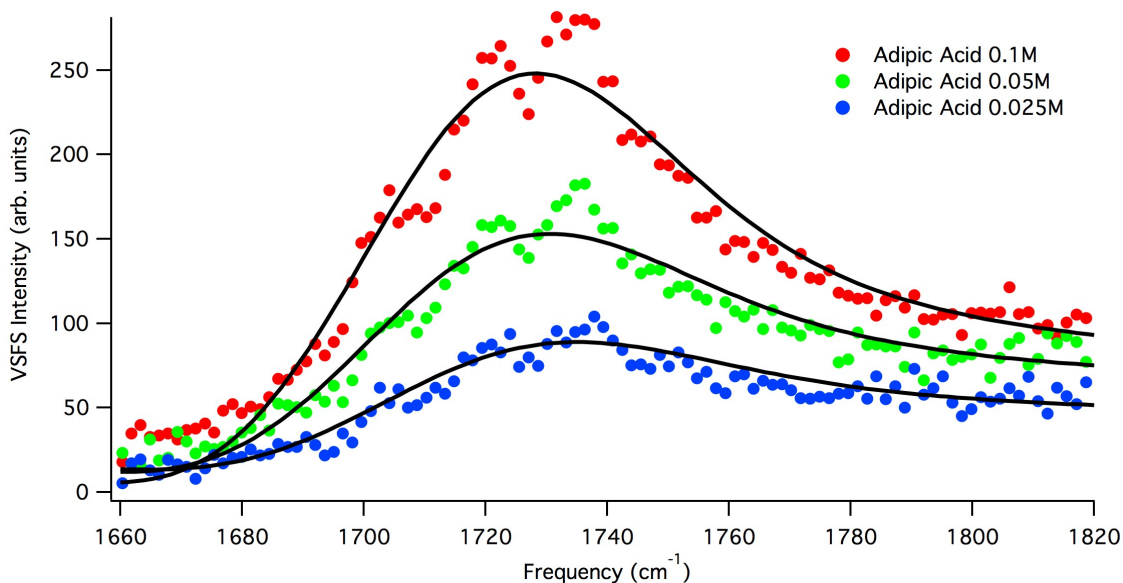
Figure 7.1. VSFS SSP of the C=O region for aqueous adipic acid at 0.025, 0.05, and 0.1M. Fits are shown in black.

The carboxylic C=O was also probed in the SPS polarization scheme and is shown with fitted curve in Figure 7.2. The VSFS signal intensity for this mode was less than that probed in SSP at the same bulk concentration 0.1M. The presence of signal under the SPS polarization scheme indicates that one or both of the C=O carboxylic acid modes have C=O dipole components in the plane of the surface. The fit to the spectrum reveal a peak centrally located at 1717 +/- 1 cm^{-1} with a Gaussian width of 35 +/- 1 cm^{-1}. All of the VSFS signals from the C=O region of adipic acid are relatively weak and as a consequence, the normally negligible non-resonant signal interferes with the resonant C=O mode. This manifests itself spectrally through interference with the blue-side of the spectra presented and results in the VSFS signal not returning to zero on the blue-side of the spectra. This has been shown for the other dicarboxylic acids and is noted in other VSFS studies.[7,8] This does not change any of the spectral interpretations.
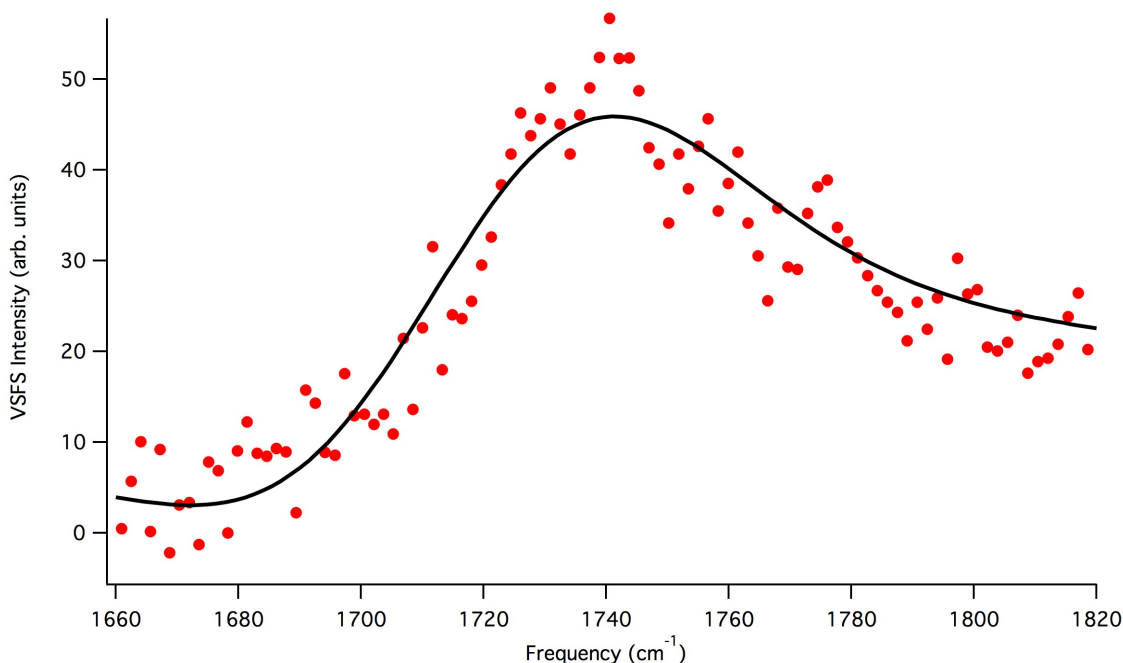
Figure 7.2. VSFS SPS of C=O region for 0.1M adipic acid. Fit is shown in black.

The C=O mode is known to be sensitive to hydrogen bonding with different frequencies reflecting the solvation around the C=O. Bulk aqueous IR studies have found the C=O mode of fully protonated adipic acid at 1707 cm^{-1} and the C=O for a singly protonated adipic acid at 1703 cm^{-19} Another spectroscopic study found the C=O mode for aqueous adipic acid at 1698 cm^{-1} for IR and 1702 cm^{-1} for Raman.[10]

Different hydrogen bonding regimes of the C=O mode for carboxylic acids have been identified through surface IR studies.[11-13] These studies have shown that specific ranges of C=O frequencies correspond to different hydrogen bonding for long-chain fatty acid monolayers at an air/water interface. These regions from ~1735-1739 cm^{-1}, ~1715-1720 cm^{-1}, and 1700-1704 cm^{-1} are assigned as having non H-bonded, singly H-bonded, and doubly H-bonded character, respectively. While long-chain fatty acids and short-chain dicarboxylic acids will have different solvation and orientation characteristics at the air/water interface, the trend will be similar for both. Adipic acid C=O frequencies show strong solvation for SSP polarization schemes with values near that of bulk C=O while the SPS polarization scheme shows slightly weaker solvation. This indicates that adipic acid is involved in multiple solvation environments at the interface with both doubly and singly H-bonded character.

In addition to surface IR, information about the solvation environment can also be gained by comparing the VSFS C=O data from adipic acid to other VSFS experiments on organic acids containing C=O moieties adsorbed to the air/water interface. The straight chain, six carbon long monocarboxylic acid hexanoic acid ($COOH(CH_2)_4(CH_3)$), was investigated with VSFS and was shown to have a C=O central frequency at 1720 cm^{-1}.[14]

The adipic acid C=O frequencies are ~10 cm^{-1} red shifted from this value and indicates that the carboxylic end groups are more strongly solvated than the monocarboxylic counterpart. Shown in Table 7.1 are the VSFS, bulk IR, and bulk Raman vibrational frequencies for malonic, succinic, glutaric, and adipic acid. When compared to the acids studies throughout this work, adipic acid has C=O frequencies which represent the most solvated in SSP. When compared to the SSP VSFS spectra, adipic acid SPS C=O frequencies are still representative of more solvation but to a lesser extent. In addition, the steric hindrances that led to the orientation and solvation of malonic and succinic acid at the air/water interface are alleviated by the carbon backbone torsion that is available for adipic acid. In essence, the longer carbon backbone can experience a number of different conformations in order to minimize the energy needed for solvation. These conformations will be explored in more depth in the computational section.

Acid	VSFS (SSP, SPS) (cm^{-1})	Bulk IR (cm^{-1})	Bulk Raman (cm^{-1})
Malonic	1740, 1730	1719	1726
Succinic	1722, 1722	1717	1717
Glutaric	1715, 1718	1709, 1707	1710, 1715
Adipic	1707, 1717	1707, 1698	1702

Table 7.1. Comparison of VSFS, bulk IR, and bulk Raman C=O vibrational frequencies for all dicarboxylic acids studied in this work.

It should be noted that the adipic acid C=O frequencies for the SSP mode are similar to bulk IR frequencies while the SPS frequencies are blue shifted to higher frequencies. This is indicative of C=O modes which are experiencing two different solvation environments based on its orientation and position in the interface. The longer carbon backbone for adipic acid provides rotational degrees of freedom that can allow the

hydrophilic carboxylic groups (and hence the C=O mode) to achieve better solvation through orientation. A possible explanation is that the C=O modes oriented more in the plane of the interface (SPS) are less likely to attain the most favorable solvation environment while C=O modes pointed more normal to the surface can achieve almost bulk like solvation environments.
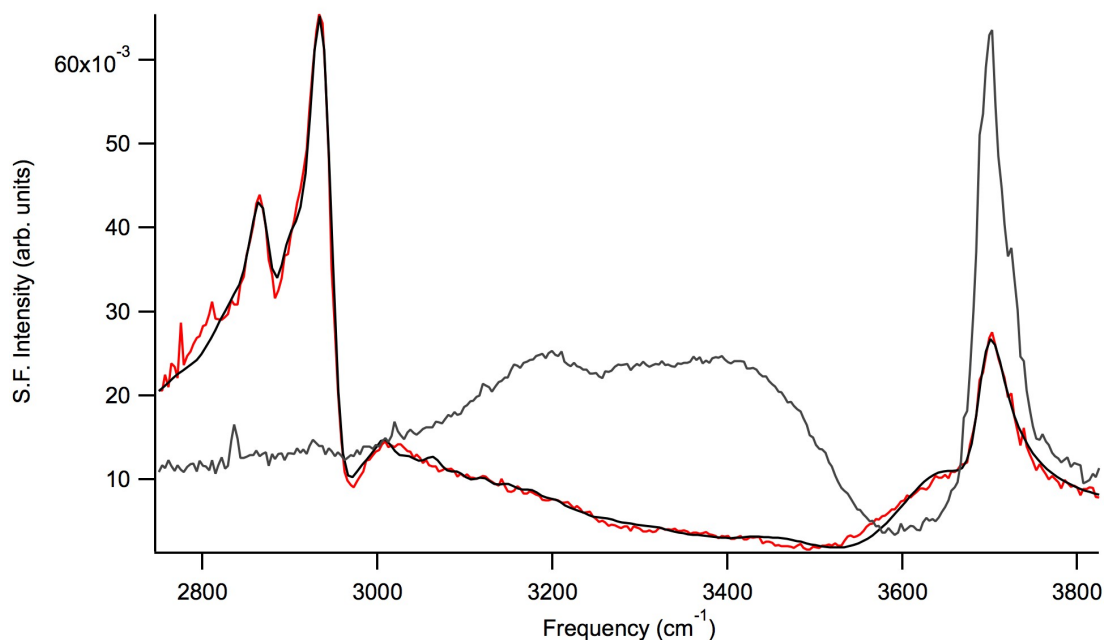
Figure 7.3. VSFS SSP spectrum in the CH/OH region of 0.1M adipic acid. The pure water spectrum is shown in gray and the fit to the data is shown in black.

Moving to the CH/OH region provides further information on the adsorption characteristics of aqueous adipic acid. The VSFS response of the OH region in the SSP polarization scheme for 0.1M adipic acid is plotted in Figure 7.3. The neat water response is plotted in gray. As was seen for glutaric acid in Chapter VI, there are large changes between the neat water VSFS spectra and the 0.1M adipic acid solutions. The

free OH signal is reduced compared to the neat water surface but there is still significant contribution from the uncoupled OH oscillators. This once again indicates that the surface of these solutions is not completely covered by adsorbed adipic acid. The presence of a peak near 3650 cm^{-1} is attributed to solvation of adipic acid in a manner similar to glutaric acid.[15-17] Below 3600 cm^{-1}, the VSFS signal from the coordinated OH region is suppressed by the presence of adipic acid. A new peak does appear below 3200 cm^{-1}, representative of strong water coordination and hydrogen bonding seen for acidic solutions.[18,19] In addition, a broad peak located around 2940 cm^{-1} is fit based on the spectral analysis of succinic acid in Chapter V and is assigned to the carboxylic OH of adipic acid.

The CH region for adipic acid is similar to glutaric acid in that there are multiple intense peaks in the CH region, which arise from CH_2 groups on adipic acid. Based on the chemical environment that the methylenes reside in, there can be shifting of the vibrational responses by a few wavenumbers.[20] There are two obvious peaks between 3000-2800 cm^{-1}; a strong peak around ~2950 cm^{-1} with a small shoulder on the red side of the peak as well as a less intense peak around 2880 cm^{-1}. Spectra were taken in D_2O to unambiguously assign these CH_2 peak frequencies and can be seen in Figure 7.4. Three peaks are fit to the data and agree with the VSFS data taken in H_2O. The first peak is located at 2873 cm^{-1}, the second peak (seen as a shoulder in the OH data) is located at 2915 cm^{-1}, and the final and most intense peak is located at 2940 cm^{-1}. All three peaks are assigned to CH_2 stretching modes. These are in general agreement with bulk aqueous adipic IR values[10] of 2880 cm^{-1}, 2921cm^{-1}, and 2955 cm^{-1}.
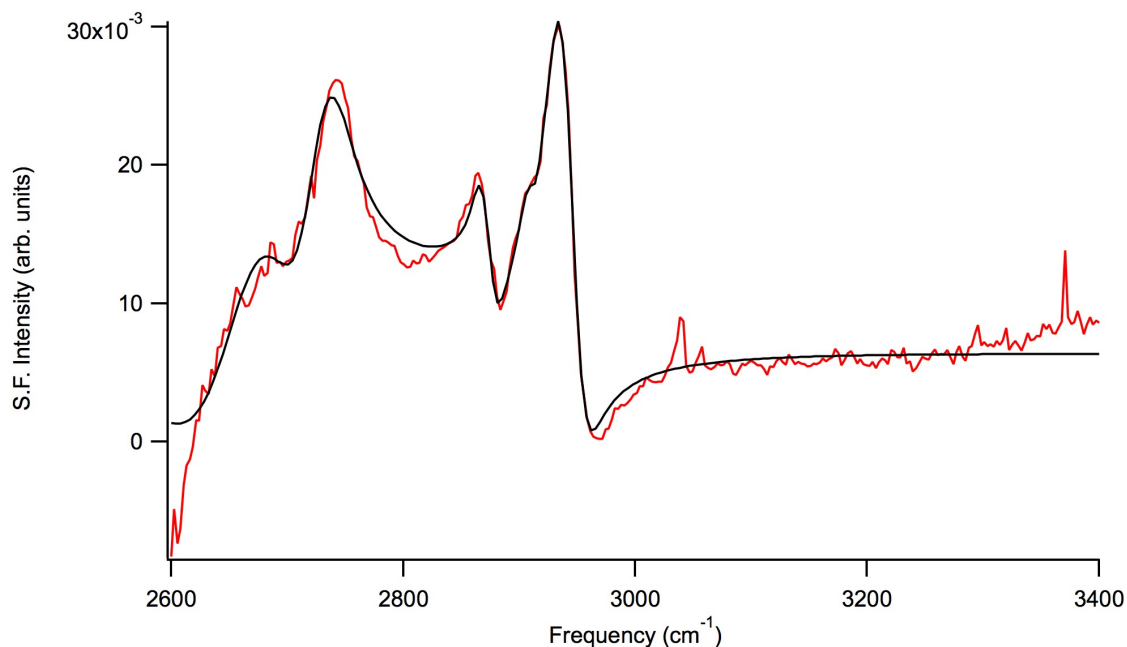
Figure 7.4. VSFS SSP spectrum of 0.1M adipic acid in D_2O. Fit is shown in black.

As shown in Chapter VI for glutaric acid, the presence of CH_2 modes is evidence of gauche conformations in the methylene backbone indicating that there is torsion along the backbone from the competing forces of solvation by the hydrophilic carboxylic groups and the hydrophobic methylene groups. It should be noted that an all trans configuration of methylene modes could result in the destructive interference of the CH_2 VSFS signal.[21] The carbon backbone conformations will be addressed further in the computational section.

Concentration Dependent Surface Tension

Surface tension data was taken for concentrations of adipic acid at 0.025, 0.05, and 0.1M and are plotted with square root VSFS C=O SSP fitted amplitudes in Figure 7.5. These values agree well with previous investigations by other laboratories.[22-24] The Gibbs adsorption equation (using concentration not corrected for activity) was used to determine the surface area per molecule and was found to be ~192 $Å^2$. The Frumkin
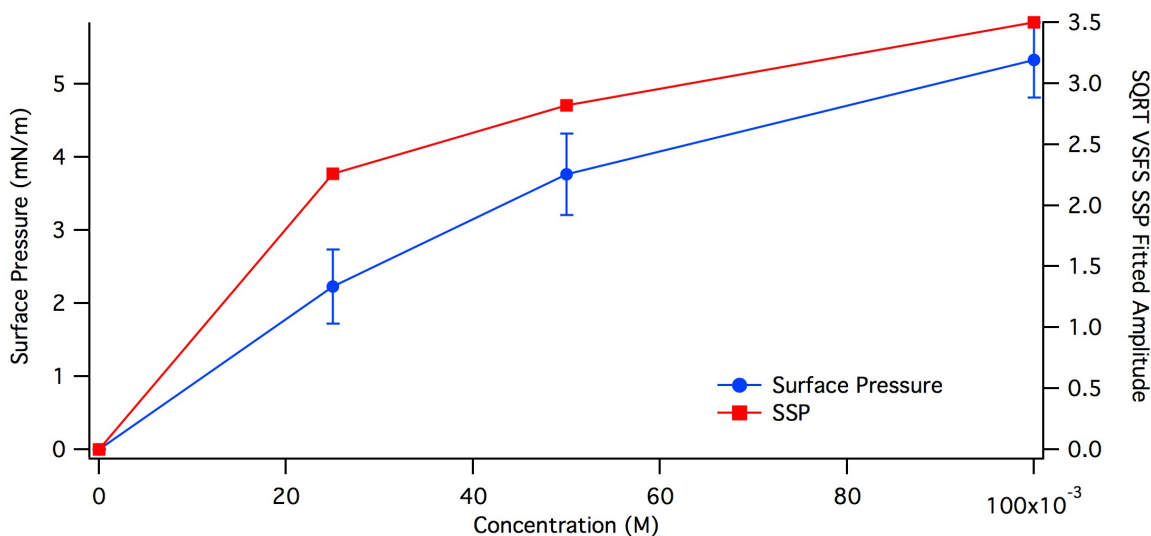
Figure 7.5. Surface pressure and square root of fitted VSFS SSP amplitudes of adipic acid plotted versus concentration.

equation[25] was used to determine the surface excess concentrations corresponding to each bulk concentration. The surface excess concentrations are plotted against the VSFS fitted amplitudes for the C=O SSP spectral data in Figure 7.6. The linear dependence of the data suggests that there are no large changes in orientation of adipic acid at the vapor/water interface as the bulk concentration of adipic acid increases.

135
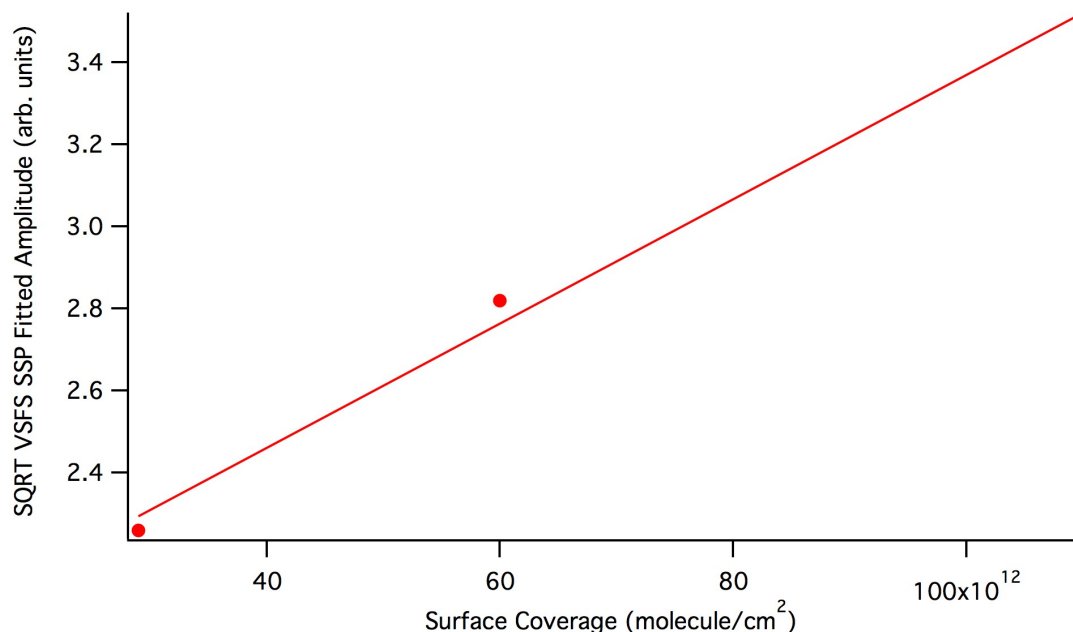
Figure 7.6. Square root of VSFS SSP fitted amplitudes versus surface coverage of adipic acid. Solid line is linear fit to data.

Although the difference between glutaric and adipic acid is only a CH_2 along the alkane backbone, this results in widely different solubilities. This phenomenon, as well as other properties, has been documented before for aliphatic dicarboxylic acids.[26-28] While both diacids show interfacial activity based on the increases in surface pressure, adipic acid has a much larger surface area per molecule than glutaric acid. In fact, the surface area per molecule for adipic acid is very similar to both malonic and succinic acid. The large surface area per molecule for these acids is indicative of two important results. The first is that these molecules are expected to be isolated at the interface. This means that malonic, succinic, and adipic acids are unlikely to coagulate at the surface and interact in a cooperative manner. The second effect is that the large surface area per molecule indicates that these acids do not flip orientations from lying flat at the interface

136

to pointing up like is seen for longer chain, traditional surfactants. The well solvated C=O frequencies for adipic acid corroborate this effect.

Computational Calculations

The VSFS and surface tension measurements performed as a function of concentration for adipic acid demonstrate that this acid has potentially different solvation environments, a carbon backbone with torsion resulting in gauche orientations, and a large surface area per molecule which does not pack tightly at the surface. By pursuing a molecular approach through the use of molecular dynamics (MD) trajectory, the adipic acid surface behavior can be further examined. Shown in Figure 7.7 is a representative density profile of ~0.1M adipic acid solution. The water density profile is also shown and fit to a hyperbolic tangent function to confirm the stability of the calculations. The plot shows a peak in concentration at the interface representative of surface adsorption of adipic acid similar to the behavior seen spectrally and through surface tension measurements. After the peak at the interface, the concentration of adipic acid levels off to bulk concentrations. These results provide validation that the MD simulations are behaving similarly to experimental results.

Following the procedure done in Chapter V and VI, the different molecular conformations present in the MD trajectory are identified. DFT structures are computed and 6 stationary point structures are shown in Figure 7.8. The longer carbon backbone for adipic acid allows for a much larger sample of backbone conformations than succinic
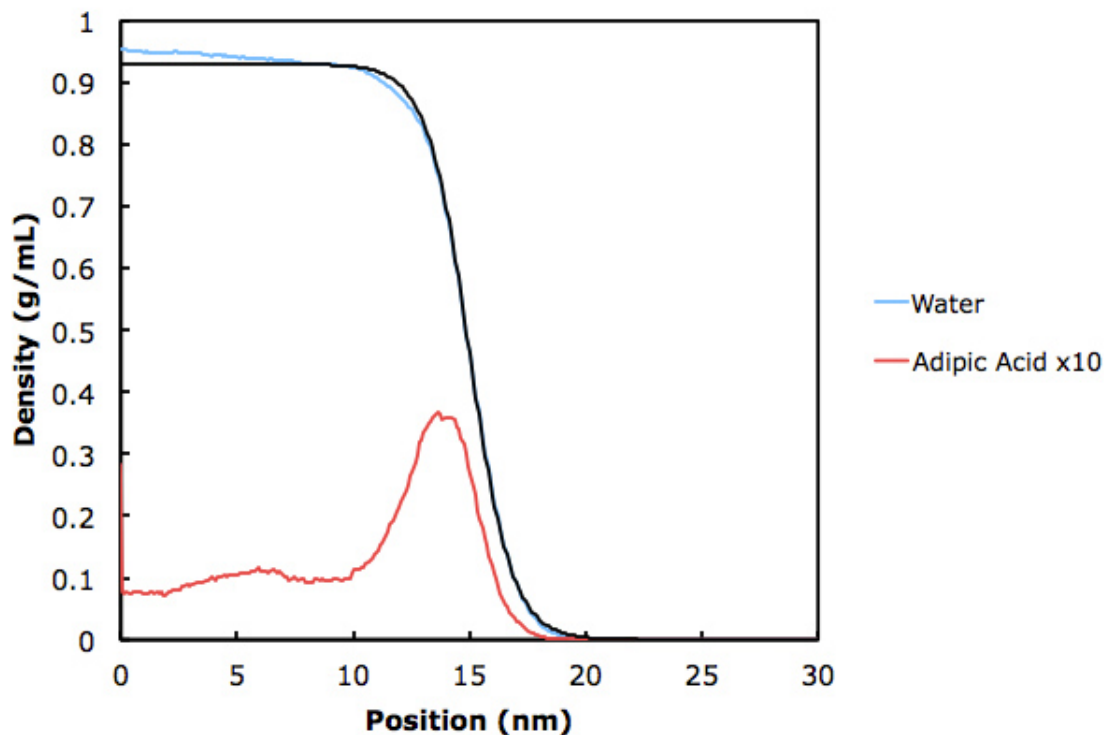
Figure 7.7. Representative depth profile of 0.1 M adipic acid MD trajectory.

and glutaric acids. Therefore, the carbon backbone structures are represented by families that define whether there are anti or gauche conformations. For example, the AAA structure contains only anti methylene conformations. The structure AAG has only one gauche methylene (next to one of the carboxylic groups) whereas the structure AGA has the gauche defect in the center of the carbon backbone. As before, the MD structures are fit to the representative DFT structures by examining the torsion and dihedral angles with a range defined around the values of each angle determined from the DFT calculations. Conformations of adipic acid that do not substantially contribute to the average state of the molecule in the MD trajectory are ignored.

138
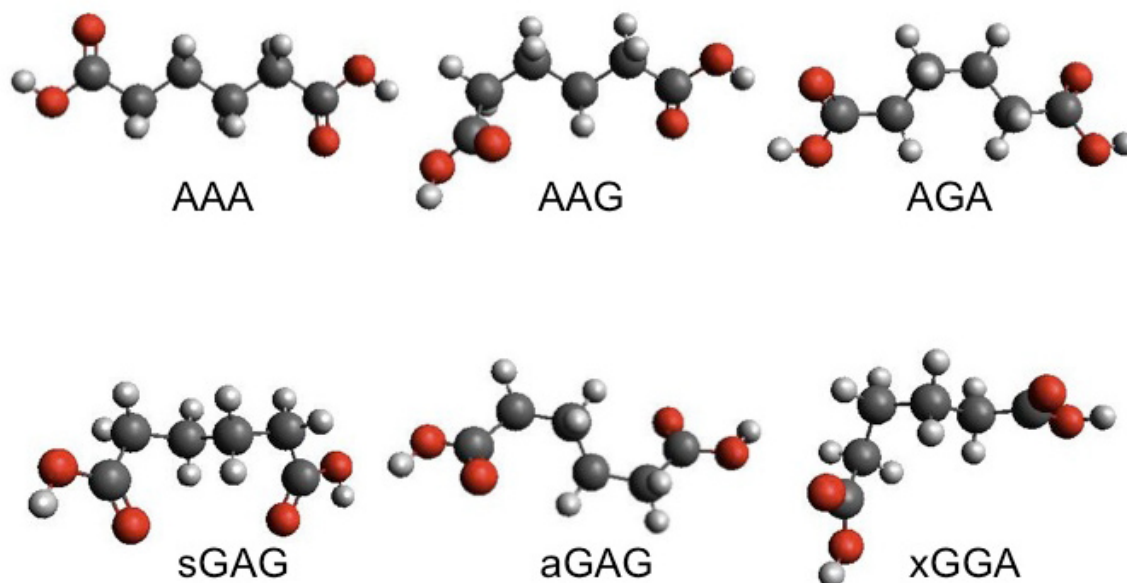
Figure 7.8. Stationary point DFT structures for representation of MD geometries.

The MD structures are fit to the DFT and the depth specific responses are plotted for the six conformers in Figure 7.9. The adipic acid conformations that contribute the most are the AAA and AGA conformers. Conformations with more than one gauche defect along the backbone do not contribute as greatly. The fully anti conformation (AAA) is unlikely to contribute to VSFS for either the C=O mode or the CH_2 mode since the net dipole orientations are in opposing directions.

The MD simulations were performed at three different concentrations (0.06M and 0.12M shown here as well as 0.25M which is above the physical solubility limit and is thus not used in the analysis). For these concentrations, there is no change in the distribution of conformations, confirming that the adsorption of adipic acid does not change as a function of concentration.
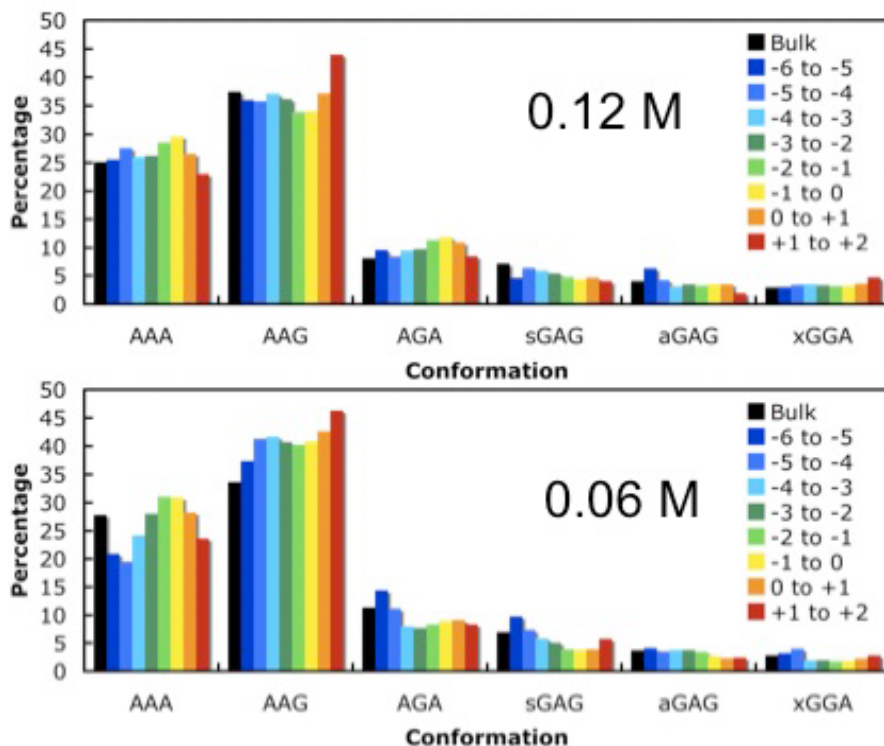
Figure 7.9. Percentages of conformations as function of depth for 0.06 M and 0.12 M adipic acid.

The final piece necessary to describe the orientation of the conformers is the pointing angles of the carbonyl bonds. The plots are similar to those of Chapter V and VI. The orientational distribution of carbonyl pointing directions for the AAG conformer is shown in Figure 7.10. At depths near the interface, the carbonyl pointing angles are isotropic, with no preference for a given direction. As this conformer approaches and resides at the interface, the isotropy is lifted and the carbonyls tend to point either in the plane (90º) or towards the bulk (angles greater than 90º). The distribution of angles is wider than that of succinic or glutaric acid and reflect the larger distribution of conformations that can exist for adipic acid. In essence, the longer chain of adipic acid is less sterically rigid and the carboxylic end groups can therefore adopt a larger range of

140

geometries. The VSFS data showed evidence of multiple solvation environments that is also captured in the MD analyses.
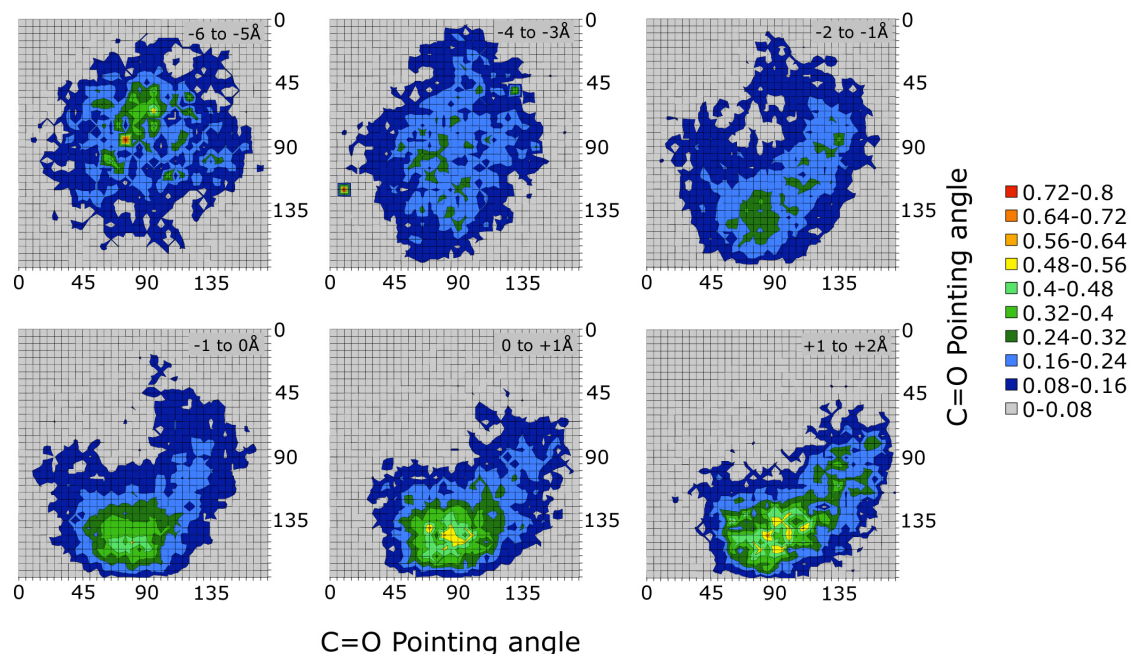
Figure 7.10. Orientational distribution of C=O pointing angles for the conformation AAG.

Another orientational distribution for conformer xGGA is shown in Figure 7.11. While this conformer is not as populous as the AAG conformer, information about the carbonyl directions can be obtained by looking at these plots and provide elucidation to spectral analyses. The conformer shows that at depths near the bulk the carbonyls tend to point in the same direction. Unlike what has been seen previously, there is no large change in the carbonyl pointing directions as this conformation moves towards the interface. There is a shifting towards a prevalence of the distribution near the center of the graph, indicating that both carbonyls are pointing more or less in the plane of the interface. In general, the carbonyls continue to point in the same direction with a wide

distribution around the 90º. Therefore these carbonyls can point slightly above, in, and below the plane of the interface.
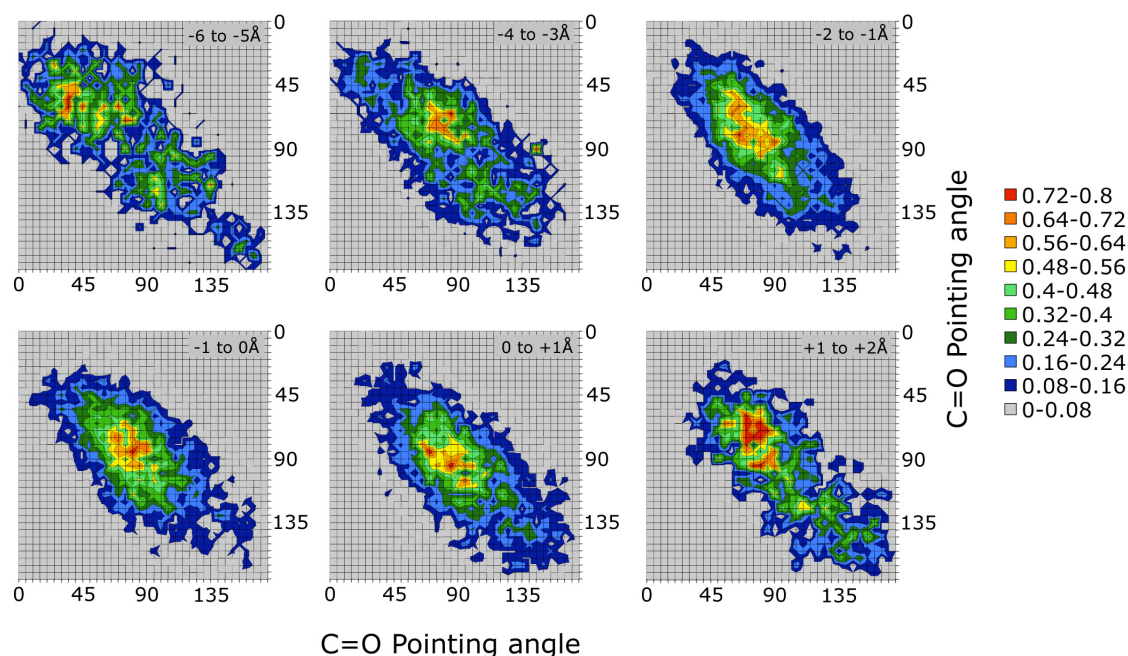
Figure 7.11. Orientational distribution of C=O pointing angles for the conformation xGGA.

These two plots demonstrate that as the carbon backbone has more degrees of freedom introduced through more methylene units, the carbonyl pointing directions become more isotropic. The spectral analysis indicated that the carbonyls may have different solvation environments based on the differences between the frequencies of the SSP and SPS polarized spectra. The computational results here paint a similar picture. As the carbon backbone becomes longer, three results become clear: 1) The torsions along the carbon back bone allow for a higher number of conformers, 2) The highly distorted carbon backbone conformations do not greatly contribute to the surface conformations, 3) The overall distribution of conformations in going from bulk to surface

142

is mostly invariant. This is somewhat different than what was seen for glutaric acid in where there was a loss of one of the main conformations that resulted in more strained conformations becoming prevalent at the interface.

The MD results provided for adipic acid show agreement with spectral analysis while also giving more structure specific details about the orientation as a function of concentration. It is evident that for the main conformation, the carbonyls point both in the plane and down towards the bulk but that for conformations which contribute less, the carbonyls can adopt orientations where the are mostly in the plane. The clear presence of CH_2 vibrations in the VSFS spectra is confirmed by the contribution of all conformers except one (AAA). Additionally, there is no evidence of conformation orientations where one carboxylic group becomes unsolvated, i.e. an orientation where the molecule has one head group solvated, the alkyl backbone pointing away from the surface, and the other head group in the gas phase.

pH Dependent Vibrational Spectroscopy

The previous sections detail the adsorption of adipic acid as a function of concentration. Adipic acid is diprotic and the surface adsorption may be dependent upon these acid groups like what was seen for malonic and succinic acid or may be more similar to glutaric acid. The adsorption of pH adjusted adipic acid is achieved by changing the bulk pH of the solutions and monitoring changes via VSFS and surface tension measurements. The C=O signal arising from the carboxylic moiety will disappear as the pH is increased since the loss of a proton from a carboxylic unit results in a change to a resonance stabilized carboxylate ion. Adipic acid has two carboxylic

moieties and thus two distinct pK_a values. By monitoring the C=O signal using VSFS as well as changes to surface tension, the adsorption of adipic acid under different pH conditions can be elucidated and compared to the shorter chain dicarboxylic acids.

The pK_a values for adipic acid[29] are 4.42 and 5.41. The percentages of protonated species are plotted in Figure 7.12. At a pH of 4, the fully protonated species represent over 70% with the remaining species being singly prononated. At a pH of 5, the fully
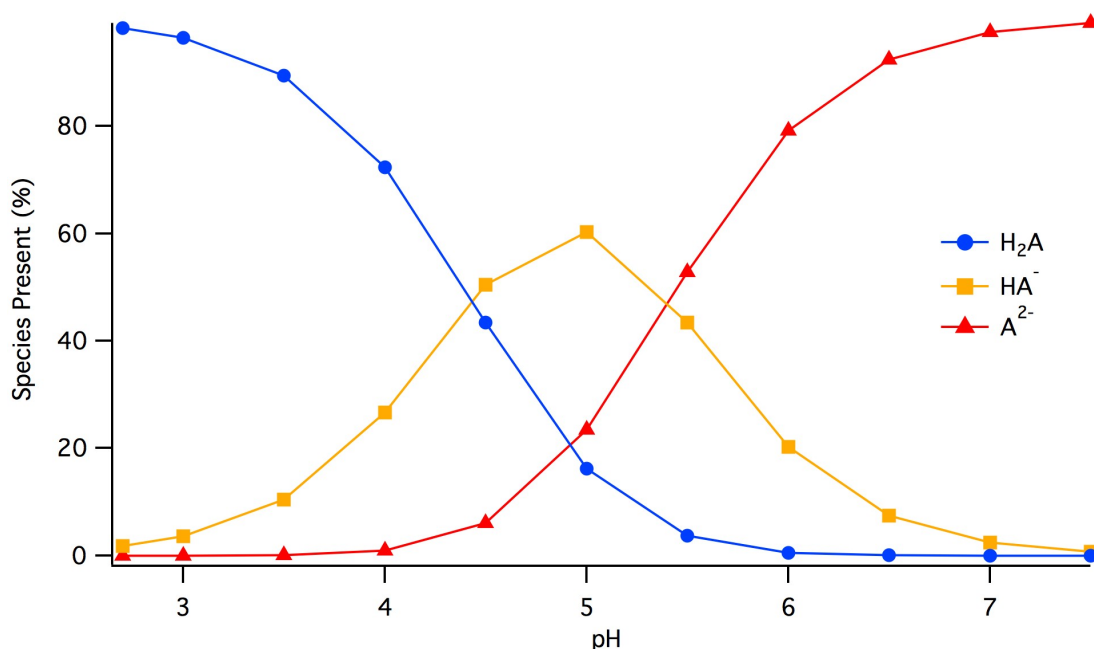
Figure 7.12. Percent of fully protonated, singly protonated, and fully deprotonated aqueous adipic acid solutions based on pK_a values.

protonated species only makes up about 16%, with the singly protonated species dominating the solution at around 60% and the fully dissociated species making up about 24%. At a pH of 6, there is virtually no doubly protonated species left (0.5%), with a fifth of the species being singly protonated and the remaining 80% completely dissociated.

At a constant concentration (0.1M), the bulk pH was adjusted and VSFS data was taken in both SSP and SPS schemes. Figure 7.13 shows the spectral response of adipic acid in the C=O region for SSP as a function of bulk adjusted pH as well as the respective fits. The spectral fits reveal a peak centrally located at 1708 ± 2 cm^{-1} with a Gaussian width of 37 ± 3cm^{-1}. There is a small decrease in intensity for pH of 4 and the intensity decreases monotonically as the pH increases. At a pH of 5.5, there is very little VSFS signal remaining in the C=O region and at a pH of 6, the signal has disappeared.
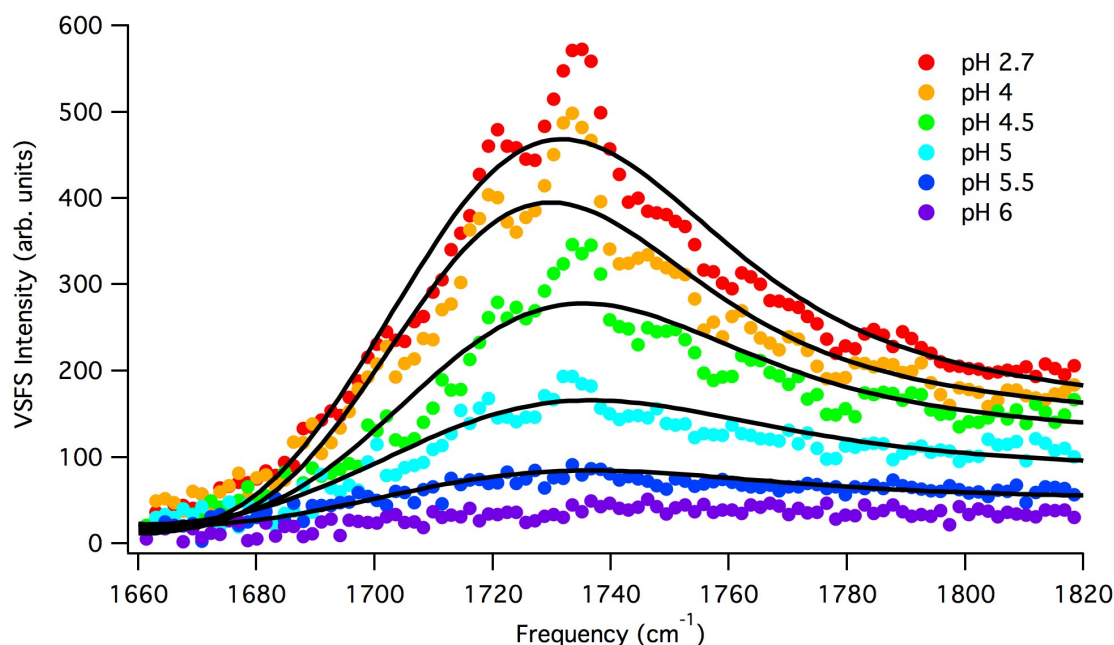
Figure 7.13. VSFS SSP of the C=O region for bulk pH adjusted 0.1M adipic acid. Fits are shown in black.

Figure 7.14 shows the spectral response of adipic acid in the C=O region for SPS as a function of bulk adjusted pH as well as the respective fits. The spectral fits reveal a peak centrally located at 1719 ± 2 cm^{-1} with a Gaussian width of 40 ± 2cm^{-1}. As was seen for SSP, the change in intensity for pH of 4 is small and the intensity decreases

monotonically as the pH increases. At a pH of 5.5, there is no VSFS signal remaining in the C=O region. Attempts were made to probe the carboxylate region (~1400 cm^{-1}) for acidic acid solutions of a high pH (4 and above) but no VSFS signal was found. The VSFS results in the C=O region therefore provide evidence that the surface-active species of adipic acid is the fully protonated moiety. By monitoring the surface tension of these diacids as a function of pH, the results from the VSFS experiments can be further elucidated.
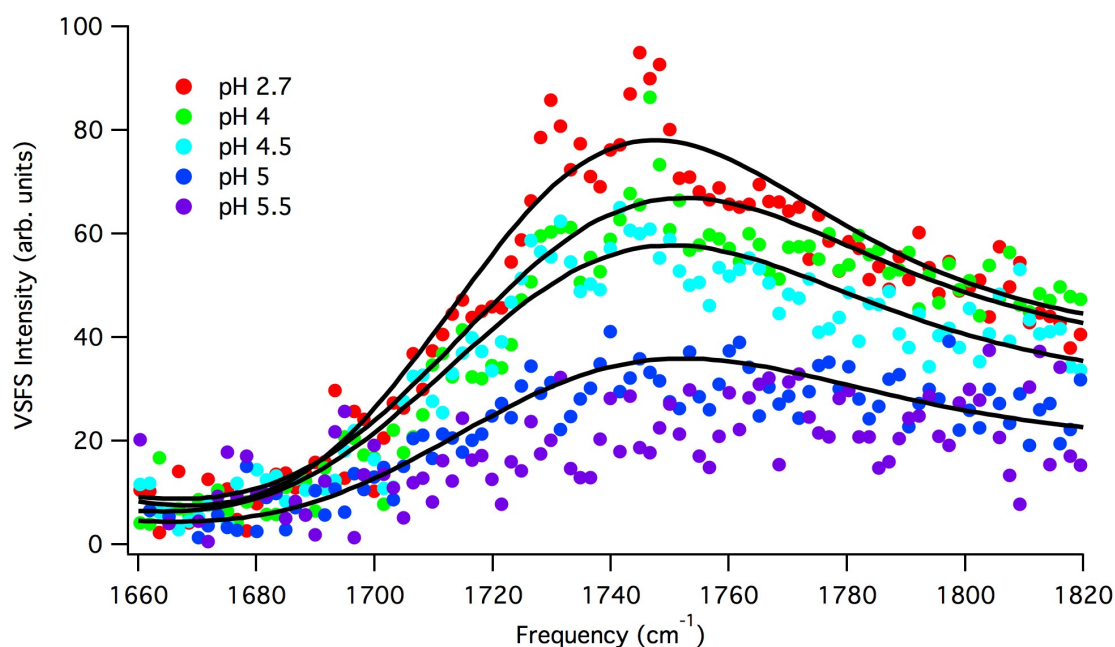
Figure 7.14. VSFS SPS of the C=O region for bulk pH adjusted 0.1M adipic acid. Fits are shown in black.

In addition to the C=O modes, the presence of CH$_2$ modes permit pH analysis based on the CH region. Bulk pH adjusted adipic acid spectra show spectral changes that show desorption as the pH is increased. The strong CH$_2$ signals for native pH adipic acid disappear at pH of 5 and 6, indicating desorption from the interface. The coordinated water region for pH 5 is diminished compared to water but returns to the same intensity

146

for pH 6. The free OH signals also show an increase in going from native pH to pH 5 and 6. In fact, the entire OH region for adipic acid at pH 6 is nearly identical to a pure water spectrum.

These experiments provide further detail to the pH dependent adsorption of adipic acid to the air/water interface. The bulk pH adjusted C=O signal for adipic acid persists to a pH of 5.5 which would indicate that the surface-active species is the fully protonated adipic acid. VSFS in the CH/OH region also show similar results. The CH_2 signal from adipic acid is not detectable at pH of 5 or higher and the OH region is nearly identical to pure water at a pH of 6. This indicates that the adsorption of adipic acid is pH dependent with only the fully protonated species being surface active. This makes adipic acid much more similar to malonic and succinic acid in its surface pH dependence.

pH Dependent Surface Tension

Surface tension measurements provide another method of determining the effect of bulk pH changes on the surface adsorption of adipic acid. Shown in Figure 7.15 is surface pressure of bulk pH adjusted adipic acid (left axis) as well as the percentage of fully protonated species in the bulk (right axis). The surface pressure values decrease as the pH value is adjusted to higher pH values indicating desorption from the interface. The surface pressure reaches a value near that of pure water (indicative of little to no adsorption at the air/water interface) around a pH of 5.5 with little to no change at higher pH values. These surface pressure values closely follow the bulk species percentages.

147
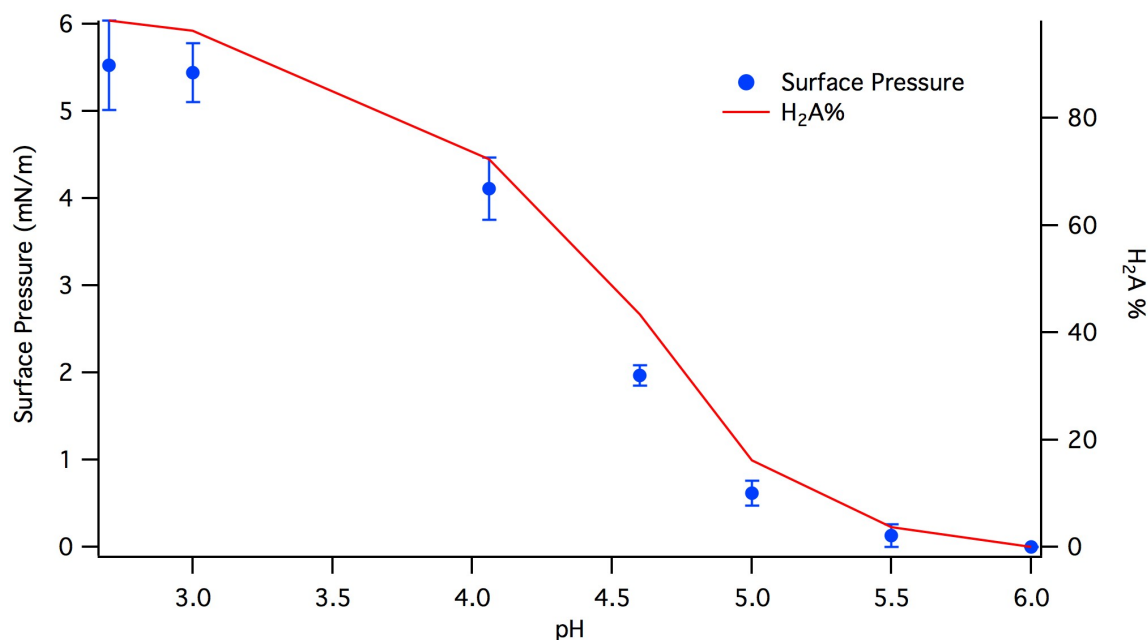
Figure 7.15. Surface pressure and percentage of fully protonated adipic acid versus bulk pH values.

Plotted in Figure 7.16 is the surface pressure of bulk pH adjusted adipic acid (left axis) along with the square root of the VSFS fitted amplitudes for the C=O mode for both SSP and SPS (right axis). The VSFS signal from the C=O decreases monotonically for both polarization schemes and follow the surface pressure data. With the surface pressure and VSFS data combined, it is clear that the adsorption of adipic is highly sensitive to changes in pH because the fully protonated form of adipic acid is the surface-active species. This places adipic acid in the same category as malonic and succinic acid.

A combined photoelectron spectroscopy and computational modeling paper investigated the solvation of dicarboxylate anions in small water clusters (1-20 water molecules).[30] Their results for the adipate ion indicated that this ion prefers bulk solvation, which is completely consistent with the results of this study. Additionally,
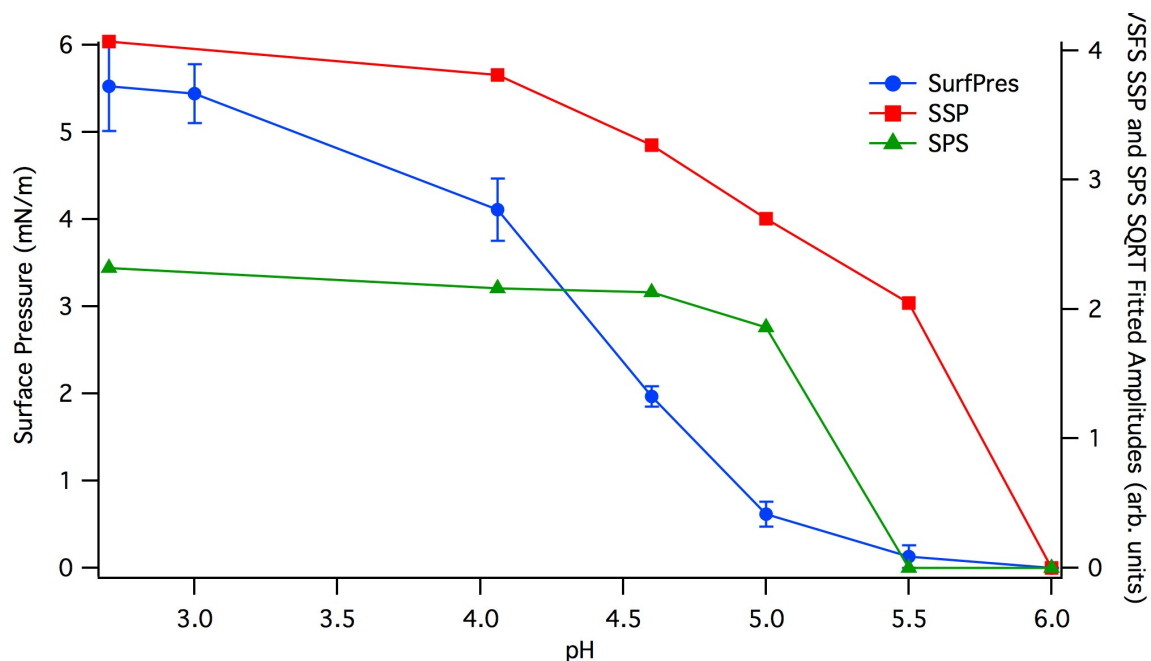
Figure 7.16. Surface pressure and square root of VSFS SSP and SPS fitted amplitudes for bulk pH adjusted 0.1 M adipic acid.

they also investigated[31] the suberate dianion ($^-O_2C(CH_2)_6CO_2^-$), which is two methylene units longer than adipic acid. For this anion, they found evidence of preferential surface adsorption due to the longer hydrophobic alkyl chain's ability to overcome the hydrophilic desire of the charged carboxylates. It is therefore likely that the pH dependence of surface adsorbed dicarboxylic acids longer than adipic acid will result in surface species beyond just the fully protonated species.

Conclusions

The behavior of adipic acid at the air/water interface is fully described through correlation of VSFS, surface tension, and computational modeling. The results show that adipic acid is strongly solvated at the interface and participates in different levels of hydrogen bonding with the water network due to increased degrees of freedom along the

carbon backbone. The surface area per molecule of adipic acid is large and does not pack tightly at the interface. Adipic acid adsorption at the air/water interface is also shown to be pH dependent with only the fully protonated surface species being surface active. Despite the stronger solvation evidenced by the C=O modes, the surface behavior of adipic acid resembles that of malonic and succinic acid. The additional methylene unit on adipic acid increases the surface activity (at a given concentration) as well as decreasing the bulk solubility when compared to the other dicarboxylic acids studied in this work. It might be expected then that this additional hydrophobicity would lead to behavior similar to that of glutaric acid. However, despite the additional methylene unit, adipic acid behavior is similar to the shorter chain dicarboxylic acids, malonic and succinic.

CHAPTER VIII

CONCLUSIONS AND FUTURE WORK

Aerosols are an integral part of our atmosphere and as such are the subject of numerous studies, from detection in the atmosphere[1] and laboratory studies[2] to thermodynamic modeling[3,4] and computational trajectories.[5] Due to the incredible diversity of material in these particles, which affects their size and fate, studying the behavior of aerosols is not trivial. Indeed, even the size of aerosols spans multiple orders of magnitude, from small clusters on the order of 10's of nanometers up to hundreds of micrometers.[6] The smaller end of this size range presents difficulties in studying due to many issues including a large surface to volume ratio.

This dissertation fully describes the surface adsorption behavior of a prevalent class of water-soluble organic material, low molecular weight dicarboxylic acids. By using a combination of surface specific experimental techniques as well computational modeling, the surface behavior of these acids has been characterized. At first glance, the differences between these molecules seem inconsequential, with only a small change to an alkyl spacer between two identical carboxylic acid groups. Upon closer inspection, however, the surface behavior of these acids is not so straightforward.

One important difference between these acids at the surface is the solvation environment of the carboxylic head group. Malonic acid displayed frequencies blue shifted from bulk vibrational frequencies indicating weak solvation. One explanation for this unique behavior is because it is adopting a ring structure that is intramolecularly bonded. Succinic acid displayed surface vibrational frequencies of the carbonyl mode that are indicative of surfactant-like solvation. The C=O frequency for succinic acid is in

a range similar to monocarboxylic acids that have been previously studied vis VSFS.[7,8] Glutaric acid showed a further shifting in C=O frequencies that are nearly bulk–like, demonstrating that the carboxylic head groups for this acid are better solvated at the air/water interface than the shorter chain dicarboxylic acids. In addition, evidence of dimerization at the air/water interface was seen for glutaric acid but not for other species. Adipic acid exhibited different frequency responses for the C=O mode indicating that there are multiple solvation environments around these head groups, with one that is less solvated (more surfactant-like) and one more solvated (more bulk-like). Because the carbonyl mode is sensitive to the solvation environment around it, a greater understanding of how dicarboxylic acids orient at the air/water surface is gained from VSFS studies. The increasing solvation as a function of alkyl chain length is a unique property at the surface since the solvation of a carboxylic headgroup for small monocarboxylic acids does not change.[7,8]

In addition to the solvation environment, the surface area per molecule indicates that this class of molecules does not pack tightly at the interface. All of these acids have much larger surface areas than traditional surfactants. For example, the monocarboxylic acid hexanoic acid has a surface area per molecule that is around ~60 $Å^2$ while adipic acid, which has the same number of carbons, has a surface area three times as large (~190 $Å^2$). The loosely packed surface behavior of these dicarboxylic acids also implies that it is unlikely there will be synergistic effects at the surface. For example, fatty acids, which are long chain monocarboxylic acids and are a common surfactant, will have closer packing at the interface as the length of the hydrophobic group (i.e. the alkyl chain) increases.[9] As the surfactant chain length is increased, the molecular packing between

the surfactant molecules at the interface becomes tighter due to van der Waals interactions. Thus, the surface concentration (moles/cm^2) increases and the area per molecule decreases.[10] In a recent study,[11] researchers investigated the surface tension of N-lauroylaminomalonic acid, N-laurylaspartic acid, and N-laurylglutamic acid which are surfactant analogs of malonic, succinic, and glutaric acid, respectively. The area per molecule for these surfactants was between 70-100 Å^2. The lack of a strong hydrophobic group on dicarboxylic acids therefore results in loose packing at the air/water surface. This isolated adsorption at the interface is also seen through the VSFS studies in the OH region. The free OH signal does not disappear for molar concentrations of malonic or glutaric, or for the highest concentrations possible for succinic and adipic. Since the free OH signal is an indicator of the top most surface layer at an air/water interface, there must remain water molecules at this layer, which are not disrupted by the organic adsorption.

The comparatively large surface area per molecule for this class is also indicative of an orientation that lies mostly flat at the interface. Once again, this is in contrast to a traditional surfactant that will orient more normal to the interface, with its hydrophobic backbone sticking into the vapor phase and the hydrophilic head group remaining solvated by water at the interface. The "flat" orientation is seen and confirmed by spectral experiments in the CH$_2$ region as well as computational modeling. In both, evidence of gauche conformations along the carbon backbone is found. The use of computational modeling provides even further information by allowing depth specific percentages of conformations to be accessed. Molecular orientations derived from computational modeling are used not only to confirm spectral analyses but also elucidate

153

those results. For example, the absolute direction of the C=O bonds in computational modeling can differentiate between the ambiguity of directionality arising from SSP VSFS spectra as was seen in Chapter IV for malonic acid.

Organic coated aerosol surfaces are expected to undergo processing from oxidation reactions as they are transported through the atmosphere.[12,13] The organic material in aerosols will therefore have a higher oxygen:carbon ratio as these oxidation reactions occur. The formation of dicarboxylic acids has been tied to this secondary organic aerosol (SOA) formation,[14,15] in addition to known primary sources.[16,17] The fate of aerosols is thus dependent upon the surface behavior of oxidized organic material. The combination of the experimental and computational results in this work describes the adsorption conditions at an air/water interface by varying concentration. Isolated at the surface (with the exception of highly concentrated glutaric acid solutions), these molecules orient their carbon backbone mostly flat at the interface. In addition, as the backbone grows longer, the added degrees of freedom allow the headgroups to solvate more efficiently with the surface water network. There is no evidence that these acids will orient themselves in a manner similar to a surfactant. It is also evident that the water surface is not completely covered.

Since these acids are diprotic, the pH dependencies of surface adsorption were investigated. Due to the very small volumes that aerosols can exist in the atmosphere, the pH of aerosols is a difficult area of study.[18] Despite these difficulties, measurements have been made on larger fog, cloud, and rain droplets.[19] Depending upon the location, time of day, season, and other environmental factors, the pH can vary by multiple pH units.[20,21] In general, the pH of large aerosols is in the range of 3-5,[22,23] with smaller

154

aerosols being more acidic. Since dicarboxylic acids are preferentially separated in the aerosol phase due to their low vapor pressure[24] and contain more than one acid group, the surface behavior as a function of pH is fundamentally important. The pH experiments in this work provide a complete description of the pH dependence of dicarboxylic acids adsorbed to an air/water interface and can be used as a model for aerosol surfaces.

Malonic, succinic, and adipic acid have surface activity that is completely dependent upon the protonation state. Since only the fully protonated species is surface active, the role of these molecules at the surface will be explicitly tied to the intrinsic pH of the aerosol. On the other hand, glutaric acid is shown to be less sensitive to changes in the pH and will remain surface active at relevant atmospheric pH values. It is somewhat surprising that the strong solvation seen for the C=O mode does not translate to a stabilization of charge at the air/water interface. Since the deprotonated forms are more soluble, the loss of a proton from increasing the pH of these solutions results in a diminished surface activity. Since organic coatings are imperative in controlling aerosol dynamics, the pH dependent surface studies done in this work are extremely important for a better understanding of how pH can affect more than just bulk properties.

Atmospheric gasses that can affect the pH of an aerosol via their dissolution into the aqueous bulk are expected to affect aerosols containing low molecular weight dicarboxylic acids. For example, adsorption of SO_2 (g), a common atmospheric pollutant, into an aerosol leads to acidification.[6,25] A study[26] looking at the effect of SO_2 (g) uptake on an aqueous succinic acid surface indicated that succinic acid does not disrupt the surface complexation of SO_2 at the air/water interface. Therefore, an aerosol containing succinic acid will be expected to have increased surface adsorption for alkaline aerosols.

Based on the results of these studies, malonic and adipic acid may also display similar behavior due to their isolated surface areas and pH dependence. Thus, gasses that will increase the pH of an aerosol (e.g. SO_2 and CO_2) through adsorption into the bulk will drive the dicarboxylic acids to the aqueous surface. Likewise, gasses that will decrease the pH of an aerosol (e.g. NH_3) will drive dicarboxylic acids into the bulk.

Future Directions and Preliminary Studies

The microphysical structure of tropospheric aerosol is highly uncertain despite the overwhelming necessity of knowing the physical state.[27] The studies conducted in this work not only elucidated the behavior of short chain dicarboxylic acids but also provided a framework to begin studying more complicated systems. For example, soot particles impact air quality and cloud formation and are emitted as complex aggregates. A recent study has shown that dicarboxylic acids can affect the structure and hygroscopic behavior of soot particles.[28] The role of dicarboxylic acids beyond their own aqueous surface behavior is of obvious relevance.

The inorganic fraction in aerosols is well described as aqueous binary systems, but the addition of organic material causes uncertainty in the structure of aerosols. For example, there can be inorganic/organic mixing in the liquid phase or phase segregation of organics.[29] The phase segregation of organics is even more difficult to describe since there can be phase separation between liquids (liquid-liquid phase separation) which can result in multiple morphologies including core-shell structures and partially engulfed structures.[30,31] These ternary systems are currently of great interest. Since dicarboxylic acids represent prevalent water soluble organic material, the behavior of these organic

156

molecules with additional inorganic components is necessary to gain a fundamental understanding of how aerosol behavior may change. As these fractions are changed (in both organic and inorganic materials), is there evidence of a particular morphology such as a core-shell structure or do the acids prefer bulk solvation? Is there evidence of phase separation and organic "lensing" at the interface? In order to answer these questions, spectra of malonic acid with some atmospherically relevant ions have been probed in the C=O region and through surface tension measurements. The preliminary results are shown below.

Preliminary studies on ternary aqueous dicarboxylic acid and atmospherically relevant ions have shown interesting behavior. Shown in Figure 8.1 is the surface tension of malonic acid with various ions added at two different concentrations. The addition of
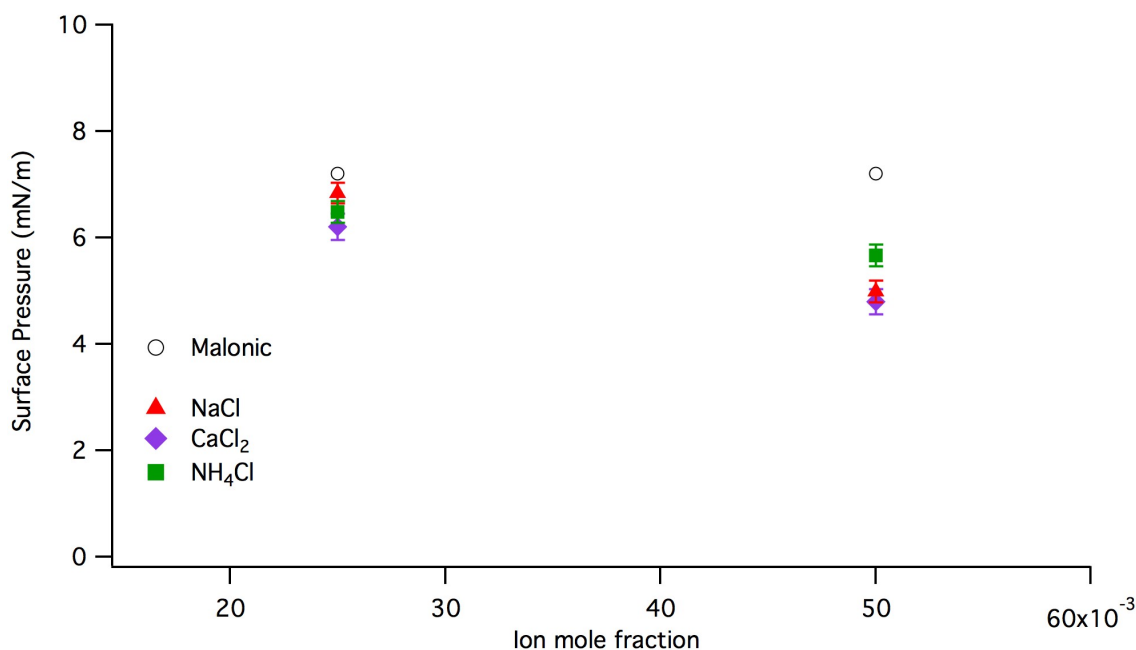
Figure 8.1. Surface pressure of 0.05mf malonic acid (black circles) with additional ions added at 0.025mf and 0.05mf.

ions to the aqueous system results in a decrease in surface pressure for all ions. This is not surprising since it is known that ions in an aqueous system increase surface tension,[32,33] due to an increase in the water structure at the interface. A common scheme when discussing ion affects in aqueous organic systems is the Hofmeister series.[34,35] In this scheme, ions are classified by their ability to "salt out" or "salt in" proteins. While the hofmeister series has been shown to be involved in a myriad of different processes beyond protein behavior,[35] it is still considered a phenomenological effect. For the studies here, the chloride anion is considered neutral in the series, displaying neither salting in or salting out behavior. The cations represent salting out, salting in, and neutral species; NH^{4+} is considered a strong salting out agent, Na^+ is considered neutral, while Ca^{2+} is considered a strong salting in agent. The general trend of the surface pressure data is a decrease in surface pressure as the ion concentration increase with $CaCl_2$ being the strongest. The effect of a dicarboxylic acid at the aqueous surface with additional ions is then in question. Does the surface pressure decrease merely reflect an increase in water structure with no change in the organic concentration? Does the decrease in surface pressure indicate a loss of organic concentration at the interface? Or is it an additive system resulting in a combination of both phenomena?

In Figure 8.2, the VSFS spectra of the C=O region for malonic acid at 0.05mf with NaCl added is shown for SSP and SPS. It is clear that the resonant peaks of the C=O mode in SSP gain intensity as the amount of ion added increases in both polarization schemes. For the SPS spectra, the increase doesn't occur for 0.025mf but

158
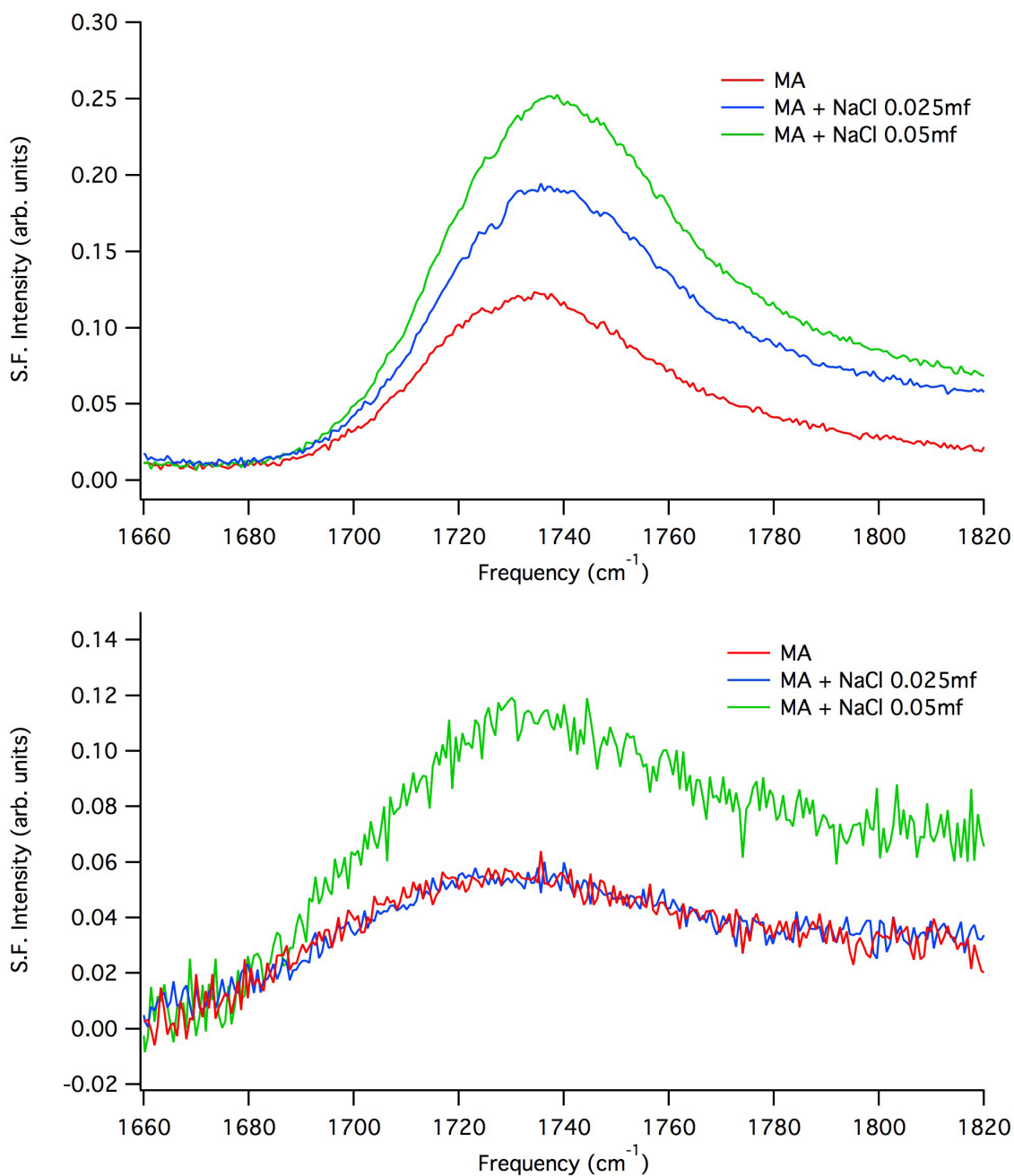
Figure 8.2. VSFS SSP of C=O mode for 0.05mf malonic acid (red trace) with 0.025mf NaCl (blue trace) and 0.05mf NaCl (green trace).

does at equivalent ion and organic concentrations. When performed at lower organic concentrations (0.025mf), the SSP data showed a monotoninc increase as the ion concentration increased for both polarizations.

In Figure 8.3, the VSFS spectra of the C=O region for malonic acid at 0.05mf with CaCl$_2$ added is shown for SSP and SPS. Much like what was seen for NaCl, the addition of CaCl$_2$ results in a large increase in the intensity of the C=O peak for SSP.
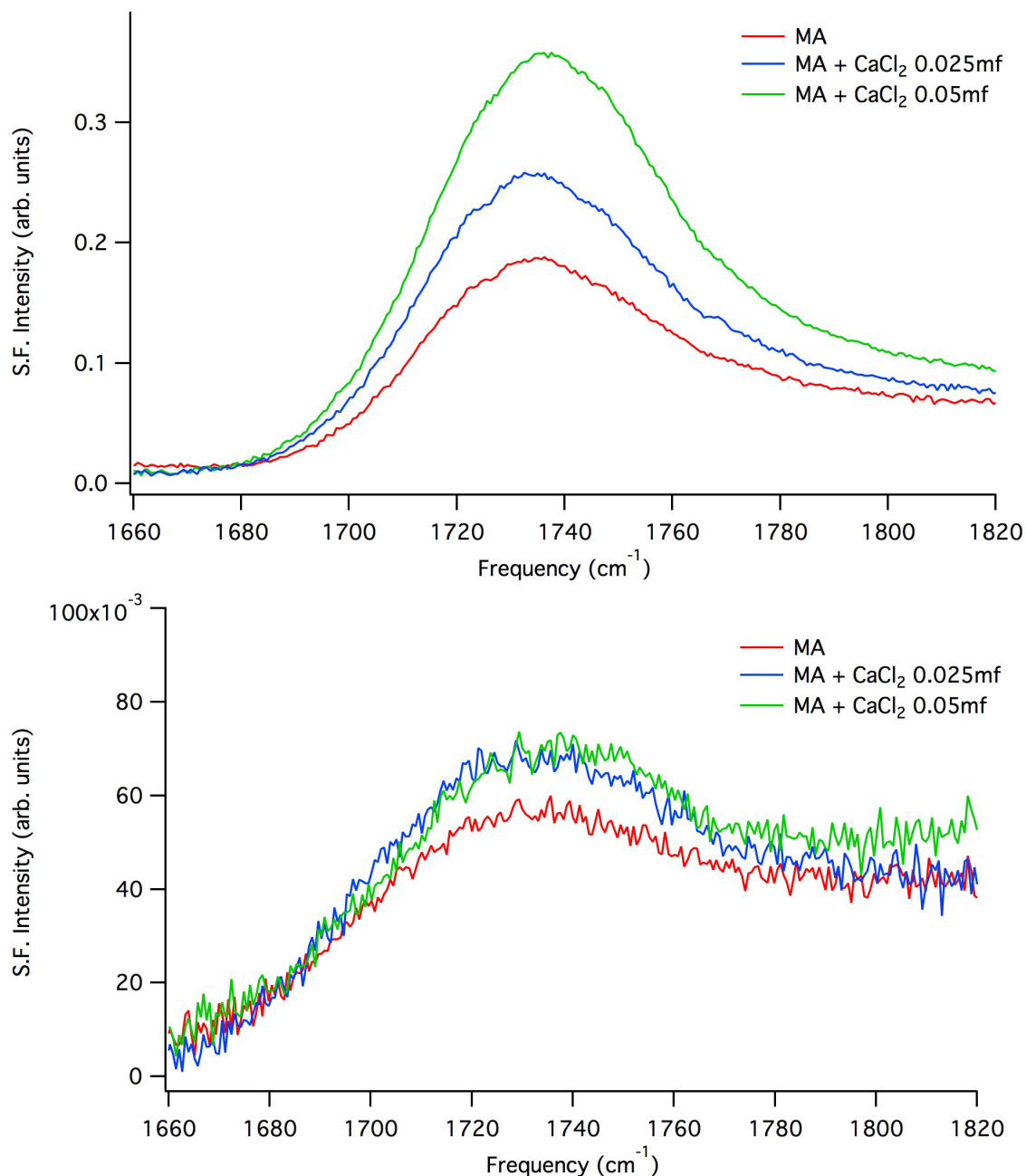
Figure 8.3. VSFS SSP of C=O mode for 0.05mf malonic acid (red trace) with 0.025mf CaCl$_2$ (blue trace) and 0.05mf CaCl$_2$ (green trace).

160

However, the SPS data shows an increase in the C=O intensity as the ion concentration increases. When performed at lower organic concentrations (0.025mf), the same effect was observed. Therefore both NaCl and CaCl$_2$ are behaving in an analogous manner.

Shown in Figure 8.4 is the VSFS spectra of the C=O region for malonic acid at
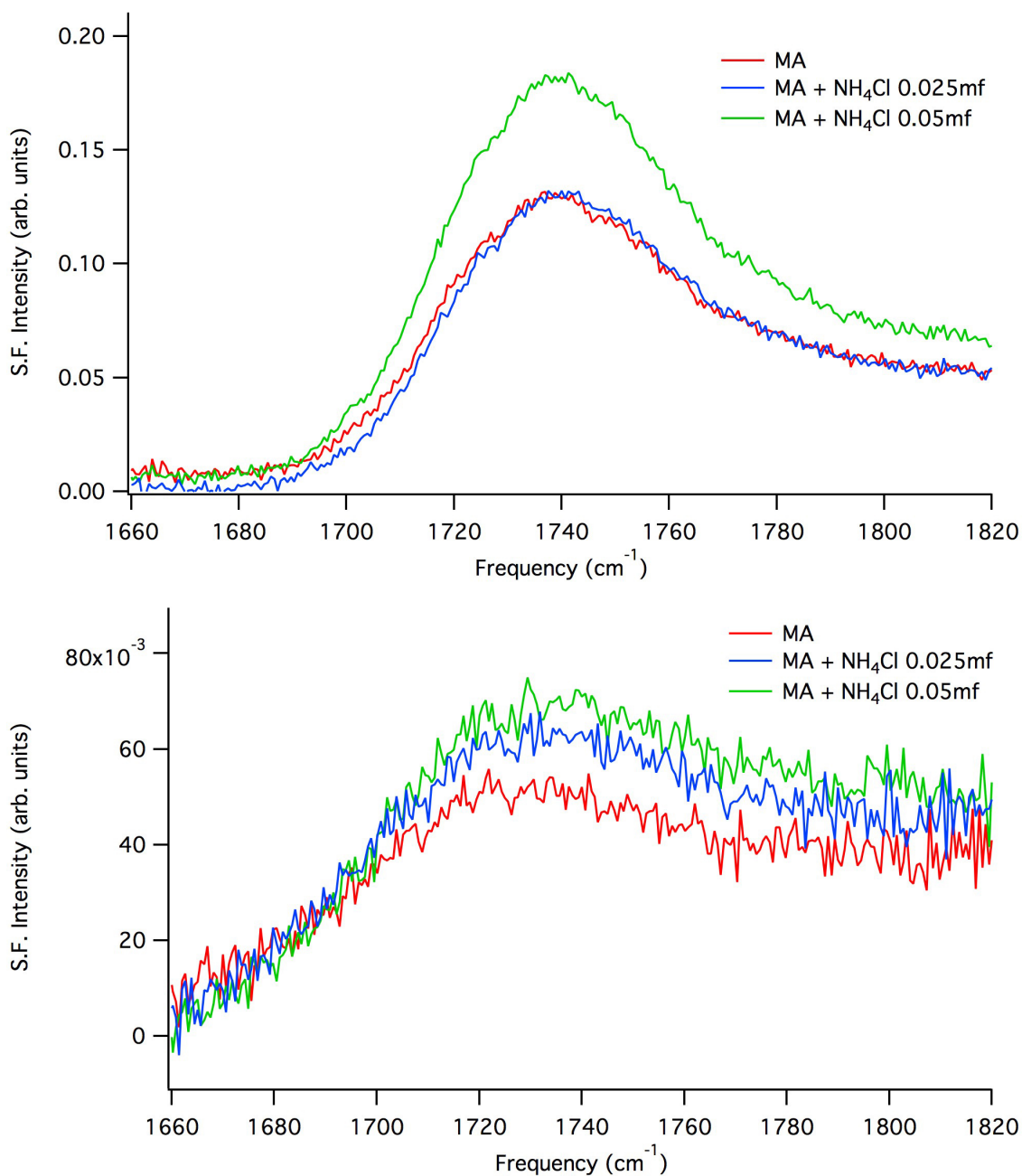
Figure 8.4. VSFS SSP of C=O mode for 0.05mf malonic acid (red trace) with 0.025mf NH$_4$Cl (blue trace) and 0.05mf NH$_4$Cl (green trace).

161

0.05mf with NH$_4$Cl added for SSP and SPS. In the SSP spectra, there is an increase in the signal intensity of the C=O mode but only once the addition of the ion reaches equivalent concentration to malonic acid. However, the change for SPS is a monotonic increase in intensity. For the lower organic concentration (0.025mf), there is very little increase in intensity as the ions are added for both polarizations.

The surface pressure data and the VSFS data show similar trends in that there is a general decrease in surface pressure as ions are added to the aqueous system while there is a general increase in the intensity of the C=O signal. The increase in signal in the VSFS data indicates that malonic acid is not desorbing from the interface. This may be evidence of a core-shell morphology in which the organic is being phase separated to the surface. Some questions immediately arise including: 1) Does the decrease in surface pressure result from water restructuring at air/water interface, 2) Does the addition of ions cause electrostriction, causing in effect a higher organic concentration, and 3) Is the increase in the C=O signal resulting from a field being set up at the interface that causes a smaller distribution in orientation leading to an increased signal? These questions require careful experimentation and can reveal exciting results about the nature of these atmospherically important surfaces.

REFERENCES CITED

CHAPTER I

(1)   Seinfeld, J. H.; Pandis, S. N. *Atmospheric Chemistry and Physics*; Wiley-Interscience: New York, 1998.

(2)   Finlayson-Pitts, B. J.; James N. Pitts, J. *Chemistry of the Lower and Upper Atmosphere*; Academic Press: San Diego, 2000.

(3)   Parsons, M. T.; Mak, J.; Lipetz, S. R.; Bertram, A. K. Deliquescence of malonic, succinic, glutaric, and adipic acid particles. *J. Geophys. Res.* **2004**, *109*, 8.

(4)   Chebbi, A.; Carlier, P. Carboxylic Acids in the Troposphere, Occurrence, Sources, and Sinks: A Review. *Atmos. Environ.* **1996**, *30*, 4233-4249.

(5)   Kawamura, K.; Usukura, K. Distributions of Low Molecular Weight Dicarboxylic Acids in the North Pacific Aerosol Samples. *J. Oceanogr.* **1993**, *49*, 271-283.

(6)   Kawamura, K.; Kasukabe, H.; Barrie, L. A. Source and reaction pathways of dicarboxylic acids, ketoacids and dicarbonyls in arctic aerosols: One year of observations. *Atmos. Environ.* **1996**, *30*, 1709-1722.

(7)   Kawamura, K.; Sakaguchi, F. Molecular distributions of water soluble dicarboxylic acids in marine aerosols over the Pacific Ocean including tropics. *J. Geophys. Res.* **1999**, *104*, 3501-3509.

(8)   Sempéré, R.; Kawamura, K. Comparative distributions of dicarboxylic acids and related polar compounds in snow, rain, and aerosols from urban atmosphere. *Atmos. Environ.* **1994**, *28*, 449-459.

(9)   Sempéré, R.; Kawamura, K. Low molecular weight dicarboxylic acids and related polar compounds in the remote marine rain samples collected from western Pacific. *Atmos. Environ.* **1996**, *30*, 1609-1619.

(10)   Aggarwal, S. G.; Kawamura, K. Molecular distributions and stable carbon isotopic compositions of dicarboxylic acids and related compounds in aerosols from Sapporo, Japan: Implications for photochemical aging during long-range atmospheric transport. *J. Geophys. Res.* **2008**, *113*, 13.

(11)   Hsieh, L.-Y.; Kuo, S.-C.; Chen, C.-L.; Tsai, Y. I. Origin of low-molecular-weight dicarboxylic acids and their concentration and size distribution variation in suburban aerosol. *Atmos. Environ.* **2007**, *41*, 6648-6661.

(12)   Hsieh, L.-Y.; Kuo, S.-C.; Chen, C.-L.; Tsai, Y. I. Size distributions of nano/micron dicarboxylic acids and inorganics ions in suburban PM episode and non-episodic aerosol. *Atmos. Environ.* **2009**, *43*, 4396-4406.

(13)   Pavuluri, C. M.; Kawamura, K.; Swaminathan, T. Water-soluble organic carbon, dicarboxylic acids, ketoacids, and α-dicarbonyls in the tropical Indian aerosols. *J. Geophys. Res.* **2010**, *115*, 15.

(14)   Kawamura, K.; Kaplan, I. R. Motor Exhaust Emissions as a Primary Source for Dicarboxylic Acids in Los Angeles Ambient Air. *Environ. Sci. Tech.* **1987**, *21*, 108-110.

(15)   Rogge, W. F.; Hildemann, L. M.; Mazurek, M. A.; Cass, G. R. Sources of Fine Organic Aerosol. 9. Pine, Oak, and Synthetic Log Combustion in Residential Fireplaces. *Environ. Sci. Technol.* **1998**, *32*, 13-22.

(16)   Kawamura, K.; Gagosian, R. B. Implications of ω-oxocarboxylic acids in the remote marine atmosphere for photo-oxidation of unsaturated fatty acids. *Nature* **1987**, *325*, 330-332.

(17)   Ellison, G. B.; Tuck, A. F.; Vaida, V. Atmospheric Processing of Organic Aerosols. *J. Geophys. Res.* **1999**, *104*, 11633-11641.

(18)   Donaldson, D. J.; Vaida, V. The Influence of Organic Films at the Air-Aqueous Boundary on Atmospheric Processes. *Chem. Rev.* **2006**, *106*, 1445-1461.

(19)   Braban, C. F.; Carroll, M. F.; Styler, S. A.; Abbatt, J. P. D. Phase Transitions of Malonic and Oxalic Acid Aerosols. *J. Phys. Chem. A* **2003**, *107*, 6594-6602.

(20)   Hansen, A. R.; Beyer, K. D. Experimentally Determined Thermochemical Properties of the Malonic Acid/Water System: Implications for Atmospheric Aerosols. *J. Phys. Chem. A* **2004**, *108*, 3457-3466.

(21)   Hyvärinen, A.-P.; Lihavainen, H.; Gaman, A.; Vairila, L.; Ojala, H.; Kulmala, M.; Viiasnen, Y. Surface tensions and densities of oxalic, malonic, succinic, maleic, malic, and cis-pinonic acids. *J. Chem. Eng. Data* **2006**, *51*, 255-260.

(22)   Booth, A. M.; Topping, D. O.; McFiggans, G.; Percival, C. J. Surface tension of mixed inorganic and dicarboxylic acid aqueous solutions at 298.15 K and their importance for cloud activation predictions. *Phys. Chem. Chem. Phys.* **2009**, *11*, 8021-8028.

(23)   Riipinen, I.; Koponen, I. K.; Frank, G. P.; Hyärinen, A.-P.; Vanhanen, J.; Lihavainen, H.; Lehtinen, K. E. J.; Bilde, M.; Markku, K. Adipic and Malonic Acid Aqueous Solutions: Surface Tensions and Saturation Vapor Pressures. *J. Phys. Chem. A* **2007**, *111*, 12995-13002.

(24)   Varga, Z.; Kiss, G.; Hansson, H.-C. Modelling the cloud condensation nucleus activity of organic acids on the basis of surface tension and osmolality measurements. *Atmos. Chem. Phys.* **2007**, *7*, 4601-4611.

(25)   Giebl, H.; Berner, A.; Reischl, G.; Puxbaum, H.; Kasper-Giebl, A.; Hitzenberger, R. CCN activation of oxalic and malonic acid test aerosols with the University of Vienna cloud condensation nuclei counter. *J. Aerosol Sci.* **2002**, *33*, 1623-1634.

(26)   Finlayson-Pitts, B. J. Reactions at surfaces in the atmosphere: integration of experiments and theory as necessary (but not necessarily sufficient) for predicting the physical chemistry of aerosols. *Phys. Chem. Chem. Phys.* **2009**, *11*, 7760-7779.

(27)   Hayase, S.; Yabushita, A.; Kawasaki, M.; Enami, S.; Hoffman, M. R.; Colussi, A. J. Weak Acids Enhance Halogen Activation on Atmospheric Water's Surfaces. *J. Phys. Chem. A* **2011**, *115*, 4935-4940.

(28)   Cruz, C. N.; Pandis, S. N. The effect of organic coatings on the cloud condensation nuclei activation of inorganic atmospheric aerosol. *J. Geophys. Res. Atmos.* **1998**, *103*, 13111-13123.

(29)   Cappa, C. D.; Lovejoy, E. R.; Ravishankara, A. R. Determination of Evaporation Rates and Vapor Pressures of Very Low Volatility Compounds: A Study of the C4-C10 and C12 Dicarboxylic Acids. *J. Phys. Chem. A* **2007**, *111*, 3099-3109.

(30)   Bilde, M.; Svenningsson, B.; Mønster, J.; Rosenørn, T. Even-odd alternation of evaporation ratesand vapor pressures of C3-C9 dicarboxylic acid aerosols. *Environmental Science & Technology* **2003**, *37*, 1371-1378.

(31)   Thalladi, V. R.; Nüsse, M.; Boese, R. The melting point alternation in α,ω-Alkanedicarboxylic acids. *Journal of the American Chemical Society* **2000**, *122*, 9227-9236.

(32)   Rozaini, M. Z. H.; Brimblecone, P. The odd-even behaviour of dicarboxylic acids solubility in the atmpospheric aerosols. *Water Air Soil and Pollution* **2009**, *198*, 65-75.

CHAPTER II

(1)   Shen, Y. R. *The Principles of Nonlinear Optics*; John Wiley & Sons: New York, 1984.

(2)   Boyd, R. W. *Nonlinear Optics*; Third ed.; Academic Press: Burlington, MA, 2008.

(3)   Lambert, A. G.; Davies, P. B.; Neivandt, D. J. Implementing the Theory of Sum Frequency Generation Vibrational Spectroscopy: A Tutorial Review. *Appl. Spectrosc. Rev.* **2005**, *40*, 103-145.

(4)   Kido-Soule, M. C., University of Oregon, 2007.

(5)   Tarbuck, T. L., University of Oregon, 2006.

(6)   Rao, Y.; Li, X.; Lei, X.; Jockusch, S.; George, M. W.; Turro, N. J.; Eisenthal, K. B. Observations of Interfacial Population and Organization of Surfactants with Sum Frequency Generation and Surface Tension. *J. Phys. Chem. C* **2001**, *115*, 12064-12067.

(7)   Davies, J. T.; Rideal, E. K. *Interfacial Phenomena*; 2nd ed.; Academic Press: New York, 1963.

(8)   Rosen, M. J. *Surfactants and Interfacial Phenomena*; 3rd ed.; John Wiley & Sons, Inc., 2004.

(9)   Joos, P. *Dynamic Surface Phenomena*; VSP: Utrecht, Netherlands, 1999.

(10)   Lyklema, J. *Fundamentals of Interface and Colloid Science*, 1991; Vol. Volume 1: Fundamentals.

CHAPTER III

(1)   Kido-Soule, M. C., University of Oregon, 2007.

(2)   Richter, L. J.; Petralli-Mallow, T. P.; Stephenson, J. C. Vibrationally resolved sum-frequency generation with broad-bandwidth infrared pulses. *Opt. Lett.* **1998**, *23*, 1594-1596.

(3)   Silverstein, R. M.; Webster, F. X. *Spectrometric Identification of Organic Compounds*; 6th ed.; John Wiley & Sons, Inc., 1998.

(4)   Bain, C. D.; Davies, P. B.; Ong, T. H.; Ward, R. N. Quantitative Analysis of Monolayer Composition by Sum-Frequency Vibrational Spectroscopy. *Langmuir* **1991**, *7*, 1563-1566.

(5)   Davies, J. T.; Rideal, E. K. *Interfacial Phenomena*; 2nd ed.; Academic Press: New York, 1963.

(6)   Borkowski, M.; 1.0.3.15 ed. 2008.

(7)   Case, D. A.; Darden, T. A.; T.E. Cheatham, I.; Simmerling, C. L.; Wang, J.; Duke, R. E.; Luo, R.; Walker, R. C.; Zhang, W.; Merz, K. M.; Roberts, B.; Wang, B.; Hayik, S.; Roitberg, A.; Seabra, G.; Kolossváry, I.; Wong, K. F.; Paesani, F.; Vanicek, J.; Liu, J.; Wu, X.; Brozell, S. R.; Steinbrecher, T.; Gohlke, H.; Cai, Q.; Ye, X.; Wang, J.; Hsieh, M.-J.; Cui, G.; Roe, D. R.; Mathews, D. H.; Seetin, M. G.; Sagui, C.; Babin, V.; Luchko, T.; Gusarov, S.; Kovalenko, A.; Kollman, P. A.; University of California, San Francisco: 2010.

(8)   Pearlman, D. A.; Case, D. A.; Caldwell, J. W.; Ross, W. S.; Cheatham, T. E.; Debolt, S.; Ferguson, D.; Seibel, G.; Kollman, P. *Comput. Phys. Commun.* **1995**, *91*, 1-41.

(9)   Martinez, L.; Andrade, R.; Birgin, E.; Martinez, J. PACKMOL: A package for building initial configurations for molecular dynamics simulations. *J. Comput. Chem.* **2009**, *30*, 2157-2164.

(10)   Caldwell, J. W.; Kollman, P. A. Structure and Properties of Neat Liquids Using Nonadditive Molecular Dynamics: Water, Methanol, and N-Methylacetamide. *J. Phys. Chem.* **1995**, *99*, 6208-6219.

(11)   Case, D. A.; Cheatham, T. E.; Darden, T.; Gohlke, H.; Luo, R.; Merz, K. M.; Onufriev, A.; Simmerling, C.; Wang, B.; Woods, R. J. The Amber biomolecular simulation programs. *J. Comput. Chem.* **2005**, *26*, 1668-1688.

(12)   Shamay, E. S.; Johnson, K.; Richmond, G. L. Dancing on Water: The Choreography of Sulfur Dioxide Adsorption to Aqueous Surfaces. *J. Phys. Chem. C* **2011**, *115*, 25304-25314.

(13)   Case, D. A.; Darden, T. A.; III, T. E. C.; Simmerling, C. L.; Wang, J.; Duke, R. E.; Luo, R.; Walker, R. C.; Zhang, W.; Merz, K. M.; Roberts, B.; Hayik, S.; Roitberg, A.; Seabra, G.; Swails, J.; Gotz, A. W.; Kolossvary, I.; Wong, K. F.; Paesani, F.; Vanicek, J.; Wolf, R. M.; Liu, J.; Wu, X.; Brozell, S. R.; Steinbrecher, T.; Gohlke, H.; Cai, Q.; Ye, X.; Wang, J.; Hsieh, M.-J.; Cui, G.; Roe, D. R.; Mathews, D. H.; Seetin, M. G.; Salomon-Ferrer, R.; Sagui, C.; Babin, V.; Luchko, T.; Gusarov, S.; Kovalenko, A.; Kollman, P. A. University of California, San Francisco, 2012.

CHAPTER IV

(1)   Kawamura, K.; Kaplan, I. R. Motor Exhaust Emissions as a Primary Source for Dicarboxylic Acids in Los Angeles Ambient Air. *Environ. Sci. Tech.* **1987**, *21*, 108-110.

(2)   Rogge, W. F.; Hildemann, L. M.; Mazurek, M. A.; Cass, G. R. Sources of Fine Organic Aerosol. 9. Pine, Oak, and Synthetic Log Combustion in Residential Fireplaces. *Environ. Sci. Technol.* **1998**, *32*, 13-22.

(3)   Chebbi, A.; Carlier, P. Carboxylic Acids in the Troposphere, Occurrence, Sources, and Sinks: A Review. *Atmos. Environ.* **1996**, *30*, 4233-4249.

(4)   Kawamura, K.; Usukura, K. Distributions of Low Molecular Weight Dicarboxylic Acids in the North Pacific Aerosol Samples. *J. Oceanogr.* **1993**, *49*, 271-283.

(5)   Kawamura, K.; Kasukabe, H.; Barrie, L. A. Source and reaction pathways of dicarboxylic acids, ketoacids and dicarbonyls in arctic aerosols: One year of observations. *Atmos. Environ.* **1996**, *30*, 1709-1722.

(6)   Kawamura, K.; Sakaguchi, F. Molecular distributions of water soluble dicarboxylic acids in marine aerosols over the Pacific Ocean including tropics. *J. Geophys. Res.* **1999**, *104*, 3501-3509.

(7)   Sempéré, R.; Kawamura, K. Comparative distributions of dicarboxylic acids and related polar compounds in snow, rain, and aerosols from urban atmosphere. *Atmos. Environ.* **1994**, *28*, 449-459.

(8)   Sempéré, R.; Kawamura, K. Low molecular weight dicarboxylic acids and related polar compounds in the remote marine rain samples collected from western Pacific. *Atmos. Environ.* **1996**, *30*, 1609-1619.

(9)   Aggarwal, S. G.; Kawamura, K. Molecular distributions and stable carbon isotopic compositions of dicarboxylic acids and related compounds in aerosols from Sapporo, Japan: Implications for photochemical aging during long-range atmospheric transport. *J. Geophys. Res.* **2008**, *113*, 13.

(10)   Hsieh, L.-Y.; Kuo, S.-C.; Chen, C.-L.; Tsai, Y. I. Origin of low-molecular-weight dicarboxylic acids and their concentration and size distribution variation in suburban aerosol. *Atmos. Environ.* **2007**, *41*, 6648-6661.

(11)   Hsieh, L.-Y.; Kuo, S.-C.; Chen, C.-L.; Tsai, Y. I. Size distributions of nano/micron dicarboxylic acids and inorganics ions in suburban PM episode and non-episodic aerosol. *Atmos. Environ.* **2009**, *43*, 4396-4406.

(12)   Pavuluri, C. M.; Kawamura, K.; Swaminathan, T. Water-soluble organic carbon, dicarboxylic acids, ketoacids, and   -dicarbonyls in the tropical Indian aerosols. *J. Geophys. Res.* **2010**, *115*, 15.

(13)   Cabaniss, S. E.; Leenheer, J. A.; McVey, I. F. Aqueous infrared carboxylate absorbances: aliphatic di-acids. *Spectrochim Acta A* **1998**, *54*, 449-458.

(14)   Socrates, G. *Infrared Characteristic Group Frequencies*; 2nd ed.; Wiley Interscience: Chichester, 1994.

(15)   Gericke, A.; Huhnerfuss, H. In Situ Investigations of Saturated Long-Chain Fatty Acids at the Air/Water Interface by External Infrared Reflection-Absorption Spectroscopy. *J. Phys. Chem.* **1993**, *97*, 12899-12908.

(16)   Johann, R.; Vollhardt, D.; Mohwald, H. Study of the pH dependence of head group bonding in arachidic acid monolayers by polarization modulation infrared reflection absorption spectroscopy. *Colloid Surface A* **2001**, *182*, 311-320.

(17)   Wolfs, I.; Dessyn, H. O. Characteristic Vibrational Pattern for the Cyclic Dimer Carboxylic Acid Function in the Solid State. *Appl. Spectrosc.* **1996**, *50*, 1000-1006.

(18)   Ghorai, S.; Laskin, A.; Tivanski, A. V. Spectroscopic Evidence of Keto-Enol Tautomerism in Deliquesced Malonic Acid Particles. *J. Phys. Chem. A* **2011**, *115*, 4373-4380.

(19)   Lambert, A. G.; Davies, P. B.; Neivandt, D. J. Implementing the Theory of Sum Frequency Generation Vibrational Spectroscopy: A Tutorial Review. *Appl. Spectrosc. Rev.* **2005**, *40*, 103-145.

(20)   Johnson, C. M.; Tyrode, E.; Baldelli, S.; Rutland, M. W.; Leygraf, C. A Vibrational Sum Frequency Spectroscopy Study of the Liquid-Gas Interface of Acetic Acid-Water Mixtures: 1. Surface Speciation. *J. Phys. Chem. B* **2005**, *109*, 321-328.

(21)   Soule, M. C. K.; Blower, P. G.; Richmond, G. L. Nonlinear Vibrational Spectroscopic Studies of the Adsorption and Speciation of Nitric Acid at the Vapor/Acid Solution Interface. *J. Phys. Chem. A* **2007**, *111*, 3349-3357.

(22)   Soule, M. C. K.; Blower, P. G.; Richmond, G. L. Effects of Atmospherically Important Solvated ions on Organic Acid Adsorption at the Surface of Aqueous Solutions. *J. Phys. Chem. B* **2007**, *111*, 13703-13713.

(23)   Richmond, G. L. Molecular Bonding and Interactions at Aqueous Surfaces as Probed by Vibrational Sum Frequency Spectroscopy. *Chem. Rev.* **2002**, *102*, 2693-2724.

(24)   Sovago, M.; Campen, R. K.; Bakker, H. J. Hydrogen bonding strength of interfacial water determined with surface sum-frequency generation. *Chem. Phys. Lett.* **2009**, *470*, 7-12.

(25)   Raymond, E. A.; Tarbuck, T. L.; Brown, M. G.; Richmond, G. L. Hydrogen-Bonding Interactions at the Vapor/Water Interface Investigated by Vibrational Sum-Frequency Spectroscopy of HOD/H2O/D2O Mixtures and Molecular Dynamics Simulations. *J. Phys. Chem. B* **2003**, *107*, 546-556.

(26)   Tian, C.-S.; Shen, Y. R. Isotopic Dilution Study of the Water/Vapor Interface by Phase-Sensitive Sum-Frequency Vibrational Spectroscopy. *J. Am. Chem. Soc.* **2009**, *131*, 2790-2791.

(27)   Buch, V. Molecular Structure and OH-Stretch Spectra of Liquid Water Surface. *J. Phys. Chem. B* **2005**, *109*, 17771-17774.

(28)   Morita, A.; Hynes, J. T. A Theoretical Analysis of the Sum Frequency Generation Spectrum of the Water Surface. II. Time-Dependent Approach. *J. Phys. Chem. B* **2002**, *106*, 673-685.

(29)   Walker, D. S.; Hore, D. K.; Richmond, G. L. Understanding the Population, Coordination, and Orientation of Water Species Contributing to the Nonlinear Optical Spectroscopy of the Vapor-Water Interface through Molecular Dynamics Simulations. *J. Phys. Chem. B* **2006**, *110*, 20451-20459.

(30)   Ota, S. T., University of Oregon, 2011.

(31)   Lin-Vien, D.; Colthup, N. B.; Fateley, W. G.; Grasselli, J. G. *The Handbook of Infrared and Raman Characteristic Frequencies of Organic Molecules*; Academic Press, 1991.

(32)   Mitsui, K.; Ukaji, T. Infrared Spectra of Some Aqueous Solutions. *Research Reports of Ikutoku Tech. Univ.* **1977**, *B-2*, 77-82.

(33)   Tarbuck, T. L.; Ota, S. T.; Richmond, G. L. Spectroscopic Studies of Solvated Hydrogen and Hydroxide Ions at Aqueous Surfaces. *J. Am. Chem. Soc.* **2006**, *128*, 14519-14527.

(34)   Tyrode, E.; Johnson, C. M.; Kumpulainen, A.; Rutland, M. W.; Claesson, P. M. Hydration State of Nonionic Surfactant Monolayers at the Liquid/Vapor Interface: Structure Determination by Vibrational Sum Frequency Spectroscopy. *J. Am. Chem. Soc.* **2005**, *127*, 16848-16859.

(35)   Hyvärinen, A.-P.; Lihavainen, H.; Gaman, A.; Vairila, L.; Ojala, H.; Kulmala, M.; Viiasnen, Y. Surface tensions and densities of oxalic, malonic, succinic, maleic, malic, and cis-pinonic acids. *J. Chem. Eng. Data* **2006**, *51*, 255-260.

(36)   Varga, Z.; Kiss, G.; Hansson, H.-C. Modelling the cloud condensation nucleus activity of organic acids on the basis of surface tension and osmolality measurements. *Atmos. Chem. Phys.* **2007**, *7*, 4601-4611.

(37)   Rosen, M. J. *Surfactants and Interfacial Phenomena*; 3rd ed.; John Wiley & Sons, Inc., 2004.

(38)   Clegg, S. L.; Seinfeld, J. H. Thermodynamic Models of Aqueous Solutions Containing Inorganic Electrolytes and Dicarboxylic Acids at 298.15 K 1. The Acids as Nondissociating Components. *J. Phys. Chem. A* **2006**, *110*, 5692-5717.

(39)   Rao, Y.; Li, X.; Lei, X.; Jockusch, S.; George, M. W.; Turro, N. J.; Eisenthal, K. B. Observations of Interfacial Population and Organization of Surfactants with Sum Frequency Generation and Surface Tension. *J. Phys. Chem. C* **2001**, *115*, 12064-12067.

(40)   Pool, R. E.; Versluis, J.; Backus, E. H. G.; Bonn, M. Comparative Study of Direct and Phase-Specific Vibrational Sum-Frequency Generation Spectroscopy: Advantages and Limitations. *J. Phys. Chem. B* **2011**, *115*, 15362-15369.

(41)   Shamay, E. S.; Johnson, K.; Richmond, G. L. Dancing on Water: The Choreography of Sulfur Dioxide Adsorption to Aqueous Surfaces. *J. Phys. Chem. C* **2011**, *115*, 25304-25314.

(42)   Nguyen, T. H.; Hibbs, D. E.; Howard, S. T. Conformatioms, Energies, and Intramolecular Hydrogen Bonds in Dicarboxylic Acids: Implications of the Design of Synthetic Dicarboxylic Acid Receptors. *J. Comput. Chem.* **2005**, *26*, 1233-1241.

(43)   Merchan, M.; Tomas, F.; Nebot-Gil, I. An *ab initio* study of intramolecular hydrogen bonding in malonic acid and its monoanion. *J. Mol. Struc-Theochem* **1984**, *109*, 51-60.

(44)   *CRC Handbook of Chemistry and Physics*; 85 ed.; CRC Press: Boca Raton, 2004.

(45)   Lange, N. A. *Handbook of Chemistry*; Revised 10th ed.; McGraw-Hill, 1967.

CHAPTER V

(1)   Chebbi, A.; Carlier, P. Carboxylic Acids in the Troposphere, Occurrence, Sources, and Sinks: A Review. *Atmos. Environ.* **1996**, *30*, 4233-4249.

(2)   Kawamura, K.; Usukura, K. Distributions of Low Molecular Weight Dicarboxylic Acids in the North Pacific Aerosol Samples. *J. Oceanogr.* **1993**, *49*, 271-283.

(3) Kawamura, K.; Kasukabe, H.; Barrie, L. A. Source and reaction pathways of dicarboxylic acids, ketoacids and dicarbonyls in arctic aerosols: One year of observations. *Atmos. Environ.* **1996**, *30*, 1709-1722.

(4) Kawamura, K.; Sakaguchi, F. Molecular distributions of water soluble dicarboxylic acids in marine aerosols over the Pacific Ocean including tropics. *J. Geophys. Res.* **1999**, *104*, 3501-3509.

(5) Sempéré, R.; Kawamura, K. Comparative distributions of dicarboxylic acids and related polar compounds in snow, rain, and aerosols from urban atmosphere. *Atmos. Environ.* **1994**, *28*, 449-459.

(6) Sempéré, R.; Kawamura, K. Low molecular weight dicarboxylic acids and related polar compounds in the remote marine rain samples collected from western Pacific. *Atmos. Environ.* **1996**, *30*, 1609-1619.

(7) Aggarwal, S. G.; Kawamura, K. Molecular distributions and stable carbon isotopic compositions of dicarboxylic acids and related compounds in aerosols from Sapporo, Japan: Implications for photochemical aging during long-range atmospheric transport. *J. Geophys. Res.* **2008**, *113*, 13.

(8) Hsieh, L.-Y.; Kuo, S.-C.; Chen, C.-L.; Tsai, Y. I. Origin of low-molecular-weight dicarboxylic acids and their concentration and size distribution variation in suburban aerosol. *Atmos. Environ.* **2007**, *41*, 6648-6661.

(9) Hsieh, L.-Y.; Kuo, S.-C.; Chen, C.-L.; Tsai, Y. I. Size distributions of nano/micron dicarboxylic acids and inorganics ions in suburban PM episode and non-episodic aerosol. *Atmos. Environ.* **2009**, *43*, 4396-4406.

(10) Pavuluri, C. M.; Kawamura, K.; Swaminathan, T. Water-soluble organic carbon, dicarboxylic acids, ketoacids, and -dicarbonyls in the tropical Indian aerosols. *J. Geophys. Res.* **2010**, *115*, 15.

(11) Bilde, M.; Svenningsson, B.; Mønster, J.; Rosenørn, T. Even-odd alternation of evaporation rates and vapor pressures of C3-C9 dicarboxylic acid aerosols. *Environmental Science & Technology* **2003**, *37*, 1371-1378.

(12) Thalladi, V. R.; Nüsse, M.; Boese, R. The melting point alternation in α,ω-Alkanedicarboxylic acids. *Journal of the American Chemical Society* **2000**, *122*, 9227-9236.

(13) Cappa, C. D.; Lovejoy, E. R.; Ravishankara, A. R. Determination of Evaporation Rates and Vapor Pressures of Very Low Volatility Compounds: A Study of the C4-C10 and C12 Dicarboxylic Acids. *J. Phys. Chem. A* **2007**, *111*, 3099-3109.

(14)   Saxena, P.; Hildemann, L. M. Water-Soluble Organics in Atmospheric Particles: A Critical Review of the Literature and Application of Thermodynamics to Identify Candidate Compounds. *J. Atmos. Chem.* **1996**, *24*, 57-109.

(15)   Johnson, C. M.; Tyrode, E.; Baldelli, S.; Rutland, M. W.; Leygraf, C. A Vibrational Sum Frequency Spectroscopy Study of the Liquid-Gas Interface of Acetic Acid-Water Mixtures: 1. Surface Speciation. *J. Phys. Chem. B* **2005**, *109*, 321-328.

(16)   Soule, M. C. K.; Blower, P. G.; Richmond, G. L. Effects of Atmospherically Important Solvated ions on Organic Acid Adsorption at the Surface of Aqueous Solutions. *J. Phys. Chem. B* **2007**, *111*, 13703-13713.

(17)   Soule, M. C. K.; Blower, P. G.; Richmond, G. L. Nonlinear Vibrational Spectroscopic Studies of the Adsorption and Speciation of Nitric Acid at the Vapor/Acid Solution Interface. *J. Phys. Chem. A* **2007**, *111*, 3349-3357.

(18)   Vinaykin, M.; Benderskii, A. V. Vibrational Sum-Frequency Spectrum of the Water Bend at the Air/Water Interface. *J. Phys. Chem. Lett.* **2012**, *3*, 3348-3352.

(19)   Walrafen, G. E.; Hokmabadi, M. S.; Yang, W. H. Raman Investigation of the Temperature Dependence of the Bending ν_2 and Combination $\nu_2 + \nu_L$ Bands from Liquid Water *J. Phys. Chem.* **1988**, *92*, 2433-2438.

(20)   Pavlovic, M.; Baranovic, G.; Lovrekovic, D. Raman study of the bending band of water. *Spectrochim Acta* **1991**, *47A*, 897-906.

(21)   Larouche, P.; Max, J.-J.; Chapados, C. Isotope effects in liquid water by infrared spectroscopy. II. Factor analysis of the temperature effect on H2O and D2O. *J. Chem. Phys.* **2008**, *129*, 064503.

(22)   Cabaniss, S. E.; Leenheer, J. A.; McVey, I. F. Aqueous infrared carboxylate absorbances: aliphatic di-acids. *Spectrochim Acta A* **1998**, *54*, 449-458.

(23)   Bardet, L.; Maillols, J.; Maillols, H. Spectre Raman de l'acide succinique en solution aqueuse saturee. *G. R. Acad. Sc. Paris* **1970**, *270, Serie B*, 158-161.

(24)   Gericke, A.; Huhnerfuss, H. In Situ Investigations of Saturated Long-Chain Fatty Acids at the Air/Water Interface by External Infrared Reflection-Absorption Spectroscopy. *J. Phys. Chem.* **1993**, *97*, 12899-12908.

(25)   Johann, R.; Vollhardt, D.; Mohwald, H. Study of the pH dependence of head group bonding in arachidic acid monolayers by polarization modulation infrared reflection absorption spectroscopy. *Colloid Surface A* **2001**, *182*, 311-320.

(26)   Muro, M.; Itoh, Y.; Hasegawa, T. A Conformation and Orientation Model of the Carboxylic Group of Fatty Acids Dependent on Chain Length in a Langmuir Monolayer Film Studied by Polarization-Modulation Infrared Reflection Absorption Spectroscopy. *J. Phys. Chem. B* **2010**, *114*, 11496-11501.

(27)   Ota, S. T., University of Oregon, 2011.

(28)   Tyrode, E.; Johnson, C. M.; Kumpulainen, A.; Rutland, M. W.; Claesson, P. M. Hydration State of Nonionic Surfactant Monolayers at the Liquid/Vapor Interface: Structure Determination by Vibrational Sum Frequency Spectroscopy. *J. Am. Chem. Soc.* **2005**, *127*, 16848-16859.

(29)   Raymond, E. A.; Richmond, G. L. Probing the Molecular Structure and Bonding of the Surface of Aqueous Salt Solutions. *J. Phys. Chem. B* **2004**, *108*, 5051-5059.

(30)   Tarbuck, T. L.; Richmond, G. L. Adsorption of Organosulfur Species at Aqueous Surfaces: Molecular Bonding and Orientation. *J. Phys. Chem. B* **2005**, *109*, 20868–20877.

(31)   Tarbuck, T. L.; Ota, S. T.; Richmond, G. L. Spectroscopic Studies of Solvated Hydrogen and Hydroxide Ions at Aqueous Surfaces. *J. Am. Chem. Soc.* **2006**, *128*, 14519-14527.

(32)   Schnitzer, C.; Baldelli, S.; Campbell, D. J.; Schultz, M. J. Sum Frequency Generation of O−H Vibrations on the Surface of H2O/HNO3 Solutions and Liquid HNO3. *J. Phys. Chem. A* **1999**, *103*, 6383–6386.

(33)   Schnitzer, C.; Baldelli, S.; Schultz, M. J. Sum Frequency Generation of Water on NaCl, NaNO3, KHSO4, HCl, HNO3, and H2SO4 Aqueous Solutions. *J. Phys. Chem. B* **2000**, *104*, 585–590.

(34)   Booth, A. M.; Topping, D. O.; McFiggans, G.; Percival, C. J. Surface tension of mixed inorganic and dicarboxylic acid aqueous solutions at 298.15 K and their importance for cloud activation predictions. *Phys. Chem. Chem. Phys.* **2009**, *11*, 8021-8028.

(35)   Varga, Z.; Kiss, G.; Hansson, H.-C. Modelling the cloud condensation nucleus activity of organic acids on the basis of surface tension and osmolality measurements. *Atmos. Chem. Phys.* **2007**, *7*, 4601-4611.

(36)   Hyvärinen, A.-P.; Lihavainen, H.; Gaman, A.; Vairila, L.; Ojala, H.; Kulmala, M.; Viiasnen, Y. Surface tensions and densities of oxalic, malonic, succinic, maleic, malic, and cis-pinonic acids. *J. Chem. Eng. Data* **2006**, *51*, 255-260.

(37)   Rosen, M. J. *Surfactants and Interfacial Phenomena*; 3rd ed.; John Wiley & Sons, Inc., 2004.

(38)   Rao, Y.; Li, X.; Lei, X.; Jockusch, S.; George, M. W.; Turro, N. J.; Eisenthal, K. B. Observations of Interfacial Population and Organization of Surfactants with Sum Frequency Generation and Surface Tension. *J. Phys. Chem. C* **2001**, *115*, 12064-12067.

(39)   *CRC Handbook of Chemistry and Physics*; 85 ed.; CRC Press: Boca Raton, 2004.

CHAPTER VI

(1)   Grosjean, D.; Cauwenberghe, K. V.; Schmid, J. P.; Kelley, P. E.; James N. Pitts, J. Identification of C3-C10 Aliphatic Dicarboxylic Acids in Airborne Particulate Matter. *Environ. Sci. Technol.* **1978**, *12*, 313-317.

(2)   Chebbi, A.; Carlier, P. Carboxylic Acids in the Troposphere, Occurrence, Sources, and Sinks: A Review. *Atmos. Environ.* **1996**, *30*, 4233-4249.

(3)   Legrand, M.; Preunkert, S.; Oliveira, T.; Pio, C. A.; Hammer, S.; Gelecser, A.; Kasper-Giebl, A.; Laj, P. Origin of C2-C5 dicarboxylic acids in the European atmosphere inferred from year-round aerosol study conducted at a west-east transect. *J. Geophys. Res.* **2007**, *112*.

(4)   Rogge, W. F.; Hildemann, L. M.; Mazurek, M. A.; Cass, G. R. Sources of Fine Organic Aerosol. 9. Pine, Oak, and Synthetic Log Combustion in Residential Fireplaces. *Environ. Sci. Technol.* **1998**, *32*, 13-22.

(5)   Hatakeyama, S.; Ohno, M.; Weng, J.-h.; Takagi, H.; Akimoto, H. Mechanism for the Formation of Gaseous and Particulate Products from Ozone-Cycloalkene Reactions in Air. *Environ. Sci. Technol.* **1987**, *21*, 52-57.

(6)   Hatakeyama, S.; Tanonaka, T.; Weng, J.-h.; Bandow, H.; Takagi, H.; Akimoto, H. Ozone-Cyclohexene Reaction in Air: Quantitative Analysis of Particulate Products and the Reaction Mechanism. *Environ. Sci. Technol.* **1985**, *19*.

(7)   Johnson, C. M.; Tyrode, E.; Baldelli, S.; Rutland, M. W.; Leygraf, C. A Vibrational Sum Frequency Spectroscopy Study of the Liquid-Gas Interface of Acetic Acid-Water Mixtures: 1. Surface Speciation. *J. Phys. Chem. B* **2005**, *109*, 321-328.

(8)   Soule, M. C. K.; Blower, P. G.; Richmond, G. L. Nonlinear Vibrational Spectroscopic Studies of the Adsorption and Speciation of Nitric Acid at the Vapor/Acid Solution Interface. *J. Phys. Chem. A* **2007**, *111*, 3349-3357.

(9)   Cabaniss, S. E.; Leenheer, J. A.; McVey, I. F. Aqueous infrared carboxylate absorbances: aliphatic di-acids. *Spectrochim Acta A* **1998**, *54*, 449-458.

(10)   Yeung, M. C.; Chan, C. K. Water Content and Phase Transitions in Particles of Inorganic and Organic Species and their Mixtures Using Micro-Raman Spectroscopy. *Aerosol Science and Technology* **2010**, *44*, 269-280.

(11)   Delarbre, J. L.; Fabregue, E.; Maury, L.; Bardet, L. Analyse Vibrationelle et Structurale en Série Aliphatique Saturée. *J. Raman Spectrosc.* **1988**, *19*, 167-174.

(12)   Gericke, A.; Huhnerfuss, H. In Situ Investigations of Saturated Long-Chain Fatty Acids at the Air/Water Interface by External Infrared Reflection-Absorption Spectroscopy. *J. Phys. Chem.* **1993**, *97*, 12899-12908.

(13)   Johann, R.; Vollhardt, D.; Mohwald, H. Study of the pH dependence of head group bonding in arachidic acid monolayers by polarization modulation infrared reflection absorption spectroscopy. *Colloid Surface A* **2001**, *182*, 311-320.

(14)   Muro, M.; Itoh, Y.; Hasegawa, T. A Conformation and Orientation Model of the Carboxylic Group of Fatty Acids Dependent on Chain Length in a Langmuir Monolayer Film Studied by Polarization-Modulation Infrared Reflection Absorption Spectroscopy. *J. Phys. Chem. B* **2010**, *114*, 11496-11501.

(15)   Soule, M. C. K.; Blower, P. G.; Richmond, G. L. Effects of Atmospherically Important Solvated ions on Organic Acid Adsorption at the Surface of Aqueous Solutions. *J. Phys. Chem. B* **2007**, *111*, 13703-13713.

(16)   Raymond, E. A.; Richmond, G. L. Probing the Molecular Structure and Bonding of the Surface of Aqueous Salt Solutions. *J. Phys. Chem. B* **2004**, *108*, 5051-5059.

(17)   Tarbuck, T. L.; Richmond, G. L. Adsorption of Organosulfur Species at Aqueous Surfaces: Molecular Bonding and Orientation. *J. Phys. Chem. B* **2005**, *109*, 20868–20877.

(18)   Tarbuck, T. L.; Ota, S. T.; Richmond, G. L. Spectroscopic Studies of Solvated Hydrogen and Hydroxide Ions at Aqueous Surfaces. *J. Am. Chem. Soc.* **2006**, *128*, 14519-14527.

(19)   Schnitzer, C.; Baldelli, S.; Campbell, D. J.; Schultz, M. J. Sum Frequency Generation of O−H Vibrations on the Surface of H2O/HNO3 Solutions and Liquid HNO3. *J. Phys. Chem. A* **1999**, *103*, 6383–6386.

(20)   Schnitzer, C.; Baldelli, S.; Schultz, M. J. Sum Frequency Generation of Water on NaCl, NaNO3, KHSO4, HCl, HNO3, and H2SO4 Aqueous Solutions. *J. Phys. Chem. B* **2000**, *104*, 585–590.

(21)   Lu, R.; Gan, W.; Wu, B.-h.; Chen, H.; Wang, H.-f. Vibrational Polarization Spectroscopy of CH Stretching Modes of the Methylene Group at the Vapor/Liquid Interfaces with Sum Frequency Generation. *J. Phys. Chem. B* **2004**, *108*, 7297-7306.

(22)   Booth, A. M.; Topping, D. O.; McFiggans, G.; Percival, C. J. Surface tension of mixed inorganic and dicarboxylic acid aqueous solutions at 298.15 K and their importance for cloud activation predictions. *Phys. Chem. Chem. Phys.* **2009**, *11*, 8021-8028.

(23)   Varga, Z.; Kiss, G.; Hansson, H.-C. Modelling the cloud condensation nucleus activity of organic acids on the basis of surface tension and osmolality measurements. *Atmos. Chem. Phys.* **2007**, *7*, 4601-4611.

(24)   Rosen, M. J. *Surfactants and Interfacial Phenomena*; 3rd ed.; John Wiley & Sons, Inc., 2004.

(25)   Clegg, S. L.; Seinfeld, J. H. Thermodynamic Models of Aqueous Solutions Containing Inorganic Electrolytes and Dicarboxylic Acids at 298.15 K 1. The Acids as Nondissociating Components. *J. Phys. Chem. A* **2006**, *110*, 5692-5717.

(26)   Rao, Y.; Li, X.; Lei, X.; Jockusch, S.; George, M. W.; Turro, N. J.; Eisenthal, K. B. Observations of Interfacial Population and Organization of Surfactants with Sum Frequency Generation and Surface Tension. *J. Phys. Chem. C* **2001**, *115*, 12064-12067.

(27)   Chen, H.; Gan, W.; Lu, R.; Guo, Y.; Wang, H.-f. Determination of Structure and Energetics for Gibbs Surface Adsorption Layers of Binary Liquid Mixture 2. Methanol + Water. *J. Phys. Chem. B* **2005**, *109*.

(28)   Barnette, A. L.; Kim, S. H. Coadsorption of n-Propanol and Water on SiO2: Study of Thickness, Composition, and Structure of Binary Adsorbate Layer Using Attenuated Total Reflectance Infrared and Sum Frequency Generation (SFG) Vibration Spectroscopy. *J. Phys. Chem. C* **2012**, *116*, 9909-9916.

(29)   *CRC Handbook of Chemistry and Physics*; 85 ed.; CRC Press: Boca Raton, 2004.

(30)   Lange, N. A. *Handbook of Chemistry*; Revised 10th ed.; McGraw-Hill, 1967.

CHAPTER VII

(1)   Grosjean, D.; Cauwenberghe, K. V.; Schmid, J. P.; Kelley, P. E.; James N. Pitts, J. Identification of C3-C10 Aliphatic Dicarboxylic Acids in Airborne Particulate Matter. *Environ. Sci. Technol.* **1978**, *12*, 313-317.

(2)   Chebbi, A.; Carlier, P. Carboxylic Acids in the Troposphere, Occurrence, Sources, and Sinks: A Review. *Atmos. Environ.* **1996**, *30*, 4233-4249.

(3)   Legrand, M.; Preunkert, S.; Oliveira, T.; Pio, C. A.; Hammer, S.; Gelecser, A.; Kasper-Giebl, A.; Laj, P. Origin of C2-C5 dicarboxylic acids in the European atmosphere inferred from year-round aerosol study conducted at a west-east transect. *J. Geophys. Res.* **2007**, *112*.

(4)   Hatakeyama, S.; Ohno, M.; Weng, J.-h.; Takagi, H.; Akimoto, H. Mechanism for the Formation of Gaseous and Particulate Products from Ozone-Cycloalkene Reactions in Air. *Environ. Sci. Technol.* **1987**, *21*, 52-57.

(5)   Hatakeyama, S.; Tanonaka, T.; Weng, J.-h.; Bandow, H.; Takagi, H.; Akimoto, H. Ozone-Cyclohexene Reaction in Air: Quantitative Analysis of Particulate Products and the Reaction Mechanism. *Environ. Sci. Technol.* **1985**, *19*.

(6)   Saxena, P.; Hildemann, L. M. Water-Soluble Organics in Atmospheric Particles: A Critical Review of the Literature and Application of Thermodynamics to Identify Candidate Compounds. *J. Atmos. Chem.* **1996**, *24*, 57-109.

(7)   Johnson, C. M.; Tyrode, E.; Baldelli, S.; Rutland, M. W.; Leygraf, C. A Vibrational Sum Frequency Spectroscopy Study of the Liquid-Gas Interface of Acetic Acid-Water Mixtures: 1. Surface Speciation. *J. Phys. Chem. B* **2005**, *109*, 321-328.

(8)   Soule, M. C. K.; Blower, P. G.; Richmond, G. L. Nonlinear Vibrational Spectroscopic Studies of the Adsorption and Speciation of Nitric Acid at the Vapor/Acid Solution Interface. *J. Phys. Chem. A* **2007**, *111*, 3349-3357.

(9)   Cabaniss, S. E.; Leenheer, J. A.; McVey, I. F. Aqueous infrared carboxylate absorbances: aliphatic di-acids. *Spectrochim Acta A* **1998**, *54*, 449-458.

(10)   Ramsis, H.; Monmouton, P.; Delarbe, J. L.; Maury, L. Analyse Vibrationelle et Structurale en Série Aliphatique Saturée X - Specres de Vibration de l'Acide Adipique et des ses Sels Alcalins de Potassium en Solution Aqueuse. *J. Raman Spectrosc.* **1995**, *26*, 265-272.

(11)   Gericke, A.; Huhnerfuss, H. In Situ Investigations of Saturated Long-Chain Fatty Acids at the Air/Water Interface by External Infrared Reflection-Absorption Spectroscopy. *J. Phys. Chem.* **1993**, *97*, 12899-12908.

(12)   Johann, R.; Vollhardt, D.; Mohwald, H. Study of the pH dependence of head group bonding in arachidic acid monolayers by polarization modulation infrared reflection absorption spectroscopy. *Colloid Surface A* **2001**, *182*, 311-320.

(13)   Muro, M.; Itoh, Y.; Hasegawa, T. A Conformation and Orientation Model of the Carboxylic Group of Fatty Acids Dependent on Chain Length in a Langmuir Monolayer Film Studied by Polarization-Modulation Infrared Reflection Absorption Spectroscopy. *J. Phys. Chem. B* **2010**, *114*, 11496-11501.

(14)   Soule, M. C. K.; Blower, P. G.; Richmond, G. L. Effects of Atmospherically Important Solvated ions on Organic Acid Adsorption at the Surface of Aqueous Solutions. *J. Phys. Chem. B* **2007**, *111*, 13703-13713.

(15)   Raymond, E. A.; Richmond, G. L. Probing the Molecular Structure and Bonding of the Surface of Aqueous Salt Solutions. *J. Phys. Chem. B* **2004**, *108*, 5051-5059.

(16)   Tarbuck, T. L.; Richmond, G. L. Adsorption of Organosulfur Species at Aqueous Surfaces: Molecular Bonding and Orientation. *J. Phys. Chem. B* **2005**, *109*, 20868–20877.

(17)   Tarbuck, T. L.; Ota, S. T.; Richmond, G. L. Spectroscopic Studies of Solvated Hydrogen and Hydroxide Ions at Aqueous Surfaces. *J. Am. Chem. Soc.* **2006**, *128*, 14519-14527.

(18)   Schnitzer, C.; Baldelli, S.; Campbell, D. J.; Schultz, M. J. Sum Frequency Generation of O−H Vibrations on the Surface of H2O/HNO3 Solutions and Liquid HNO3. *J. Phys. Chem. A* **1999**, *103*, 6383–6386.

(19)   Schnitzer, C.; Baldelli, S.; Schultz, M. J. Sum Frequency Generation of Water on NaCl, NaNO3, KHSO4, HCl, HNO3, and H2SO4 Aqueous Solutions. *J. Phys. Chem. B* **2000**, *104*, 585–590.

(20)   Lu, R.; Gan, W.; Wu, B.-h.; Chen, H.; Wang, H.-f. Vibrational Polarization Spectroscopy of CH Stretching Modes of the Methylene Group at the Vapor/Liquid Interfaces with Sum Frequency Generation. *J. Phys. Chem. B* **2004**, *108*, 7297-7306.

(21)   Tyrode, E.; Hedburg, J. A Comparative Study of the CD and CH Stretching Spectral Regions of Typical Surfactants Systems Using VSFS: Orientation Analysis of the Terminal CH3 and CD3 Groups. *J. Phys. Chem. C* **2012**, *116*, 1080-1091.

(22)   Riipinen, I.; Koponen, I. K.; Frank, G. P.; Hyärinen, A.-P.; Vanhanen, J.; Lihavainen, H.; Lehtinen, K. E. J.; Bilde, M.; Markku, K. Adipic and Malonic Acid Aqueous Solutions: Surface Tensions and Saturation Vapor Pressures. *J. Phys. Chem. A* **2007**, *111*, 12995-13002.

(23)   Booth, A. M.; Topping, D. O.; McFiggans, G.; Percival, C. J. Surface tension of mixed inorganic and dicarboxylic acid aqueous solutions at 298.15 K and their importance for cloud activation predictions. *Phys. Chem. Chem. Phys.* **2009**, *11*, 8021-8028.

(24)   Varga, Z.; Kiss, G.; Hansson, H.-C. Modelling the cloud condensation nucleus activity of organic acids on the basis of surface tension and osmolality measurements. *Atmos. Chem. Phys.* **2007**, *7*, 4601-4611.

(25)   Rosen, M. J. *Surfactants and Interfacial Phenomena*; 3rd ed.; John Wiley & Sons, Inc., 2004.

(26)   Bilde, M.; Svenningsson, B.; Mønster, J.; Rosenørn, T. Even-odd alternation of evaporation rates and vapor pressures of C3-C9 dicarboxylic acid aerosols. *Environmental Science & Technology* **2003**, *37*, 1371-1378.

(27)   Rozaini, M. Z. H.; Brimblecone, P. The odd-even behaviour of dicarboxylic acids solubility in the atmpospheric aerosols. *Water Air Soil and Pollution* **2009**, *198*, 65-75.

(28)   Thalladi, V. R.; Nüsse, M.; Boese, R. The melting point alternation in α,ω-Alkanedicarboxylic acids. *Journal of the American Chemical Society* **2000**, *122*, 9227-9236.

(29)   *CRC Handbook of Chemistry and Physics*; 85 ed.; CRC Press: Boca Raton, 2004.

(30)   Minofar, B.; Mucha, M.; Jungwirth, P.; Yang, X.; Fu, Y.-J.; Wang, X.-B.; Wang, L.-S. Bulk versus Interfacial Aqueous Solvation of Dicarboxylate Dianions. *J. Am. Chem. Soc.* **2004**, *126*, 11691-11698.

(31)   Yang, X.; Fu, Y.-J.; Wang, X.-B.; Slavicek, P.; Mucha, M.; Jungwirth, P.; Wang, L.-S. Solvent-Mediated Folding of a Doubly Charged Anion. *J. Am. Chem. Soc.* **2004**, *126*, 876-883.

CHAPTER VIII

(1)   Chebbi, A.; Carlier, P. Carboxylic Acids in the Troposphere, Occurrence, Sources, and Sinks: A Review. *Atmos. Environ.* **1996**, *30*, 4233-4249.

(2)   Kolb, C. E.; Worsnop, D. R. Chemistry and Composition of Atmospheric Aerosol Particles. *Annu. Rev. Phys. Chem.* **2012**, *63*, 471-491.

(3)   Clegg, S. L.; Seinfeld, J. H. Thermodynamic Models of Aqueous Solutions Containing Inorganic Electrolytes and Dicarboxylic Acids at 298.15 K 1. The Acids as Nondissociating Components. *J. Phys. Chem. A* **2006**, *110*, 5692-5717.

(4)   Clegg, S. L.; Seinfeld, J. H. Thermodynamic Models of Aqueous Solutions Containing Inorganic Electrolytes and Dicarboxylic Acids at 298.15 K 2. Systems Including Dissociation Equilibria. *J. Phys. Chem. A* **2006**, *110*, 5718-5734.

(5)   Ma, X.; Chakraborty, P.; Henz, B. J.; Zachariah, M. R. Molecular dynamic simulation of dicarboxylic acid coated aqueous aerosol: strucutre and processing of water vapor. *Physical Chemistry Chemical Physics* **2011**, *13*, 9374-9384.

(6)   Seinfeld, J. H.; Pandis, S. N. *Atmospheric Chemistry and Physics*; Wiley-Interscience: New York, 1998.

(7)   Johnson, C. M.; Tyrode, E.; Baldelli, S.; Rutland, M. W.; Leygraf, C. A Vibrational Sum Frequency Spectroscopy Study of the Liquid-Gas Interface of Acetic Acid-Water Mixtures: 1. Surface Speciation. *J. Phys. Chem. B* **2005**, *109*, 321-328.

(8)   Soule, M. C. K.; Blower, P. G.; Richmond, G. L. Effects of Atmospherically Important Solvated ions on Organic Acid Adsorption at the Surface of Aqueous Solutions. *J. Phys. Chem. B* **2007**, *111*, 13703-13713.

(9)   Rosen, M. J. *Surfactants and Interfacial Phenomena*; 3rd ed.; John Wiley & Sons, Inc., 2004.

(10)   Kanicky, J. R.; Poniatowski, A. F.; Mehta, N. R.; Shah, D. O. Cooperativity among Molecules at Interfaces in Relation to Various Technological Processes: Effect of Chain Length on the pKa of Fatty Acid Salt Solutions. *Langmuir* **2000**, *16*, 172-177.

(11)   Bordes, R.; Tropsch, J.; Holmberg, K. Counterion specificity of surfactants based on dicarboxylic amino acids. *J. Colloid. Interf. Sci.* **2009**, *338*, 529-536.

(12)   Donaldson, D. J.; Vaida, V. The Influence of Organic Films at the Air-Aqueous Boundary on Atmospheric Processes. *Chem. Rev.* **2006**, *106*, 1445-1461.

(13)   Ellison, G. B.; Tuck, A. F.; Vaida, V. Atmospheric Processing of Organic Aerosols. *J. Geophys. Res.* **1999**, *104*, 11633-11641.

(14)   Kawamura, K.; Imai, Y.; Barrie, L. A. Photochemical production and loss of organic acids in high Arctic aerosols during long-range transport and polar sunrise ozone depletion events. *Atmos Environ* **2005**, *39*, 599-614.

(15)   Kawamura, K.; Sakaguchi, F. Molecular distributions of water soluble dicarboxylic acids in marine aerosols over the Pacific Ocean including tropics. *J. Geophys. Res.* **1999**, *104*, 3501-3509.

(16)   Kawamura, K.; Kaplan, I. R. Motor Exhaust Emissions as a Primary Source for Dicarboxylic Acids in Los Angeles Ambient Air. *Environ. Sci. Tech.* **1987**, *21*, 108-110.

(17)   Kawamura, K.; Gagosian, R. B. Implications of ω-oxocarboxylic acids in the remote marine atmosphere for photo-oxidation of unsaturated fatty acids. *Nature* **1987**, *325*, 330-332.

(18)   Crans, D. C.; Levinger, N. E. The Conundrum of pH in Water Nanodroplets: Sensing pH in Reverse Micelle Water Pools. *Accounts Chem. Res.* **2011**, *45*, 1637-1645.

(19)   Krivacsy, Z.; Molnar, A. Size distribution of ions in atmospheric aerosols. *Atmos. Res.* **1998**, *46*, 279-291.

(20)   Jeffrey L. Collett, J.; Bator, A.; Rao, X.; Demoz, B. B. Acidity variations across the cloud drop size spectrum and their influence on rates of atmospheric sulfate production. *Geophys. Res. Lett.* **1994**, *21*, 2393-2396.

(21)   Keene, W. C.; Sander, R.; Pszenny, A. A. P.; Vogt, R.; Crutzen, P. J.; Galloway, J. N. Aerosol pH in the marine boundary layer: A review and model evaluation. *J. Aerosol Sci.* **1998**, *29*, 339-356.

(22)   Keene, W. C.; Pszenny, A. A. P.; Maben, J. R.; Stevenson, E.; Wall, A. Closure evaluation of size-resolved aerosol pH in the New England coastal atmosphere during summer. *J. Geophys. Res.* **2004**, *109*, D23307.

(23)   Zhang, Q.; Jimenez, J. L.; Worsnop, D. R.; Canagaratna, M. A Case Study of Urban Particle Acidity and Its Influence on Secondary Organic Aerosol. *Environ. Sci. Technol.* **2007**, *41*, 3213-3219.

(24)   Ludwig, J.; Klemm, O. Organic acids in different size classes of atmophseric particulate materials. *Tellus* **1988**, *40B*, 340-347.

(25)   Finlayson-Pitts, B. J.; James N. Pitts, J. *Chemistry of the Lower and Upper Atmosphere*; Academic Press: San Diego, 2000.

(26)   Ota, S. T., University of Oregon, 2011.

(27)   Reid, J. P.; Dennis-Smither, B. J.; Kwamena, N.-O. A.; Miles, R. E. H.; Hanford, K. L.; Homer, C. J. The morphology of aerosol particles consisting of hydrophobic and hydrophilic phases: hydrocarbons, alcohols, and fatty acids as the hydrophobic component. *Phys. Chem. Chem. Phys.* **2011**, *13*, 15559-15572.

(28)   Xue, H.; Khalizov, A. F.; Wang, L.; Zheng, J.; Zhang, R. Effects of Coating of Dicarboxylic Acids on the Mass-Mobility Relationship of Soot Particles. *Environ. Sci. Technol.* **2009**, *43*, 2787-2792.

(29)   Bertram, A. K.; Martin, S. T.; Hanna, S. J.; Smith, M. L.; Bodsworth, A.; Chen, Q.; Kuwata, M.; Liu, A.; You, Y.; Zorn, S. R. Predicting the relative humidities of liquid-liquid phase separation, efflorescence, and deliquescence of mixed particles of ammonium sulfate, organic material, and water using the organic-to-sulfate mass ratio of the particle and the oxygen-to-carbon elemnetal ratio of the organic component. *Atmos. Chem. Phys.* **2011**, *11*, 10995-11006.

(30)   Song, M.; Marcolli, C.; Kreiger, U. K.; Zuend, A.; Peter, T. Liquid-liquid phase separation and morphology of internally mixed dicarboxylic acids/ammonium sulfate/water particles. *Atmos. Chem. Phys.* **2012**, *12*, 2691-2712.

(31)   Ciobanu, V. G.; Marcolli, C.; Krieger, U. K.; Weers, U.; Peter, T. Liquid-liquid Phase Separation in Mixed Organic/Inorganic Aerosol Particles. *J. Phys. Chem. A* **2009**, *113*, 10966-10978.

(32)   Gibbs, J. W. *The Collected Works of J. Willard Gibbs*; Yale University Press: New Haven, 1948; Vol. Volume 1: Thermodynamics.

(33)   Jungwirth, P.; Tobias, D. J. Specific Ion Effects at the Air/Water Interface. *Chem. Rev.* **2006**, *106*, 1259-1281.

(34)   Zhang, Y.; Cremer, P. S. Chemistry of Hofmeister Anions and Osmolytes. *Annu. Rev. Phys. Chem* **2010**, *61*, 63-83.

(35)   Kunz, W.; Nostro, P. L.; Ninham, B. W. The present state of affairs with Hofmeister effects. *Curr. Opin. Colloid In.* **2004**, *9*, 1-18.